MODELING RHEOLOGY OF NON-NEWTONIAN LUBRICANTS IN PISTON SKIRT ELASTOHYDRODYNAMIC LUBRICATION (EHL) DURING INITIAL ENGINE START UP CONDITIONS

BY

Mr.Usman Farooq Chaudhri
MSc (MECH)-56
SESSION 2008-2010

ADVISOR

PROFESSOR DR. MUHAMMAD AFZAAL MALIK

National University of Sciences and Technology
College of Electrical & Mechanical Engineering
Rawalpindi

4th June 2010

MODELING RHEOLOGY OF NON-NEWTONIAN LUBRICANTS IN PISTON SKIRT EHL DURING INITIAL ENGINE START UP CONDITIONS

By

Mr. Usman Farooq Chauhdri

Submitted to the Faculty of College of Electrical and Mechanical Engineering, Rawalpindi, in partial fulfillment of the requirement for the degree of

Master of Science in Mechanical Engineering

Candidate: Mr. Usman Farooq Chaudhri

Advisor: Professor Dr. Muhammad Afzaal Malik

Committee Members:

1. Prof. Dr. Mahmood Anwar Khan
2. Associate Prof. Dr. Riaz A Mufti
3. Assistant Professor. Raja Amir Azim

College of Electrical & Mechanical Engineering
National University of Sciences and Technology
Rawalpindi

4th June 2010

TABLE OF CONTENTS

S/No. DESCRIPTION
Page No

List of Figures

ABSTRACT

MODELING RHEOLOGY OF NON-NEWTONIAN LUBRICANTS IN PISTON SKIRT EHL DURING INITIAL ENGINE START UP CONDITIONS

At global level, automobile engine manufacturers ensure that piston skirts are sufficiently lubricated during normal engine operation to prevent adhesive wear of skirt and cylinder liner. This is possible as Elastohydrodynamic lubrication (EHL) between piston skirt and cylinder liner does not allow actual metal to metal contact. At the time of Engine start up, absence of EHL film between piston skirt and cylinder liner results in dry contact followed by sequential formation of boundary, mixed and then EHL films, while the Engine attains normal operating conditions after warm up. Advancements in engine design have necessitated use of synthetic, multigrade Non-Newtonian engine lubricants to reduce engine friction and wear and enhance its operational life. Multiple blends of Non-Newtonian engine lubricants cater for various aspects of engine lubrication requirements during normal operation. However their peculiar rule to minimize adhesive wear of piston skirt and liner surfaces during engine start up conditions under ideal conditions have yet to be properly modeled and thoroughly investigated. This calls for proper investigative research to model rheological behavior of non-Newtonian engine lubricants with particular focus on initial engine start up conditions. This research will mathematically model and simulate transient EHL phenomenon of piston skirts during engine start up conditions while using viscoelastic Maxwell type of Non-Newtonian engine oil as lubricant. Comparative analysis and parametric studies of Newtonian and Non-Newtonian lubricants rheology and effects on EHL of piston skirt during engine initial start up conditions are also part of this research work.

Acknowledgements

During my time at EME, I have met a number of people who have contributed to making my experience here rewarding and enjoyable from both a personal and professional standpoint.

First and foremost, I would like to thank my advisor Dr Afzaal malik for his contributions to both my work as well as my personal and professional development throughout my time at the NUST College of E&ME. I would like to thank Dr Afzaal for all of the technical insight he has provided on numerous occasions throughout the duration of the Thesis work.

I would like to thank Mr. Syed Adnan Qasim for giving me the opportunity to take on a significant amount of responsibility in my thesis work, and for encouraging me to write technical publications and attend conferences. I believe that these experiences have played an instrumental role in my professional development during my time at NUST College of E&ME.

I would like to thank my group partners, Mumtaz ali khan and Ali Usman for their support and insight in this study.

I would like to acknowledge the National University of Sciences and Technology, Pakistan for their financial support in writing technical publications and attend conferences.

I would also like to thank Dr. Riaz Mufti and Mr. Saif ullah Khalid, who have contributed significantly to my work during my research work. I consider both their technical and personal advice to have been invaluable throughout the time that we have known each other.

Finally, last but not least, I would like to thank my family for their support throughout my time here.

CHAPTER 1

NON-NEWTONIAN LUBRICANT RHEOLOGY AND PISTON LUBRICATION

1.1 Introduction

The prediction and assessment of friction, wear and load bearing capacity of a lubricated and dynamically loaded piston assembly over a wide range of operating conditions is extremely important. The modeling issues involved in dynamically loaded piston skirts and their lubrication are extensive. These include the influences of oil feed, thermal effects and cavitations, changes in viscosity with shear rate, temperature and pressure, and the effects of viscoelasticity [1]. The design and development of modern internal combustion engine is the result of investigations carried through in different scientific areas, in order to satisfy the requirements of the manufacturers in terms of performance, cost and weight. Improvements in lubrication, heat reduction and load capacity enhancement are some of the areas with interest to this work.

Piston's small oscillatory motion in a reciprocating engine significantly affects its lubrication during initial engine start up cycles. Multi grade engine lubricants show viscoelastic non-Newtonian behavior due to the presence of polymer additives [2]. Maxwell lubricant is the first viscoelastic rate type model exhibiting energy storage by characterizing lubricants elastic response and energy dissipation by its viscous nature [3]. Compared to Newtonian fluids, kinetic energy dissipation and power due to shear stress at the wall decrease in Maxwell model [4]. Polymer additives as viscosity index (VI) improvers in viscoelastic lubricants significantly improve base stock performance over wide range of automotive engine operating conditions [5]. Initial engine start up is a critical operating condition when engine lubricant must be mobile enough to assist 'cold starting' and yet viscous enough to prevent wear.

1.2 Concept of Piston Lubrication & Lubricant Rheology

Engine oil lubricants make up nearly one half of the lubricant market and therefore attract a lot of interest. The principle function of the engine oil lubricant is to extend the life of moving parts operating under many different conditions of speed, temperature and pressure. At low

temperatures the lubricant is expected to flow sufficiently in order that moving parts are not starved of oil. At higher temperatures they are expected to keep the moving parts a part to minimize wear. The lubricant does this by reducing friction and removing heat from moving parts apart from minimizing wear. An important function of the lubricant is to prevent any contamination like wear debris, sludge, soot particles, acids or peroxides from doing any damage to engine.

A typical automotive engine lubricant consists of oil (base stock) and additives. The base stock may be characterized in several different ways. For example, the base stock may be composed of petroleum that has come out of the ground and that has been distilled or separated in to a desirable molecular weight fraction for use in engine oil. This fraction may be further enhanced by such process as extraction, de-waxing, or chemical reaction to remove undesirable constituents. Such base stocks are typically called “mineral” oils.

To create suitable engine oil, additives are blended to the base stock[6]. The additives either enhance the stability of the lubricant or provide additional protection to the engine. The presence of the additives in the oil is necessary; otherwise the oil could not work in severe conditions of temperature and pressure [7].

1.3 Viscoelasticity in Non-Newtonian Lubricants and Review of Past Research

A fascinating and largely unresolved problem in tribology concerns the effect of viscoelasticity on lubrication-flow characteristics. This problem has been tackled since the mid-1950s with the appearance of the so-called multi grade oils [6], and has recently taken on added significance with the transition to lubricants of yet lower viscosity for improved energy efficiency. Any factor influencing load capacity and wear in journal bearings is clearly of renewed importance; consequently, there are good practical reasons to reopen the general question of viscoelastic effects on lubrication.

Since the mid 1950s, the addition of polymers to mineral oils has become a well established practice. These additives cause the existing lubricants to become non-Newtonian and viscoelastic [7]. Even in the simplest flow situation, it is necessary to consider more than the usual shear-stress component; indeed, the mechanical behavior of these lubricants is potentially far more complicated than that of mineral oil based lubricants, which may be regarded as

Newtonian fluids. It is known that polymeric additive containing lubricants posses a characteristic relaxation time, λ, which is the ratio of the viscosity to the elastic modulus. For lubricating oils, the fluid relaxation times might be expected to vary from 10mm to 10μm [8]. If a lubrication process time is of the same order, one could expect strong time-dependant effects. The Deborah number De=λ/T can be used to measure such time dependence, where T is the characteristic time of the flow process under consideration [9].

Attempts to interpret the time-dependent effect on the basis of the shear dependant viscosity, or based on different heat transfer characteristics of polymeric lubricants, have proved largely unproductive and the viscoelastic behavior of the lubricants has been proposed as the most likely cause for the improvements in the performance. Despite popular belief and some experimental evidence with real lubricants, it appears that unequal normal stresses and memory effects may be relatively insignificant in automotive Piston skirt and liner [10]. As a consequence, one might superficially expect that, at high shear rates encountered in piston liner, the behavior of multi grade oils may not be greatly different from that of the low viscosity base stock use to formulate oils [11]. In a recent study how ever values of film thickness obtained from direct measurements in of piston and liner in an operating engine were found to correlate not with the high temperature, high shear rate viscosity and relaxation time. Even though typical fluid relaxation times are only of the order of micro seconds, viscoelasticity can have a measureable and beneficial effect on lubrication characteristics [12], and is expected to significantly affect the film thickness and the coefficients of friction in piston skirt and liner [13]. There is some controversy as to whether viscoelastic behavior, as manifested through normal stress effects, can have any effect at all in lubrication, over and above that which arises as a result of the shear dependence of the viscosity [14]. It seems clear at present that polymeric oils are in fact better lubricants than the non polymeric oils [15] . Specifically, they appear to reduce friction and wear when compared with either their base oils or mineral oils of comparable low shear viscosity. To date, attempts to predict this improvement in performance by invoking non-Newtonian behavior have been significantly unsuccessful. It is unlikely that one could have known a priori whether viscoelasticity would give rise to any beneficial or adverse side effects; although the fact that one of nature's lubricants, synovial fluid, is elastic liquid may have been a useful pointer [16]. Over the past decades, numerous theoretical and experimental studies have been undertaken to determine whether polymer-improved oils are more efficient than their Newtonian counterparts, even after the improved viscosity-temperature

response has been accommodated [17]. It is fair to say that the situation is inconclusive and somewhat confused. At best, there have been small improvements, [18]; at worst, any effects have been within the experimental error [19].

The lubricant behavior will be modeled by the upper-convected Maxwell constitutive equation, which is the simplest viscoelastic model having a constant viscosity and a constant relaxation time. By employing characteristic lubricant relaxation times in an order of magnitude analysis, we develop a perturbation method to analyze the flow of Maxwell lubricants between two narrow surfaces and determine whether the viscoelastic properties have any effects on lubrication characteristics compared with their Newtonian counter parts. This perturbation scheme is used to derive coupled non linear partial differentiation equations governing the evolution of the fluid velocity and pressure in thin film flows. The leading order problem corresponds to Newtonian lubrication solution [20]. Numerical solution on the order of the Deborah number (De) yields corrections to the flow profiles due to viscoelasticity [21]. Attention will be paid to the mechanisms of the viscoelastic pressure driving thin film flow in the presence of viscoelasticity.

Base oils such as mineral oil and silicone oil that have traditionally been used in tribological systems can be characterized as Newtonian fluids. These fluids have a constant viscosity and follow a simple relationship for stress τ, and strain $\delta V/\delta n$, that is linear with bulk viscosity μ, such that $\tau = \mu\ \delta V/\delta n$. Non-Newtonian lubricants are described as those that "have a more complex relationship between the shear stress and the velocity derivative". For this study, we will focus only on the viscoelastic properties of non-Newtonian lubricants and describe how these properties affect the Piston-liner lubrication process.

Viscoelastic lubricants can experience shear rate dependant viscosity, stress or strain relaxation, or both. The continuity and momentum equations are valid for all flows of incompressible fluids, but the Reynolds equation is not valid for all flows since it assumes that the lubricant has a constant viscosity and a Newtonian form of the stress tensor. For non-Newtonian lubricants, an appropriate constitutive equation for the stress tensor must be found that adequately describes the response of the lubricant to the applied conditions. The appropriate form of the constitutive equation for a particular fluid depends on the molecular structure of the polymer chains that make up the fluid. The fluid relaxation time can be defined according to the Maxwell model, which has the following general constitutive equation relating the stress tensor in the fluid to the applied strain rate tensor.

$$\lambda \frac{\partial \tau}{\partial t} + \tau = -\eta \frac{\partial \gamma}{\partial t} \qquad \ldots\ldots\ldots\ldots \quad (1.1)$$

Substituting the shear stress and partial time derivative of the shear stress in to Maxwell model for an applied shear stress γ, the resulting equation gives the relaxation time as

$$\lambda(\omega) = \frac{G'}{G''\omega} \qquad \ldots\ldots\ldots\ldots \quad (1.2)$$

Hence the characteristic relaxation time for a fluid is defined as the limit of the relaxation time as the frequency **ω** goes to zero.

Earlier efforts included studies on flow rheology of non-Newtonian fluids on the time dependant film thickness history between non parallel sliding surfaces on the basis of Power law fluid model [22]. Use of poly alpha Olefins in synthetic engine oils to cater for severe engine operating conditions highlights significance of viscoelasticity aspects of non Newtonian lubricants [23]. Many researchers modeled non-Newtonian lubricants as power law fluid to characterize shear thinning, although such models do not exhibit any elastic normal stress effects [24]. Most of the researchers employed sinh law to describe shear thinning effects and primarily referred to Ree-Eyring model for the purpose. In reality 'sinh law' was not intended to characterize shear thinning lubricants [25]. While describing shear thinning aspects using Ree-Eyring model, viscoelastic effects in compression and in shear were neglected [26]. Despite this fact, researchers of late, while modeling thermal non Newtonian lubrication ignored viscoelastic effects and instead described shear stress and shear strain rate by following Eyring fluid model [27]. Incidentally, such studies also did not model engine start up conditions with emphasis on viscoelasticity.

This study covers viscoelastic aspects of non-Newtonian lubricants at engine start up, when, in reality, absence of elastohydrodynamic lubrication (EHL) may result in early engine wear. Multi-grade, viscoelastic, non-Newtonian engine lubricant is modeled as upper convected Maxwell fluid in simulated engine start up conditions. This model calculates piston eccentricities, their effect on modified hydrodynamic contact pressures, lubricant properties, piston contact geometry and shape of lubricant film.

1.4 Basic Concepts of I.C. Engine & its Lubrication

1.4.1 Rigid Hydrodynamic Lubrication Regime

This lubrication regime results from a film of separating fluid being drawn into a converging, wedge-shaped zone by the self-acting pumping action of a moving surface. Both the pressure and the frictional power loss in this film are a function of the lubricant's viscosity in combination with the geometry and shear rate imposed by bearing operating conditions. The deformation due to lubricant pressure is small. Therefore, the rigid-surface, hydrodynamic theory suffices. The Reynolds equation is used to calculate the hydrodynamic pressure, as well as the friction losses in the lubricant film.

1.4.2 Elastohydrodynamic Lubrication (EHL) Regime

In an EHL regime the piston skirt surface deformations due to lubricant pressure are of the order of lubricant film thickness. Hence, the EHD theory is needed. In this case the effect of pressure-induced deformation on the lubricant-film gap has to be accounted for although; the Reynolds equation is still applicable. The inclusion of piston skirt/rings surface deformations in the lubricant-film-gap expression renders the equation highly non-linear resulting in considerable difficulty in obtaining a solution.

1.4.3 Mixed Lubrication Regime

In this regime the load is shared by both fluid film and asperity contact. Therefore, both the Reynolds equation and elastic contact equations need to be solved simultaneously.

1.4.4 Boundary Lubrication Regime

In this regime no hydrodynamic film is sustained. The coefficient of friction is very high and friction is proportional to the applied load for a certain range of sliding velocity and temperature.

1.5. Concept of Hydrodynamic & EHD Lubrication

There are two conditions for the occurrence of hydrodynamic lubrication:

- Two surfaces must move relatively to each other with sufficient velocity for a load carrying lubricating film to be generated and,

- Surfaces must be inclined at some angle to each other, i.e., if the surfaces are parallel a pressure field will not form in the lubricating film to support the required load.

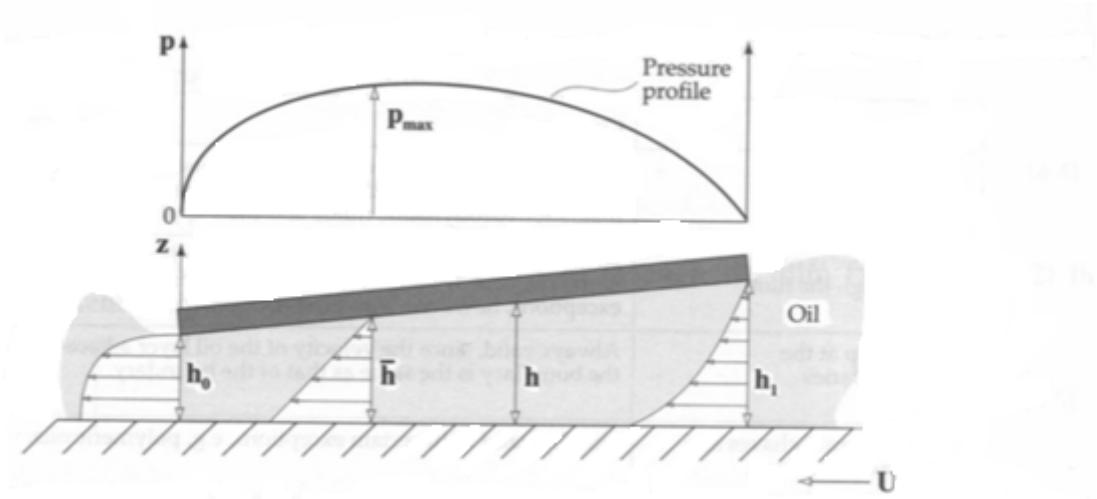

Fig 1.1 Principle of hydrodynamic pressure generation between non-parallel surfaces.**[22]**

Elastohydrodynamic lubrication can be defined as a form of hydrodynamic lubrication where the elastic deformation of the contacting bodies and the changes of viscosity with pressure play fundamental roles. The deformation of the bodies has to be included in the basic model of elastohydrodynamic lubrication. Grubin in 1940 found that elastohydrodynamic lubrication is the combination of three effects:

- Hydrodynamics
- Elastic deformation of the metal surfaces
- Increase in the viscosity of oil under extreme pressures

The lubricated contacts in which these three effects take place are said to be operating elastohydrodynamically, which effectively means that the contacting surfaces deform elastically under the hydrodynamic pressure generated in the layer of lubricating film. The lubricating films are very thin, in the range of 0.1 to 1[μm], but manage to separate the interacting surfaces, resulting in a significant reduction of wear and friction.

CHAPTER-2

PRESSURE GENERATION, REYNOLDS, NAVIER STOKES, ENERGY EQUATIONS & VISCOUS SHEARING

2.1. Introduction

Reynolds equation is an analytical proof that describes that a viscous liquid can prevent contact between two sliding surfaces by hydrodynamic pressures resulting in less friction and almost zero wear. Reynolds equation describes the process of lubrication through the generation of a viscous oil film between the moving surfaces. The two surfaces must slide over each other with adequate velocity for a load carrying oil film to be generated and must be inclined to each other at some angle. Reynolds equation is a reduction of the Navier-Stokes continuity and momentum equation. Reynolds equation is more or less derived by conceiving the equilibrium of an element of liquid submitted to viscous shear.

2.2. Principle of Hydrodynamic Pressure Generation & Reynolds Equation

Following assumptions are made to understand the principle of hydrodynamic pressure generation:-

1. Bottom surface is fully flooded and moves with some velocity.
2. Upper surface is inclined at some angle to the lower surface.
3. When lower surface moves, it drags oil film into the converging wedge, hence pressure field is generated.
4. In the start of the wedging process, the increasing pressure limits the entry flow while at the exit there is a decrease in pressure, which increases the exit flow.
5. At the inlet, the pressure gradient drives the fluid velocity profile to bend inwards whereas it causes the velocity profiles to bend outwards at the exit.

There are some simplifying assumptions, which are required in the derivation of Reynolds equation, and are as follows

1. Body forces are ignored.
2. Pressure is considered constant.
3. No slip at the boundaries.

4. Lubricant is Newtonian in nature.
5. Fluid flow is laminar.
6. Fluid inertia force is ignored.
7. Density of fluid is constant.
8. Fluid viscosity is constant.

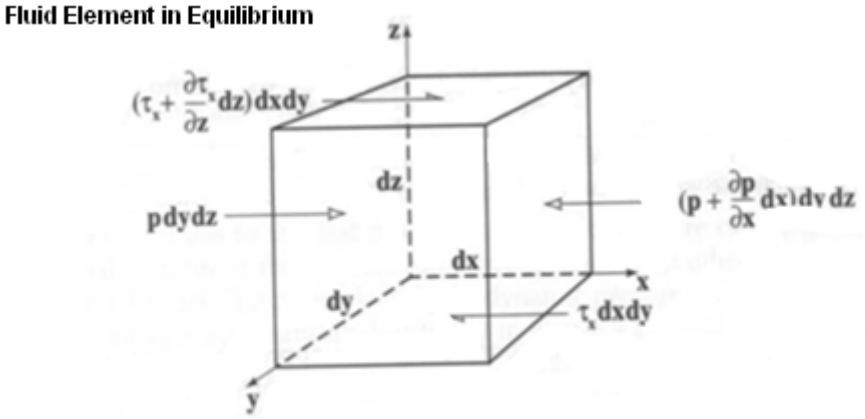

Fig 2.1 Equilibrium of an element of fluid from a hydrodynamic film; **p** is the pressure, τ_x is the shear stress acting in the '**x**' direction. **[22]**

The equilibrium of an element of fluid is considered as shown above in figure 2.1, to obtain an expression of the continuity of flow in a column. For Simplicity, assume that the forces on the element are acting initially in the 'x' direction only.

Since the fluid element is in equilibrium condition, hence the forces acting on it must balance out, so

$$pdydz + (\tau + \frac{\partial}{\partial z} + \tau_x dz)dxdy = (p + \frac{\partial p}{\partial x} dx)dydz + \tau_x dxdy \quad \text{..……..} \quad (2.1)$$

which after simplifying gives:

$$\frac{\partial}{\partial z}\tau_x dxdydz = \frac{\partial p}{\partial x} dxdydz \quad \text{…….. (2.2)}$$

Assuming non-zero volume i.e., dxdydz $\neq$ 0

$$\Rightarrow \quad \frac{\partial \tau_x}{\partial z} = \frac{\partial p}{\partial x} \quad \text{…….. (2.3)}$$

Forces that are acting in the outward direction must balance the forces that are acting in the inward direction, hence

$$pdxdz + (\tau_y + \frac{\partial}{\partial z}\tau_y dz)dxdy = (p + \frac{\partial p}{\partial y}dy)dxdz + \tau_y dxdy \quad \ldots\ldots\ldots\ldots (2.4)$$

Again assuming non-zero volume i.e., dxdydz $\neq$ 0

$$\Rightarrow \quad \frac{\partial}{\partial z}\tau_y = \frac{\partial p}{\partial y} \quad \ldots\ldots\ldots\ldots\ldots\ldots (2.5)$$

According to Assumption # 2, Pressure is constant throughout the film. Hence, $\frac{\partial p}{\partial z} = 0$

So shear stress can be expressed in terms of shear rate and lubricant viscosity, and is given as:

$$\tau_x = \eta\frac{u}{h} = \eta\frac{\partial u}{\partial z} \quad (\text{'x' component of Shear Stress}) \quad \ldots\ldots\ldots\ldots\ldots (2.6)$$

$$\tau_y = \eta\frac{v}{h} = \eta\frac{\partial v}{\partial z} \quad (\text{'y' component of Shear Stress}) \quad \ldots\ldots\ldots\ldots\ldots (2.7)$$

Putting the x component of Shear stress into equation (2.3), we obtain:

$$\frac{\partial}{\partial z}\left[\eta\frac{\partial u}{\partial z}\right] = \frac{\partial p}{\partial x} \quad \ldots\ldots\ldots\ldots (2.8)$$

Similarly, putting the y component of shear stress into equation (2.4), we obtain:

$$\frac{\partial}{\partial z}\left[\eta\frac{\partial v}{\partial z}\right] = \frac{\partial p}{\partial y} \quad \ldots\ldots\ldots\ldots (2.9)$$

According to assumption # 8, viscosity is considered constant in the entire fluid film. Hence it has no component in the 'z' direction. So equation (2.5) can be rearranged to give:

$$\frac{\partial p}{\partial x}\partial z = \partial\left[\eta\frac{\partial u}{\partial z}\right]$$

Taking Integral on both sides of the above equation:

$$\frac{\partial p}{\partial x}z + c_1 = \eta\frac{\partial u}{\partial z}$$

Integrating the above expression will give.

$$\int\left(\frac{\partial p}{\partial x}z + c_1\right)\partial z = \eta\int \partial u$$

$$\frac{\partial p}{\partial x}\left(\frac{z^2}{2}\right)+c_1 z+c_2=\eta u \qquad \text{…….. (2.10)}$$

Boundary Conditions. As there is no slip or velocity changes between the liquid film and solid surface at the boundaries of the wedge. Hence the boundary conditions are defined as

$u = U_2$ at $z = 0$; $u = U_1$ at $z = h$

Appling $u = U_2$ at $z = 0$ in equation (2.10)

$$\frac{\partial p}{\partial x}\left(\frac{(0)^2}{2}\right)+c_1\times 0+c_2=\eta U_2$$

$C_2 = \eta U_2$ ……. (2.11)

Appling $u = U_1$ at $z = h$ in equation (2.10)

$$\frac{\partial p}{\partial x}\frac{h^2}{2}+C_1 h+\eta U_2=\eta U_1$$

$$C_1+\left(\frac{\partial p}{\partial x}\frac{h^2}{2}\frac{1}{h}\right)=\frac{\eta}{h}(U_1-U_2)$$

$$C_1=(U_1-U_2)\frac{\eta}{h}-\frac{\partial p}{\partial x}\frac{h}{2} \qquad \text{…….. (2.12)}$$

Solving equations (2.10), (2.11) and (2.12)

we obtain:

$$\frac{\partial p}{\partial x}\left(\frac{z^2}{2}\right)+\left[(U_1-U_2)\frac{\eta}{h}-\frac{\partial p}{\partial x}\frac{h}{2}\right]z+\eta U_2=\eta u$$

$$u=\frac{\partial p}{\partial x}\left[\frac{z^2-zh}{2\eta}\right]+(U_1-U_2)\frac{z}{h}+U_2 \qquad \text{…….. (2.13)}$$

Equation (2.13) defines the velocity in the ‘x’ direction. Velocity profiles at the entry of the hydrodynamic film are shown in figure 2.2 below.

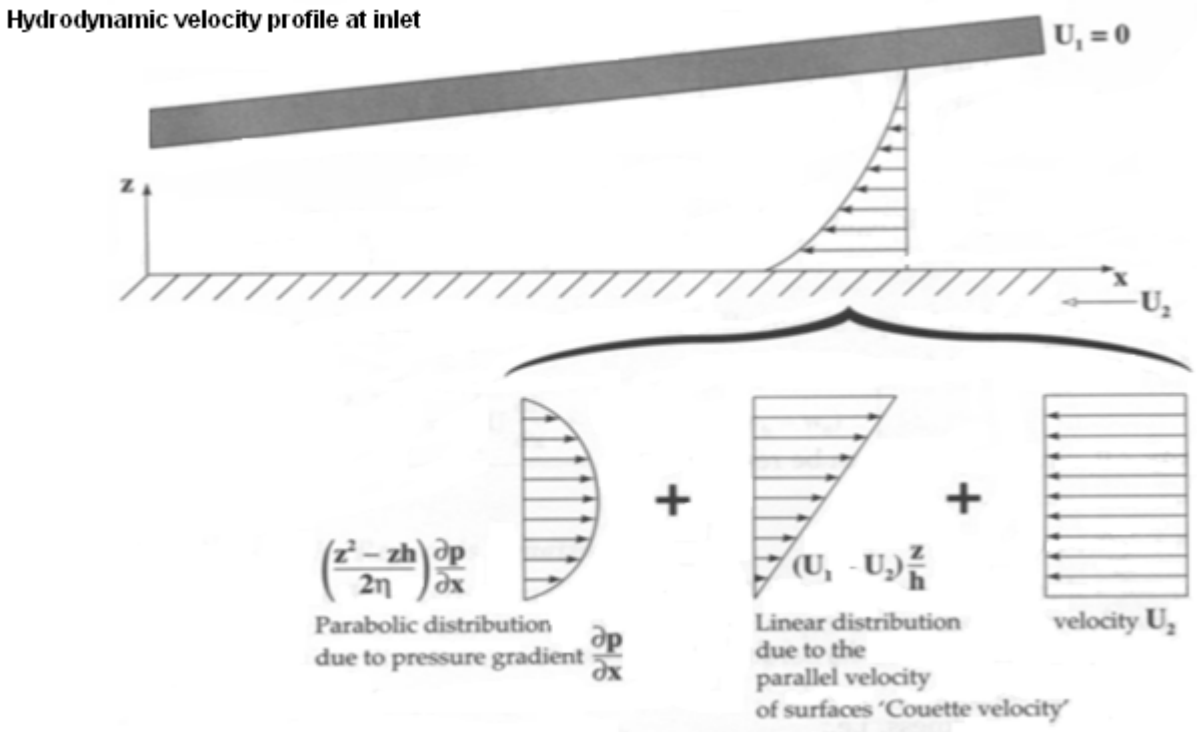

Fig 2.2 Velocity profiles at the entry of the hydrodynamic film. **[22]**

According to assumption # 8, fluid viscosity is assumed constant. Therefore it is not a function of 'z' Equation So eq (2.9) can be written as:

$$\partial\left(\eta\frac{\partial v}{\partial z}\right) = \left(\frac{\partial p}{\partial y}\right)\partial z$$

After integration it will give

$$\eta\frac{\partial v}{\partial z} = \frac{\partial p}{\partial y}z + C_1$$

Again integrating, $$\int \eta dv = \int\left(\frac{\partial p}{\partial y}z + C_1\right)\partial z$$

$$\eta v = \frac{\partial p}{\partial y}\left(\frac{z^2}{2}\right) + C_1 z + C_2 \qquad \text{……. (2.14)}$$

Keeping in view the third assumption that there is no slip or velocity change between the liquid and solid at the boundaries of the wedge, hence the boundary conditions are defined as

$v = V_2$ at $z = 0$; $v = V_1$ at $z = h$

Put $v = V_2$ at $z = 0$ in equation (2.14)

$$\eta V_2 = \frac{\partial p}{\partial y}\frac{(0)^2}{2} + C_1 \times 0 + C_2$$

$$C_2 = \eta V_2 \qquad \ldots\ldots\ldots\ldots\ldots \quad (2.15)$$

Put $v = V_1$ at $z = h$ & $C_2 = \eta V_2$ in equation (2.14)

$$\eta V_1 = \frac{\partial p}{\partial y}\frac{h^2}{2} + C_1 h + \eta V_2$$

$$C_1 = \frac{\eta}{h}(V_1 - V_2) - \frac{\partial p}{\partial y}\frac{h}{2} \qquad \ldots\ldots\ldots\ldots\ldots \quad (2.16)$$

Solving equations (2.14), (2.15) and (2.16)

We get:

$$v = \frac{\partial p}{\partial y}\left[\frac{z^2 - zh}{2\eta}\right] + (V_1 - V_2)\frac{z}{h} + V_2 \qquad \ldots\ldots\ldots\ldots\ldots \quad (2.17)$$

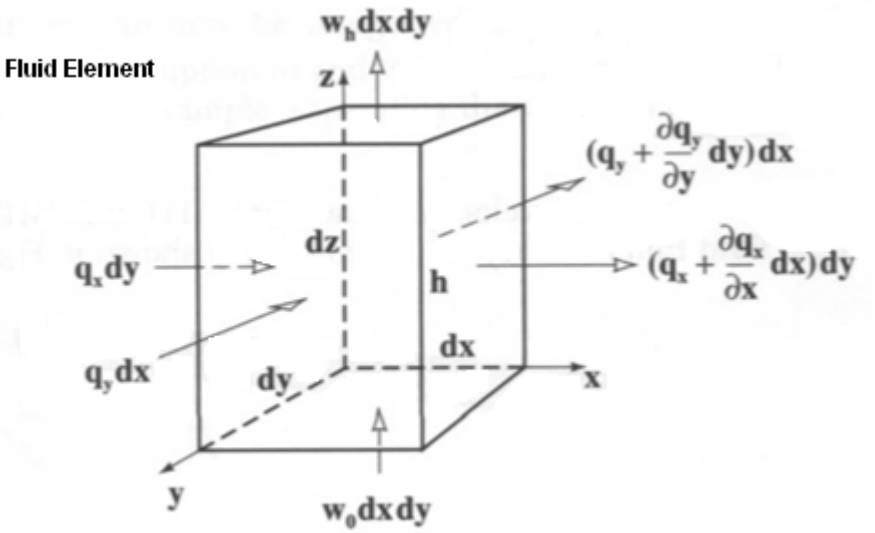

Fig 2.3 Continuity of flow in a column. **[22]**

Consider the lubricant film such that the film flows into the column horizontally at the rates of q_x and q_y as shown in figure 2.3 and in the vertical direction the lubricant flows into the column at the rate of '$w_o dxdy$' and flows out at the rate of '$w_h dxdy$'. The principle of continuity of flow

states that "the inflow of a liquid must be equal to outflow from the control volume under steady conditions". Hence following relation applies:

$$q_x dy + q_y dx + w_0 dxdy = \left(q_x + \frac{\partial q_x}{\partial x} dx\right)dy + \left(q_y + \frac{\partial q_y}{\partial y} dy\right)dx + w_h dxdy$$

$$\frac{\partial q_x}{\partial x} dxdy + \frac{\partial q_y}{\partial y} dxdy + (w_h - w_0)dxdy = 0$$

$$dxdy\left(\frac{\partial q_x}{\partial x} + \frac{\partial q_y}{\partial y} + ((w_h - w_0)\right) = 0$$

Since film area = dxdy ≠ 0, hence

$$\frac{\partial q_x}{\partial x} + \frac{\partial q_y}{\partial y} + (w_h - w_0) = 0 \qquad \text{……} \qquad (2.18)$$

If 'h' is the oil film thickness and 'u' is the oil film velocity then oil flow rate per unit length in the 'x' & 'y' direction is given by:

$$q_x = \int_0^h u dz \qquad \text{..……} \qquad (2.19)$$

$$q_y = \int_0^h v dz \qquad \text{……} \qquad (2.20)$$

Solving equations (2.13) & (2.17),

we obtain:

$$u = \frac{\partial p}{\partial x}\left[\frac{z^2 - zh}{2\eta}\right] + (U_1 - U_2)z/h + U_2$$

$$v = \frac{\partial p}{\partial y}\left[\frac{z^2 - zh}{2\eta}\right] + (V_1 - V_2)z/h + V_2$$

Put 'u' in equation (2.19)

$$q_x = \int_0^h \left[\frac{\partial p}{\partial x}\left(\frac{z^2 - zh}{2\eta}\right) + (U_1 - U_2)\frac{z}{h} + U_2\right]dz$$

$$q_x = -\left[\frac{-h^3}{12\eta}\frac{\partial p}{\partial x}\right] + \frac{h}{2} + (U_1 + U_2) \qquad \text{……} \quad (2.21)$$

which is the expression of the flow rate per unit length in the 'x' direction.

Also after putting ‘v’ from equation (2.17) in to equation (2.20), we obtain:

$$q_y = \int_0^h v\,dz$$

$$q_y = \int_0^h \left[\frac{\partial p}{\partial y}\left(\frac{z^2 - zh}{2\eta} \right) + (V_1 - V_2)\frac{z}{h} + V_2 \right] dz$$

$$q_y = \frac{\partial p}{\partial y}\frac{1}{12\eta}\left(-h^3\right) + h\left[\frac{V_1 - V_2 - 2V_2}{2} \right]$$

$$q_y = \frac{-h^3}{12\eta}\frac{\partial p}{\partial y} + \frac{h}{2}(V_1 + V_2) \qquad \ldots\ldots\ldots\ldots\ldots\ldots \qquad (2.22)$$

which is the expression for the flow rate per unit length in the ‘y’ direction.

Solving equations (2.18), (2.21) and (2.22),

$$\frac{\partial}{\partial x}(q_x) + \frac{\partial}{\partial y}(q_y) + (w_h - w_0) = 0$$

$$\frac{\partial}{\partial x}\left[-\frac{h^3}{12\eta}\frac{\partial p}{\partial x} + \frac{h}{2}(U_1 + U_2) \right] + \frac{\partial}{\partial y}\left[-\frac{h^3}{12\eta}\frac{\partial p}{\partial y} + \frac{h}{2}(V_1 + V_2) \right] + (w_h - w_0) = 0 \qquad \ldots\ldots \text{`} (2.23)$$

In order to further simplify the expression of the continuity equation of flow in a column, we define oil velocities in the ‘x’ and ‘y’ directions as follows:

$U = U_1 + U_2$; $V = V_1 + V_2$

Assuming that there is no variation in surface velocity in the ‘x’ and ‘y’ directions, i.e.,

$U \neq f(x)$; $V \neq f(y)$

Hence equation (2.23) becomes:

$$\frac{\partial}{\partial x}\left(\frac{h^3}{\eta}\frac{\partial p}{\partial x} \right) + \frac{\partial}{\partial y}\left(\frac{h^3}{\eta}\frac{\partial p}{\partial y} \right) = 6\left(\frac{Udh}{dx} + \frac{Vdh}{dy} \right) + 12(w_h - w_0) \qquad \ldots\ldots\ldots\ldots \qquad (2.24)$$

Equation (2.24) is the final expression of the 3-D Reynolds Equation.

Further simplifying the 3-DRenoylds equation, we make certain approximations.

1. Unilateral Velocity Approximation: Assuming that one of the velocities is equal to zero i.e., V = 0, hence equation (2.24) becomes

$$\frac{\partial}{\partial x}\left(\frac{h^3}{\eta}\frac{\partial p}{\partial x}\right)+\frac{\partial}{\partial y}\left(\frac{h^3}{\eta}\frac{\partial p}{\partial y}\right)=6\frac{Udh}{dx}+12\left(w_h-w_0\right) \quad \ldots\ldots\ldots\ldots\ldots\ldots \quad (2.25)$$

2. Steady Film Thickness Approximation*:* Assuming that there is no vertical flow over the oil film, i.e., $w_h - w_0 = 0$. This assumption requires that the distance between the two film surfaces remains constant during the operation. In that case equation (2.25) becomes

$$\frac{\partial}{\partial x}\left(\frac{h^3}{\eta}\frac{\partial p}{\partial x}\right)+\frac{\partial}{\partial y}\left(\frac{h^3}{\eta}\frac{\partial p}{\partial y}\right)=6\frac{Udh}{dx} \quad \ldots\ldots\ldots\ldots.. \quad (2.26)$$

3. Isoviscous Approximation: Neglecting shear heating effects and assuming that lubricant viscosity is constant over the film, i.e., η is constant.

$$\frac{1}{\eta}\left[\frac{\partial}{\partial x}\left(h^3\frac{\partial p}{\partial x}\right)+\frac{\partial}{\partial y}\left(h^3\frac{\partial p}{\partial y}\right)\right]=6\frac{Udh}{dx}$$

$$\frac{\partial}{\partial x}\left(\frac{h^3\partial p}{\partial x}\right)+\frac{\partial}{\partial y}\left(\frac{h^3\partial p}{\partial y}\right)=6U\eta\frac{dh}{dx} \quad \ldots\ldots\ldots\ldots\ldots\ldots \quad (2.27)$$

Infinitely Long Bearing Approximation: Assuming that the bearing length is infinite in the 'y' direction. Hence pressure changes in this direction are very small as compared to the bearing length. So, the pressure gradient is approximately equal to zero, i.e., $\frac{\partial p}{\partial y}=0$. So,

$$\frac{\partial}{\partial x}\left(\frac{h^3\partial p}{\partial x}\right)=6U\eta\left(\frac{dh}{dx}\right) \quad \ldots\ldots\ldots\ldots\ldots\ldots \quad (2.28)$$

Integrating both sides w.r.t. 'x',

$$\frac{h^3dp}{dx}=6U\eta h+C \quad \ldots\ldots\ldots\ldots\ldots \quad (2.29)$$

Boundary Conditions: For the value of 'C' assume that at some point along the lubricant film the value of pressure is maximum. At that point pressure gradient is zero, i.e., $\frac{dp}{dx}=0$ at $h=\bar{h}$.

Where $\bar{h}$ is the film thickness when the pressure is maximum. Apply it in equation (2.29)

$$0 = 6U\eta\bar{h}+C$$

C $= -6U\eta\bar{h}$ $\rightarrow$ Put it in equation (2.29)

$$\frac{dp}{dx} = 6U\eta\frac{\left(h-\bar{h}\right)}{h^3} \qquad \text{…….. (2.30)}$$

which is the required expression of simplified 1-D Reynolds equation.

2.3 NAVIER STOKES EQUATION

Considering a rectangular element of fluid of sides 'dx','dy' and thickness 'b'. Appling equation of motion (i.e., F = ma = $\frac{mdv}{dt}$) such that the forces acting on the element are F_x, F_y. The following equations are for the forces acting in the x and y direction.

$$F_x = m\frac{du}{dt} \quad ; \qquad F_y = m\frac{dv}{dt}$$

$$\left\{\begin{array}{l} F_x = \left(\rho bdxdy\right)\frac{du}{dt} \\ F_y = \left(\rho bdxdy\right)\frac{dv}{dt} \end{array}\right\} \qquad \text{……. (2.31)}$$

Hence, the velocity change *'du'* at time *'dt'* is expressed by the following equation:

$$du = \underbrace{\frac{\partial u}{\partial t}dt}_{\text{Progress in time}} + \underbrace{\frac{\partial u}{\partial x}dx + \frac{\partial u}{\partial y}dy}_{\text{Movement of position}}$$

$$du = dt\left[\frac{\partial u}{\partial t} + \frac{\partial u}{\partial x}\frac{\partial x}{\partial t} + \frac{\partial u}{\partial y}\frac{\partial y}{\partial t}\right]$$

but $\frac{dx}{dt} = u; \qquad \frac{dy}{dt} = v$

$$\Rightarrow \qquad \frac{du}{dt} = \frac{\partial u}{\partial t} + u\frac{\partial u}{\partial x} + v\frac{\partial u}{\partial y} \qquad \text{…… (2.32)}$$

Putting value of $\frac{du}{dt}$ in equation (2.31)

$$\left.\begin{aligned} F_x &= \rho\left(\frac{\partial u}{\partial t} + u\frac{\partial u}{\partial x} + v\frac{\partial u}{\partial y}\right) b\,dx\,dy \\ F_y &= \rho\left(\frac{\partial u}{\partial t} + u\frac{\partial u}{\partial x} + v\frac{\partial u}{\partial y}\right) b\,dx\,dy \end{aligned}\right\} \quad \ldots\ldots\ldots\ldots \quad (2.33)$$

The forces F acting on the element comprises of:

a. The Body Force F_b (B_x, B_y)

b. Pressure Force F_p (P_x, P_y)

c. Viscous Force F_s(S_x, S_y)

In simple words, F_x and F_y are expressed by following equations.

$$\left.\begin{aligned} F_x &= B_x + P_x + S_x \\ F_y &= B_y + P_y + S_y \end{aligned}\right\} \quad \ldots\ldots\ldots\ldots \quad (2.34)$$

Body Force 'F_b (B_x, B_y): These forces act throughout the mass, like force of gravity

Let,

X = x component of body forces

Y = y component of body forces

Then according to Newton's 2nd law of motion:

$$\left.\begin{aligned} B_x &= X\rho bdxdy \\ B_y &= Y\rho bdxdy \end{aligned}\right\} \quad \ldots\ldots\ldots\ldots \quad (2.35)$$

Pressure Force F_p (P_x, P_y): The pressure forces acting in the x-direction is given by deducting the outlet pressure force from the inlet pressure force, which is

$$P_x = pb\,dy - \left(p + \frac{\partial p}{\partial x}dx\right)bdy$$

Similarly

$$\left.\begin{aligned} \Rightarrow P_x &= -\frac{\partial p}{\partial x}bdxdy \\ P_y &= -\frac{\partial p}{\partial y}bdxdy \end{aligned}\right\} \quad \ldots\ldots\ldots\ldots \quad (2.36)$$

Viscous Force (S_x,S_y): In case of forces in the 'x' direction due to angular deformation (S_{x1}),

Corresponding shear stress is expressed as:

$$\tau = \mu \frac{\partial \gamma}{\partial t}$$

Where, $\frac{\partial \gamma}{\partial t}$ is the rate of relative strain. So,

$$\tau = \mu \frac{\partial \gamma}{\partial t} = \mu\left(\frac{\partial \gamma_1}{\partial t} + \frac{\partial \gamma_2}{\partial t}\right) = \mu\left(\frac{\partial u}{\partial y} + \frac{\partial v}{\partial x}\right)$$

Hence forces in the x-direction due to angular deformation are given by:

$$S_{x1} = \frac{\partial \tau}{\partial y}(b dx dy) \quad ; \quad \text{But} \quad \tau = \mu\left(\frac{\partial u}{\partial y} + \frac{\partial v}{\partial x}\right)$$

$$\Rightarrow S_{x1} = \left(\frac{\partial^2 u}{\partial y^2} - \frac{\partial^2 u}{\partial x^2}\right)\mu(b\, dx\, dy) \qquad \ldots\ldots\ldots\ldots \quad (2.37)$$

Force in the 'x' Direction Due to Elongation Transformation S_{x2}: Consider a rhombus inscribed in a cubic fluid element of thickness equal to unity.

After calculating the deformation per unit time, the velocity of angular deformation $\partial\gamma/\partial t$ becomes

$$\frac{\partial \gamma}{\partial t} = \frac{\sqrt{2}\frac{\partial u}{\partial x}}{\sqrt{2}} = \frac{\partial u}{\partial x}$$

Therefore, the shear stress 'τ' is given by:

$$\tau = \mu \frac{\partial \gamma}{\partial t} = \mu \frac{\partial u}{\partial x}$$

For equilibrium condition, the force on one face due to tensile stress σ_x and the shear force on other two faces due to shear stress are as follows,

$$\sigma_x = 2 \times \sqrt{2\tau} \cos 45^0 = 2\tau$$
$$\sigma_x = 2\mu \frac{\partial u}{\partial x}$$

let the fluid element have sides dx, dy and thickness b, then the tensile stress in 'x' direction on the face at distance dx becomes $\sigma_x + \frac{\partial \sigma_x}{\partial x} dx$. This stress acts on the face of body, so the force 'σ_{x2} in the 'x' direction is:

$$S_{x2} = -(\sigma_x)_x bdy + (\sigma_x)_{x+dx} bdy = \left\{ -\sigma_x + \left(\sigma_x + \frac{\partial \sigma_x}{\partial x} \right) \right\} bdy$$

$$= \frac{\partial \sigma_x}{\partial_x} bdxdy = 2\mu \frac{\partial^2 u}{\partial x^2} bdxdy \qquad \ldots\ldots\ldots\ldots \qquad (2.38)$$

Therefore,

$$\left.\begin{aligned} S_x &= S_{x1} + + S_{x2} = \mu \left(\frac{\partial^2 u}{\partial x^2} + \frac{\partial^2 u}{\partial y^2} \right) bdxdy \\ S_y &= \mu \left(\frac{\partial^2 v}{\partial x^2} + \frac{\partial^2 v}{\partial y^2} \right) bdxdy \end{aligned}\right\} \qquad \ldots\ldots\ldots \qquad (2.39)$$

Putting equations (2.34), (2.36) and (2.38) into equation (2.35) , the following equation is obtained.

$$\left.\begin{aligned} \rho \left(\frac{\partial u}{\partial t} + u \frac{\partial u}{\partial x} + v \frac{\partial u}{\partial y} \right) &= \rho X - \frac{\partial p}{\partial x} + \mu \left(\frac{\partial^2 u}{\partial x^2} + \frac{\partial^2 u}{\partial y^2} \right) \\ \rho \left(\frac{\partial v}{\partial t} + u \frac{\partial v}{\partial x} + v \frac{\partial v}{\partial y} \right) &= \rho Y - \frac{\partial p}{\partial y} + \mu \left(\frac{\partial^2 v}{\partial x^2} + \frac{\partial^2 v}{\partial y^2} \right) \end{aligned}\right\}$$

Inertia Term — Body force — Pressure — Viscous

These equations are called the Navier-Stokes equations. In the inertia term, the rates of velocity change with position and, $\left(u \frac{\partial u}{\partial x} + v \frac{\partial u}{\partial y} \right)$ $\left(u \frac{\partial u}{\partial x} + v \frac{\partial u}{\partial y} \right)$ and so are called the convective accelerations.

2.4 Viscous Heating and Energy Equation

A prediction of the temperature rise in the EHL contacts between machine elements is an important contribution to the engineering design process. Apart from this, the temperature rise has a significant influence on the material properties of the lubricant and thus on the performance of the contact.

The full energy equation expressing the law of conservation of energy is :

$$\rho \left[\frac{De}{Dt} + p \frac{D}{Dt} \left(\frac{1}{\rho} \right) \right] = \frac{\partial q}{\partial t} + \emptyset + \nabla . (k \nabla T) - \nabla . \mathrm{q_r} \qquad \ldots\ldots\ldots\ldots \qquad (2.40)$$

where e = specific internal energy per unit mass; $\emptyset$ = viscous dissipation function;

q_r = the radiation heat flux vector; q = internal heat generation; T = temperature;

t = time; p = pressure; k = thermal conductivity

The specific internal energy can be expressed in terms of known quantities and lubricant properties. According to the first law of thermodynamics

$$de = T\,dS - p\,dv \qquad \ldots\ldots\ldots\ldots \quad (2.41)$$

where S is the entropy and ν is specific volume, the entropy may be regarded as a function of the temperature, T , and the pressure, P , so

$$dS = \left(\frac{\partial S}{\partial T}\right)_p dT + \left(\frac{\partial S}{\partial p}\right)_T dp \qquad \ldots\ldots\ldots\ldots \quad (2.42)$$

One of Maxwell's identities states that,

$$\left(\frac{\partial S}{\partial T}\right)_T = -\left(\frac{\partial v}{\partial T}\right)_p \qquad \ldots\ldots\ldots\ldots\ldots \quad (2.43)$$

Therefore, $de = T\left(\frac{\partial S}{\partial T}\right)_p \partial T - T\left(\frac{\partial v}{\partial T}\right)_p dp - pdv$ $\ldots\ldots\ldots\ldots\ldots\ldots$ (2.44)

Thermal expansion coefficient, i.e,

$$C_p = T\left(\frac{\partial S}{\partial T}\right)_p, \varepsilon = \left(\frac{1}{v}\frac{\partial v}{\partial T}\right)_p \qquad \ldots\ldots\ldots\ldots\ldots \quad (2.45)$$

This equation can be written as

$$de = C_p dT - \varepsilon T v dp - pdv = C_p dT - \varepsilon T\left(\frac{1}{\rho}\right)dp - pd\left(\frac{1}{\rho}\right) \qquad \ldots\ldots\ldots\ldots\ldots \quad (2.46)$$

Thus, $$\left[\frac{De}{Dt} + p\frac{D}{Dt}\left(\frac{1}{\rho}\right)\right] = \rho C_p \frac{DT}{Dt} - \varepsilon T \frac{Dp}{Dt} \qquad \ldots\ldots\ldots\ldots\ldots\ldots \quad (2.47)$$

Replacing the left hand side of equation (2.40) with the right hand side of the previous equation gives:

$$\rho C_p \frac{DT}{Dt} - \varepsilon T \frac{Dp}{Dt} = \frac{\partial q}{\partial t} + \emptyset + \nabla.(k\nabla T) - \nabla.q_r \qquad \ldots\ldots\ldots\ldots\ldots\ldots \quad (2.48)$$

$$\rho C_p\left[\frac{\partial T}{\partial t} + v.\nabla T\right] = \frac{\partial q}{\partial t} + \emptyset + \nabla.(k.\nabla T) - \nabla.q_r + \varepsilon T\left[\frac{\partial p}{\partial t} + v.\nabla p\right] \qquad \ldots\ldots\ldots\ldots\ldots\ldots \quad (2.49)$$

The general energy equation can be significantly reduced when applied to a lubricant film such that:

1. Except for viscous heating, no heat is generated in the lubricant (No chemical reactions or radio activity). This cancels the ∂q/∂t term.

2. Within the lubricant radiation can be neglected. Therefore $q_r = 0$
3. For steady state situations all the time derivatives are equal to zero, this being the case when the surfaces of the bodies are considered perfectly smooth.

Due to the specific geometry and flow aspects of the lubricant film, further simplifications can be applied. Since for EHL-contacts the surfaces are almost parallel, the velocity across the film, w, is generally neglected. In concentrated contacts the oil film is very thin, i.e. of the order of 10^{-3} compared to the contact width, so:

$$\frac{\partial}{\partial x}\left(k\frac{\partial T}{\partial x}\right), \frac{\partial}{\partial y}\left(k\frac{\partial T}{\partial y}\right) \ll \frac{\partial}{\partial z}\left(k\frac{\partial T}{\partial z}\right) \qquad \text{(2.50)}$$

Applying these simplifications to equation (2.48), we get:

$$\rho C_p\left[u\frac{\partial T}{\partial x} + v\frac{\partial T}{\partial y}\right] = \emptyset + \frac{\partial}{\partial z}\left(k\frac{\partial T}{\partial z}\right) + \varepsilon T\left[u\frac{\partial p}{\partial x} + v\frac{\partial p}{\partial y}\right] \qquad \text{(2.51)}$$

For line contacts this equation can be reduced even further, since v = 0 and all the derivatives in the y direction are equal to zero:

$$\underbrace{\rho C_p u\frac{\partial T}{\partial x}}_{\text{Convection}} = \underbrace{\emptyset}_{\text{source}} + \underbrace{\frac{\partial}{\partial z}\left(k\frac{\partial T}{\partial z}\right)}_{\text{conduction}} + \underbrace{\varepsilon T u\frac{\partial p}{\partial x}}_{\text{compressive heating}}$$

CHAPTER-3

MATHEMATICAL MODEL OF PISTON SKIRTS LUBRICATION

3.1. Governing Equations of Piston Motion

The equations incorporating piston motion are described in this section. These equations are devised and used by following the approach adapted in the Zhu et al numerical analysis (1991). The analysis of Zhu was related to modeling of piston skirts in mixed lubrication regime. The equations of piston motion used in our analysis are meant for basic modeling of piston skirts in the EHL regime. Hence, some modifications are made by ignoring factors related to possible solid-to-solid contact in modeling mixed lubrication regime by Zhu. Prominent aspects of ignoring such factors are mentioned below:

1. Normal forces due to solid-to-solid contact & moment about piston-pin due to contact pressures are neglected because they are applicable only to the mixed lubrication regime.

2. Friction forces due to solid-to-solid contact & moment about piston-pin due to contact friction are neglected because they are applicable only to the mixed lubrication regime.

A schematic drawing of piston/cylinder system and all the forces & moments acting on the piston are shown in the figure below.

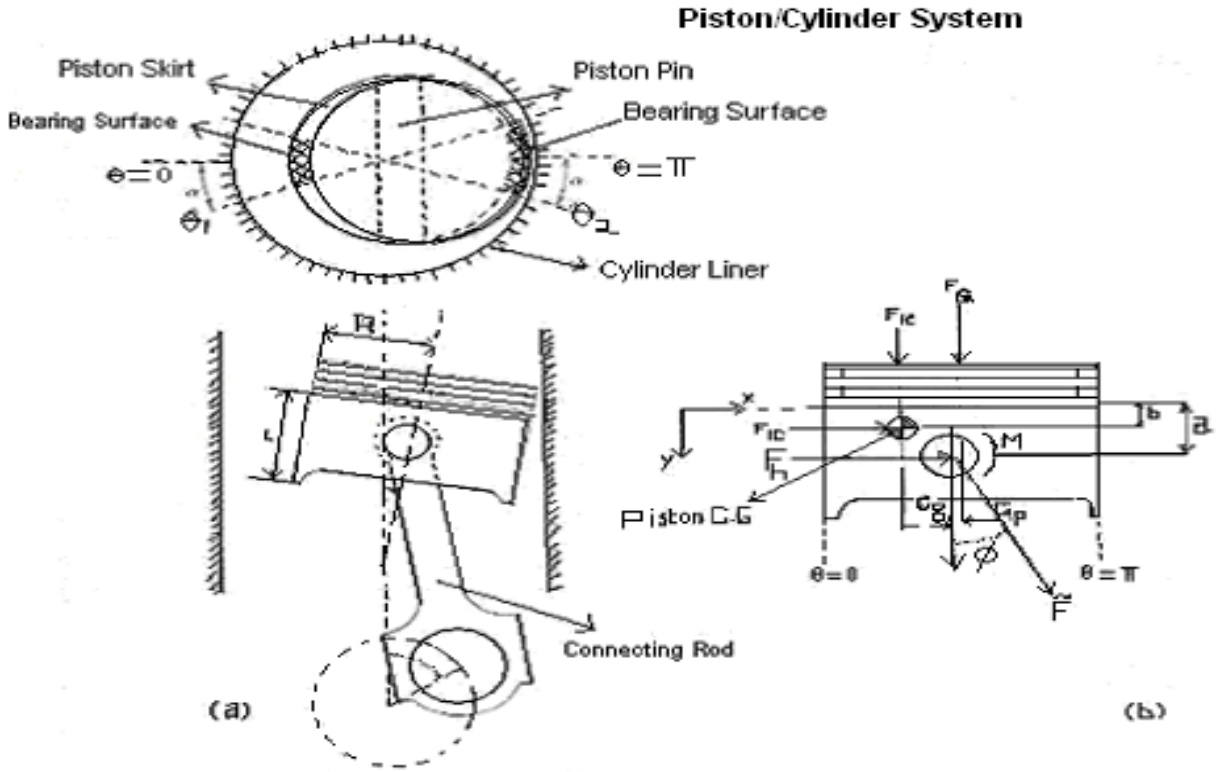

Figure 3.1 : Schematic of the Piston/Cylinder System

Equilibrium of all the forces and moments that are applied on piston are:

$$F_G + F_{fh} + \overline{F}_{IP} + \overline{F}_{IC} + \overline{F}\cos\phi = 0 \qquad \text{……..} \qquad (3.1)$$

$$F_h + F_{IP} + F_{IC} - \overline{F}\sin\phi = 0 \qquad \text{……} \qquad (3.2)$$

$$M_h + M_{IC} + F_{IC}(a-b) - \overline{F}_{IC}C_g + F_G C_P + M_f = 0 \qquad \text{……} \qquad (3.3)$$

where, F_G = Combustion gas force acting on the top of piston

F_{fh} = Friction Force due to hydrodynamic lubricant film

F_{IC} = Inertia Force due to piston mass; F_{IP} = Inertia force due to piston pin mass

F = Total normal force acting on piston skirts; ϕ = Connecting rod angle

C_g = Horizontal distance between piston center of mass and piston pin

C_p = Distance of the piston-pin from the axis of piston

M_f = Moment about piston-pin due to friction force

M_{fh} = Moment about piston-pin due to hydrodynamic friction

a = Vertical distance from the top of piston skirt to the piston-pin

b = Vertical distance from the top of piston skirt to the piston center of gravity

Elimination of connecting rod force from equations (3.1) & (3.2) gives the following force equation:

$$-F_{IP} - F_{1C} = F_s + F_h + F_{fh} \tan\phi \qquad \text{..... (3.4)}$$

The moment equation (3.3) can be rewritten as:

$$-M_{1C} - F_{1C}(a-b) = M_s + M_h + M_{fh} \qquad \text{..... (3.5)}$$

In equations (3.4) & (3.5), F_s and M_s are defined by

$$F_s = \tan\phi(F_G + \overline{F}_{IP} + \overline{F}_{IC}) \qquad \text{..... (3.6)}$$

$$M_s = F_G C_P - \overline{F}_{IC} C_g \qquad \text{..... (3.7)}$$

For constant crankshaft speed 'ω', piston position is given by:

$$Y = \left[(l+r)^2 - (C_p)^2\right]^{0.5} - (l^2 - B^2)^{0.5} - r\cos\psi \qquad \text{..... (3.8)}$$

where, l = Connecting rod length ; r = Crank radius ; ψ = Crank angle

For constant crankshaft speed 'ω', piston speed is given by:

$$V = \dot{Y} = r\omega\sin\psi + r\omega B\cos\psi(l^2 - B^2)^{0.5} \qquad \text{..... (3.9)}$$

For constant crankshaft speed 'ω', piston acceleration is given by:

$$\ddot{Y} = r\omega^2\cos\psi + (r\omega B\cos\psi)^2(l^2 - B^2)^{-1.5} + \left[(r\omega\cos\psi)^2 - r\omega^2 B\sin\psi\right](l^2 - B^2)^{-0.5} \qquad \text{..... (3.10)}$$

where, $B = C_p + r\sin\Psi$ ..... (3.11)

The reciprocating inertia forces can be given by

$$\overline{F}_{IP} = -m_{pin}\ddot{Y} \qquad \ldots\ldots\ldots\ldots\ldots\ldots \qquad (3.12)$$

$$\overline{F}_{IC} = -m_{pis}\ddot{Y} \qquad \ldots\ldots\ldots\ldots\ldots\ldots \qquad (3.13)$$

where, m_{pin} = Mass of piston-pin ; m_{pis} = Mass of piston

R = Radius of Piston ; E_1, E_2 = Young's Moduli ;

The connecting rod angle is calculated by

$$\Phi = \tan^{-1}\left[B(l^2 - B^2)^{-0.5}\right] \qquad \ldots\ldots\ldots\ldots\ldots\ldots \qquad (3.14)$$

The transverse inertia forces and moments depend upon the piston transverse acceleration related to eccentricities of piston at the bottom and top of the skirt respectively:

$$F_{IP} = -m_{pin}\left[\ddot{e}_t + \frac{a}{L}(\ddot{e}_b - \ddot{e}_t)\right] \qquad \ldots\ldots\ldots\ldots\ldots\ldots \qquad (3.15)$$

$$F_{IC} = -m_{pis}\left[\ddot{e}_t + \frac{b}{L}(\ddot{e}_b - \ddot{e}_t)\right] \qquad \ldots\ldots\ldots\ldots\ldots\ldots \qquad (3.16)$$

$$M_{IC} = -I_{pis}\frac{(\ddot{e}_t - \ddot{e}_b)}{L} \qquad \ldots\ldots\ldots\ldots\ldots\ldots \qquad (3.17)$$

where, I_{pis} = Piston rotary inertia about its center of mass; L = Piston skirt length

Substituting equations (3.15), (3.16), and (3.17) into equations (3.4) & (3.5) and simplifying these equations gives two new equations, which are written in matrix form as under:

$$\begin{bmatrix} m_{pin}\left(1-\frac{a}{L}\right)+m_{pis}\left(1-\frac{b}{L}\right) & m_{pin}\frac{a}{L}+mpis\frac{b}{L} \\ \frac{I_{pis}}{L}+m_{pis}(a-b)(1-\frac{b}{L}) & m_{pis}(a-b)\frac{b}{L}-\frac{I_{pis}}{L} \end{bmatrix} \begin{bmatrix} \ddot{e}_t \\ \ddot{e}_b \end{bmatrix} = \begin{bmatrix} F_h + F_s + F_{fh}\tan\Phi \\ M_h + M_s + M_f \end{bmatrix} \qquad (3.18)$$

Calculation of F_h & M_h: In order to calculate normal force due to hydrodynamic pressure in the film 'F_h' and the moment about piston-pin due to hydrodynamic pressure 'M_h',

hydrodynamic pressure distribution is required, which is obtained by solving the 2-D Reynolds equation.

The normal force and moments due to hydrodynamic pressures about piston-pin is calculated by the following expression:

$$F_h = R\int_A \int p_h(\theta, y)\cos\theta d\theta dy \qquad \ldots\ldots\ldots\ldots\ldots\ldots \qquad (3.19)$$

$$M_h = R\int_A \int p_h(\theta, y)(a-y)\cos\theta d\theta dy \qquad \ldots\ldots\ldots\ldots\ldots\ldots \qquad (3.20)$$

where, p_h = Hydrodynamic pressure

Hydrodynamic Friction and Average Shear Stress Factors.

The average shear stress acting on the surface of piston skirt is given as:

$$\tau = \frac{\eta U}{h} + \frac{h}{2}\frac{dp}{dy} \qquad \ldots\ldots\ldots\ldots\ldots\ldots \qquad (3.21)$$

Derivation of Expression for Shear Stress 'τ'

Shear stress is defined as product of dynamic viscosity (η) and shear rate $\left(\frac{du}{dz}\right)$

Hence, $\tau = \eta\frac{du}{dz}$ …… (a)

$$u = \left(\frac{z^2 - zh}{2\eta}\right)\frac{\partial p}{\partial y} + (U_1 + U_2)\frac{z}{h} + U_2 \qquad \ldots\ldots\ldots\ldots\ldots\ldots \qquad (b)$$

where, η = Dynamic viscosity; h = Fluid film thickness;

$\frac{\partial p}{\partial y}$ = Pressure gradient in the 'y' direction.

U_1 = Velocity of top surface (cylinder liner surface); U_2 = Velocity of bottom surface (Piston skirt surface)

Hence, $U_1 = 0$ and $U_2 = U$

Thus velocity equation i.e. equation (b) is given by

$$u = \left(\frac{z^2 - zh}{2\eta} \right) \frac{\partial p}{\partial y} - \frac{Uz}{h} + U \qquad \ldots\ldots\ldots\ldots\ldots\ldots \quad \text{(c)}$$

Differentiating equation (c) w.r.t. 'z' gives shear rate $\frac{du}{dz}$

$$\frac{du}{dz} = \left(z - \frac{h}{2} \right) \frac{1}{2\eta} \frac{dp}{dy} - \frac{U}{h} \qquad \ldots\ldots\ldots\ldots\ldots\ldots\ldots \quad \text{(d)}$$

Put equation (d) in equation (a) to get

$$\tau = \eta \left[\left(z - \frac{h}{2} \right) \frac{1}{\eta} \frac{dp}{dy} - \frac{U}{h} \right] \qquad \ldots\ldots\ldots\ldots\ldots\ldots\ldots \quad \text{(e)}$$

$$\tau = \eta \frac{h}{2} + \frac{h}{2} \frac{dp}{dy}$$

which is the required expression for equation (3.21).

Calculation of F_{fh} & M_{fh} The total hydrodynamic friction force 'F_{fh}' is given by

$$F_{fh} = R \int_A \int \tau(\theta, y) d\theta dy$$

$$F_{fh} = R \int_A \int \left(\eta \frac{U}{h} + \frac{h}{2} \frac{dp}{dy} \right) d\theta dy \qquad \ldots\ldots\ldots\ldots\ldots\ldots \quad (3.22)$$

The moment of total hydrodynamic friction force given by:

$$M_{fh} = R \int_A \int \tau(\theta, y)(R\cos\theta - Cp) d\theta dy$$

$$M_{fh} = R \int_A \int \left(\eta \frac{U}{h} + \frac{h}{2} \frac{dp}{dy} \right) (R\cos\theta - Cp) d\theta dy \qquad \ldots\ldots\ldots\ldots\ldots\ldots \quad (3.23)$$

Calculation of Engine Oil Film Thickness: The engine oil film thickness $\bar{h}$ is one of the inputs. Moreover, film thickness value is also required to determine the shear stress 'τ' to calculate 'F_{fh}' and 'M_{fh}' in equations (3.22) and (3.23) respectively. The piston eccentricity at skirt top (e_t) and that at skirt bottom (e_b) must be incorporated in the expression to determine lubricant film thickness. Since the piston eccentricities, e_t and e_b, are usually much smaller than

the piston skirt length 'L', the lubricant film thickness (without considering bulk elastic deformations of piston skirt) can be given by.

$$\bar{h} = C + e_t(t)\cos\theta + \left[e_b(t) - et(t)\right]\frac{y}{L}\cos\theta \qquad \ldots\ldots\ldots\ldots\ldots\ldots \quad (3.24)$$

where, C = Nominal radial clearance between piston and cylinder bore.

Calculation of Hydrodynamic Pressure (p_h). Hydrodynamic pressures are obtained by solving the Reynolds equation.

$$\frac{\partial}{\partial x}\left(\bar{h}^3\frac{\partial p_h}{\partial x}\right) + \frac{\partial}{\partial y}\left(\bar{h}^3\frac{\partial p_h}{\partial y}\right) = 6\eta U\frac{d\bar{h}}{dy} \qquad \ldots\ldots\ldots\ldots\ldots\ldots \quad (3.25)$$

Pressure obtained from (3.25) will give 'p_h' which will be used in equations (3.19 & 3.20) to determine 'F_h'&'M_h'.

Coefficient of Friction Calculation: The relationship for finding the coefficient of friction is given by:

$$\mu = \frac{Friction\,Force}{Load} = \frac{\int_0^L\int_0^B \tau\, dxdy}{\int_0^L\int_0^B p dxdy} \qquad \ldots\ldots\ldots\ldots\ldots\ldots\ldots \quad (3.26)$$

3.2. Mathematical Relationships Defining Skirts Lubrication

At every time step or crank angle we do the following:

1. We assumed the previous time step, Use this time step as the initial value for the next time step, we can calculate mean lubricant film thickness '$\bar{h}$' with equation (3.24). This '$\bar{h}$'is used to calculate the shear stress as given in equation (3.21) and in equations (3.22) & (3.23). The hydrodynamic pressure *'p_h'* are obtained from the solution of the Reynolds equation.

2. When the velocities $\dot{e}_t, \dot{e}_b$ at the previous time step are obtained we calculate present values for the current time step, the accelerations term in equation (3.18), $\ddot{e}_t, \ddot{e}_b$ are

obtained by numerical differentiation of velocities. When we get the accelerations, we check equation (3.18) is satisfied or not.

3. If equation (3.18) goes beyond our defined tolerance boundary, The method to find $\dot{e}_t, \dot{e}_b$ for the current time step will be aligned and the procedure as above will be repeated.

4. The adjustment of $\dot{e}_t, \dot{e}_b$ is done by using Runge-Kutta technique, which involves calling the solver routine.

If the values of $\dot{e}_t, \dot{e}_b$ obtained are acceptable, the position of the piston at the end of current time step is calculated by:

$$e_t(t_i + \Delta t) = e_t(t_i) + \Delta t \dot{e}_t(t_i)$$

$$e_b(t_i + \Delta t) = e_b(t_i) + \Delta t \dot{e}_b(t_i)$$

6. As the ultimate solution of piston motion is periodic and hence not dependent on initial values so, the above mentioned numerical procedure can start from any piston position.

7. Our initial guess is that, we start from $e_t(0) = e_b(0) = \dot{e}_t(0) = \dot{e}_b(0) = 0$.

The numerical procedure described above was run on matlab to achieve desired results; we see that the solution for piston basic hydrodynamic model converged at the sixth engine cycle.

If we consider a four-stroke engine, one cycle means two crankshaft revolutions. So, the converged periodic solution will always satisfy the following relationships:

$e_t(t) = e_t(t + 4\pi/\omega)$; $e_b(t) = e_b(t + 4\pi/\omega)$; $\dot{e}_t(t) = \dot{e}_t(t + 4\pi/\omega)$; $\dot{e}_b(t) = \dot{e}_b(t + 4\pi/\omega)$

3.3 Modeling Of Non-Newtonian Viscoelastic Aspects

One of the simplest viscoelastic fluid models available is the upper convected Maxwell (UCM) model incorporating a constant viscosity and relaxation time. In this study, we restrict our attention to the UCM constitutive model characterized by the small relaxation time, λ. The continuity, momentum and constitutive equations for the incompressible flow of a non-Newtonian fluids are, respectively,

$$\boldsymbol{\nabla . v = 0}, \quad \ldots\ldots\ldots\ldots\ldots \quad (3.27)$$

$$\boldsymbol{\rho\left(\frac{\partial v}{\partial t} + v.\nabla v\right) = -(\nabla P + \nabla.\tau)}, \quad \ldots\ldots\ldots\ldots\ldots \quad (3.28)$$

$$\boldsymbol{\lambda\dot{\tau} + \tau = -2\eta d}, \quad \ldots\ldots\ldots\ldots\ldots \quad (3.29)$$

where $\boldsymbol{d} = \frac{\mathbf{1}}{\mathbf{2}}(\boldsymbol{\nabla v} + (\boldsymbol{\nabla v})^{\boldsymbol{T}})$

is the rate of deformation tensor, and $\dot{\boldsymbol{\tau}}$ is the upper-convected derivative defined as

$$\dot{\boldsymbol{\tau}} = \frac{\partial \boldsymbol{T}}{\partial \boldsymbol{t}} + \boldsymbol{v}.\boldsymbol{\nabla\tau} - (\boldsymbol{\nabla v}).\boldsymbol{\tau} - \boldsymbol{\tau}.(\boldsymbol{\nabla v})^{\boldsymbol{T}}. \quad \ldots\ldots\ldots\ldots \quad (3.30)$$

In these equations, ρ is the constant lubricant density, v is the lubricant velocity vector, p is the pressure, τ, is the extra-stress tensor, λ is the fluid relaxation time, and η is the lubricant viscosity. In general, λ and η are functions of the local shear rate, pressure and temperature. In this paper they are taken to be constant. In this problem, the fluid may be assumed to incompressible and inertia less, and gravitational effects can be ignored. The continuity and momentum equations for steady flow can be rewritten in component form as

$$\frac{\partial u}{\partial x} + \frac{\partial v}{\partial y} = 0 \quad \ldots\ldots\ldots\ldots\ldots \quad (3.31)$$

$$\frac{\partial \tau_{xx}}{\partial x} + \frac{\partial \tau_{xy}}{\partial y} + \frac{\partial P}{\partial x} = 0 \quad \ldots\ldots\ldots\ldots\ldots\ldots \quad (3.32)$$

$$\varepsilon\left(\frac{\partial \tau_{xy}}{\partial x} + \frac{\partial \tau_{yy}}{\partial y}\right) + \frac{\partial P}{\partial y} = 0 \quad \ldots\ldots\ldots\ldots\ldots\ldots \quad (3.33)$$

$$\tau_{xx} + De\left(u\frac{\partial \tau_{xx}}{\partial x} + v\frac{\partial \tau_{xx}}{\partial y} - 2\frac{\partial u}{\partial y}\tau_{xy} - 2\frac{\partial u}{\partial x}\tau_{xx}\right) = -2\varepsilon\frac{\partial u}{\partial x} \quad \ldots\ldots\ldots\ldots\ldots\ldots \quad (3.34)$$

$$\tau_{xy} + De\left(u\frac{\partial \tau_{xy}}{\partial x} + v\frac{\partial \tau_{xy}}{\partial y} - \frac{\partial v}{\partial x}\tau_{xx} - \frac{\partial u}{\partial y}\tau_{yy}\right) = -\left(\frac{\partial u}{\partial y} + \varepsilon\frac{\partial v}{\partial y}\right) \quad \ldots\ldots\ldots\ldots\ldots\ldots \quad (3.35)$$

$$\tau_{yy} + De\left(u\frac{\partial \tau_{yy}}{\partial x} + v\frac{\partial \tau_{yy}}{\partial y} - 2\frac{\partial v}{\partial y}\tau_{yy} - 2\frac{\partial v}{\partial x}\tau_{xy}\right) = -2\frac{\partial v}{\partial x} \quad \ldots\ldots\ldots\ldots\ldots\ldots \quad (3.36)$$

The velocity boundary conditions are:

u=U,v=0, when y=0;

u=0,v=0, when y=h(x);

the pressure boundary conditions are

$P = P_a$, at x=0 and x=L.

Thus, the pressure at the ends of the gap reduces to that of a stationery fluid at ambient pressure P_a . In fact, there has been a long-standing controversy in the literature on lubrication as to the best end-pressure boundary conditions, as the choice of these conditions can significantly affect the prediction for a non-Newtonian model , A discussion of the pressure boundary conditions at the inlet and the exit can be found in[19],

The concept of the Deborah number highlights that it is not only the material's relaxation time, $\boldsymbol{\lambda}$, which determines material behavior, but also the time scale of the deformation process. The Deborah number is zero for a Newtonian fluid and infinite for a Hookean elastic solid [20]. Substituting the dimensionless variables and dropping the asterisks, we obtain the dimensionless governing equations

CHAPTER-4

NON-DIMENSIONALISATION & NUMERICAL PROCEDURE

4.1. Non-Dimensionalization Of The Reynolds Equation.

The Reynolds equation consists of Pressure 'p', Film thickness 'h', Entraining velocity 'U' and Dynamic viscosity 'η'. Non-Dimensionlization of the Reynolds equation forms involves following non dimensional variables:

$$\left.\begin{aligned} h^* &= \frac{h}{c} & x^* &= \frac{x}{R} \\ y^* &= \frac{y}{L} & p^* &= \frac{pc^2}{6U\eta R} \end{aligned}\right\} \qquad \ldots\ldots\ldots\ldots\ldots\ldots \quad (4.1)$$

where, h = the hydrodynamic film thickness [m]; c = the piston radial clearance [m]

R = Piston radius [m]; L = the piston axial length [m]; p = the hydrodynamic pressure [Pa]

U = the piston entraining velocity [m/s], i.e. U = (U1+U2)/2;

η = the dynamic viscosity of the piston [Pas]; x, y = the hydrodynamic film co-ordinates [m]

Reynolds equation in non-dimensional form is given by:

$$\frac{\partial}{\partial x^*}\left(h^{*3}\frac{\partial p^*}{\partial x^*}\right)+\left(\frac{R}{L}\right)^2\frac{\partial}{\partial y^*}\left(h^{*3}\frac{\partial p^*}{\partial y^*}\right)=\frac{\partial h^*}{\partial x^*} \qquad \ldots\ldots\ldots\ldots\ldots \quad (4.2)$$

4.2 Finite Difference Scheme, Solution Domain & Boundary Conditions

Piston lubrication problem is solved by using the 'finite difference' technique. This technique is based on approximating a differential quantity by the difference between two or

more adjacent nodes. For example, finite difference approximation of 'M_v'w.r.t. 'x' at 'i' node is given by:

$$\left(\frac{\partial M_v}{\partial x^*}\right) = \frac{M_{v,i+1} - M_{v,i-1}}{2\delta x^*} \qquad \ldots\ldots\ldots\ldots\ldots\ldots \quad (4.3)$$

Subscripts i-1 and i+1 denote positions immediately before and after the central position 'i' and 'δx*' is the step length between nodes. A similar expression results for second differential $\partial^2 M_v$. This expression is found according to the principle for the derivation of the finite difference approximation of the second derivative of a function as illustrated in figure 4.1 shown below.

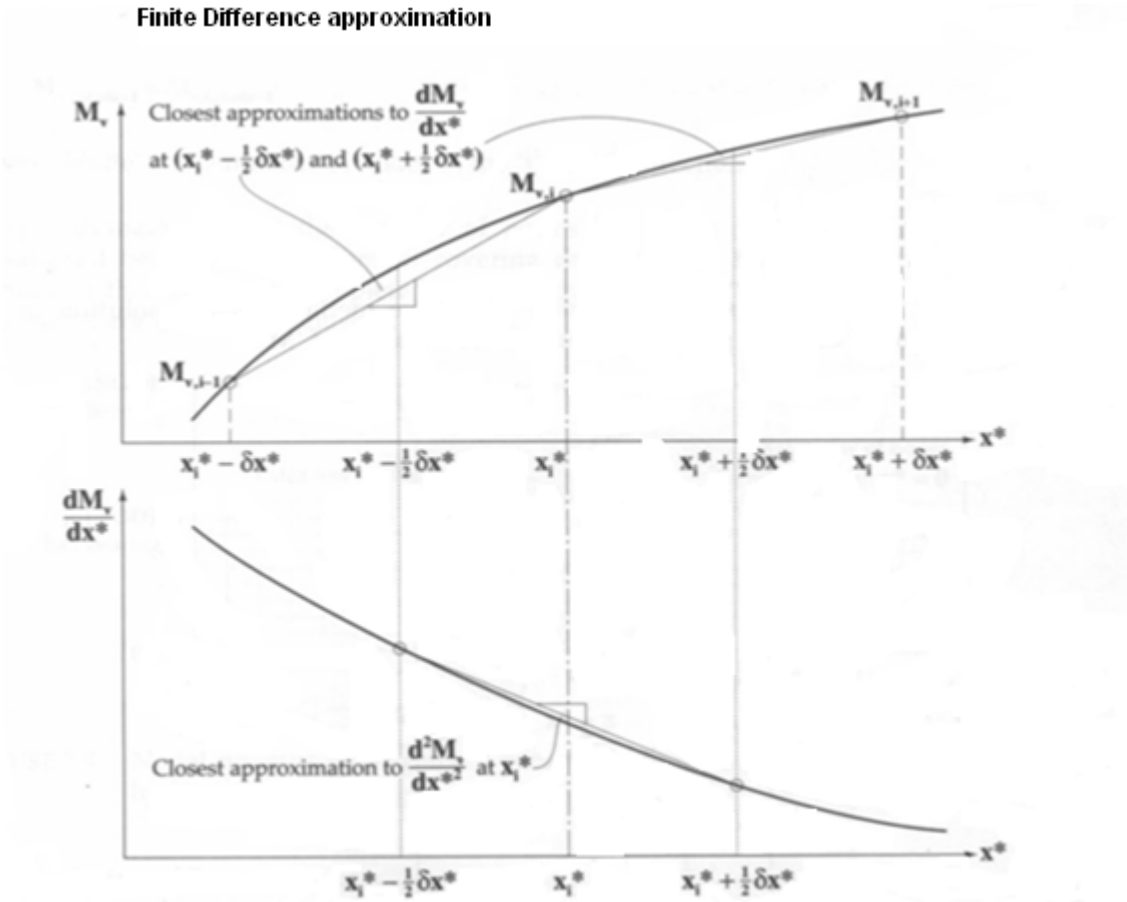

Fig 4.1 Illustration of the principle for the derivation of the finite difference approximation of the second derivative of a function. **[22]**

The second differential term $\partial^2 M_v/\partial x^{*2}$ is found by subtracting the expression of $\partial M_v/\partial x^*$, at the i-0.5 nodal position from the i+0.5 nodal position and dividing by δx*, i.e.

$$\left(\frac{\partial^2 M_v}{\partial x^{*2}}\right)_i = \frac{\left(\frac{\partial M_v}{\partial x^*}\right)_{i+0.5} - \left(\frac{\partial M_v}{\partial x^*}\right)_{i-0.5}}{\delta x^*} \qquad \ldots\ldots\ldots\ldots\ldots \qquad (4.4)$$

where;

$$\left(\frac{\partial M_v}{\partial x^*}\right)_{i+0.5} \approx \frac{M_{v,i+1} - M_{v,i}}{\delta x^*}$$

$$\left(\frac{\partial M_v}{\partial x^*}\right)_{i-0.5} \approx \frac{M_{v,i} - M_{v,i-1}}{\delta x^*}$$

The finite difference equivalent of ($\partial^2 M_v / \partial x^{*2} + \partial^2 M_v / \partial y^{*2}$) is found by considering the nodal variation of 'M_v' in two axes, i.e. the 'x' and 'y' axes. A second nodal position variable is introduced in the 'y' axis. The expressions for '$\partial M_v / \partial y^*$' and '$\partial^2 M_v / \partial y^{*2}$' are exactly the same as the expressions for the 'x' axis but with 'i' substituted by 'j'. The coefficients of 'M_v' at the 'i'-th node and adjacent nodes required by the Reynolds equation which form a 'finite difference operator' are illustrated as a 'computing molecule' as shown in figure below.

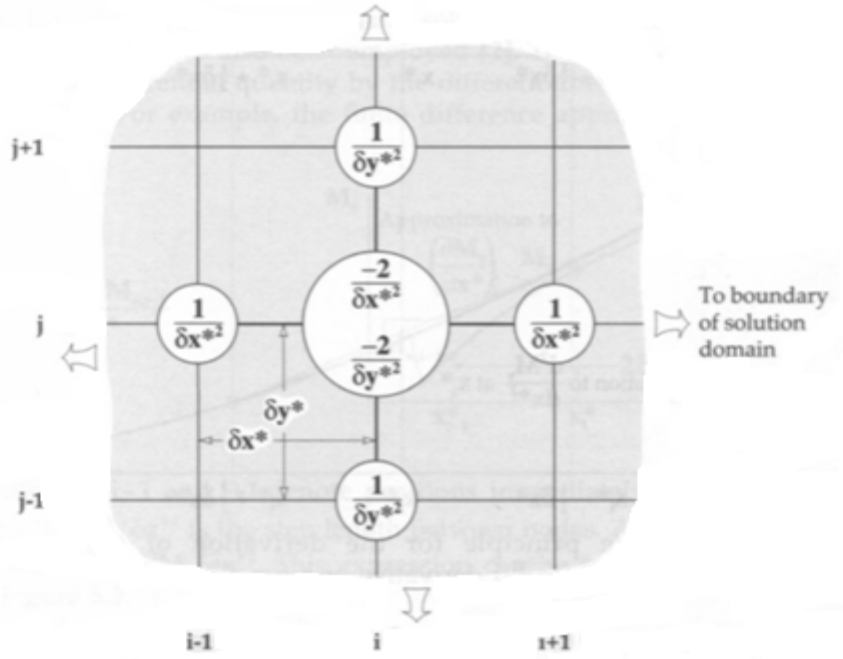

Figure 4.2 Finite difference operator and nodal scheme for numerical analysis of the Reynolds equation. **[22]**

The finite difference method is easy; less computation time is required and does not create problems while applying boundary conditions. When the finite difference operator is located at the boundary of a solution domain, special arrangements may be required with imaginary nodes outside of a boundary. In our case the solution domain is the range over which our solution is applicable. The terms 'F' and 'G' can be included with the finite difference operator to form a complete equivalent of the Reynolds equation. The equation is then rearranged to provide an expression for '$M_{v,\,i,\,j}$' i.e.:

$$M_{v,i,j} = \frac{C_1\left(M_{v,i+1,j} + M_{v,i-l,j}\right) + \left(\frac{R}{L}\right)^2 C_2\left(M_{v,i,j+l} + M_{v,i,j-i}\right) - G_{i.j}}{2C_1 + 2C_2 + F_{i,j}} \qquad \ldots\ldots\ldots\ldots \quad (4.5)$$

where, $C_1 = \frac{1}{\delta x^{*2}}$; $C_2 = \frac{1}{\delta y^{*2}}$

Solution Domain & Boundary Conditions.

We define the boundary conditions and the ranges of values to be computed after establishing the controlling equation. For piston skirts lubrication model, the boundary conditions require that 'p^*' or 'M_v' are zero at the edges of piston skirt surface and the cavitations can occur to prevent negative pressures occurring on these surfaces. The range of 'x^*' is between 0-75^o. The range of 'y^*' is from -0.5 to +0.5, if the mid-line of piston skirt surface is selected as a datum. A domain of the piston skirts where symmetry can be exploited to cover either half of the skirt area, i.e., from y* = 0 to y* = 0.5, or the whole piston skirt area is shown in figure below.

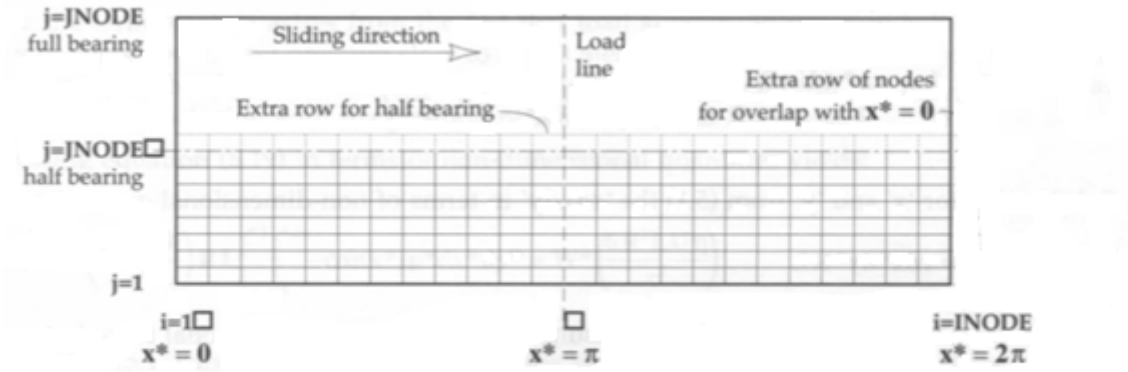

Figure 4.3 Nodal pressure or Vogelpohl parameter domains for finite difference analysis of hydrodynamic bearings. **[22]**

4.3 Calculation of Film Thickness Friction Force & Friction Coefficient.

After finding the pressure field, we calculate the friction force and friction coefficient from the film thickness. We know that the frictional force operating across the hydrodynamic film is calculated by integrating the shear stress 'τ' over the piston skirts area i.e.:

$$F = \int_0^L \int_0^{2\pi R} \tau dx dy \qquad \ldots\ldots\ldots\ldots\ldots\ldots \qquad (4.6)$$

where, the shear stress 'τ'is given by:

$$\tau = \frac{\eta U}{h} + \frac{h}{2}\frac{dp}{dx} \qquad \ldots\ldots\ldots\ldots\ldots\ldots \qquad (4.7)$$

where, τ is the shear stress [Pa]; η is the dynamic viscosity of the lubricant [Pas];

U is the entraining velocity [m/s]; h is the hydrodynamic film thickness [m];

p the hydrodynamic pressure [Pa]; F is the friction force [N]

x the distance in the direction of sliding [m]; y is the distance normal to the direction of sliding [m]

Friction force can be expressed in terms of non-dimensional quantities. From equation (4.1)

h = h***c,** **x = x***R and p = p* ($6U\eta R / c^2$);

Substituting these into (4.7) yields:

$$\tau = \frac{\eta U}{c}\frac{1}{h^*}\frac{ch^*}{2}\frac{6U\eta R}{c^2}\frac{1}{R}\frac{dp^*}{dx^*} = \left(\frac{U\eta}{c}\right)\left(\frac{1}{h^*} + 3h^*\frac{dp^*}{dx^*}\right) \quad \ldots\ldots\ldots\ldots \quad (4.8)$$

Substituting for 'x' and 'y' from equation (4.1) the 'τdxdy' in terms of non- dimensional quantities is:

$$\tau dxdy = \tau dx^* dy^* RL \quad \ldots\ldots\ldots\ldots \quad (4.9)$$

Substituting (4.7) and (4.8) into (4.9) results in an expression for frictional force in terms of dimensional quantities:

$$F = \frac{RL\eta U}{c}\int_0^1\int_0^{2\pi}\left(\frac{1}{h^*} + 3h^*\frac{dp^*}{dx^*}\right)dx^* dy^* \quad \ldots\ldots\ldots\ldots \quad (4.10)$$

It can be seen from equation (4.10) that the non-dimensional shear stress 'τ^*' is expressed as:

$$\tau^* = \frac{1}{h^*} + 3h^*\frac{dp^*}{dx^*} \quad \ldots\ldots\ldots\ldots \quad (4.11)$$

Equation (4.10) can be re-written in the following form:

$$F = \frac{RL\eta U}{c}\int_0^1\int_0^{2\pi}\tau^* dx^* dy^* = F^*\left(\frac{RL\eta U}{c}\right) \quad \ldots\ldots\ldots\ldots \quad (4.12)$$

The coefficient of friction is obtained by dividing the friction force by the axial load. A similar quantity is also found when the dimensionless friction is divided by the dimensionless load.

$$\mu = \frac{F}{W} = \frac{\int_0^L\int_0^{2\pi R}\tau dxdy}{\int_0^L\int_0^{2\pi R} p dxdy} \quad \ldots\ldots\ldots\ldots \quad (4.13)$$

where, μ is the coefficient of friction & W is the bearing load [N].

Load on the piston is expressed as:

$$W = \int_0^L \int_0^{2\pi R} -\cos(x^*)\, p\, dx\, dy \qquad \ldots\ldots\ldots\ldots\ldots\ (4.14)$$

where the term –cos(x*) arises from the fact that load supporting pressure is located near to x*=π or cos(x*)= -1.

Any pressure close to x* = 0 merely imposes an extra load on the piston since it acts in the direction of the load. The negative sign tells the fact that the load vector does not coincide with the position of maximum film thickness.

Expressing Equation (4.14) in the terms of non-dimensional quantities yields:

$$W = \left(\frac{6U\eta R}{c^2}\right) RL \int_0^l \int_0^{2\pi} -\cos(x^*)\, p^*\, dx^*\, dy^* = W^* \left(\frac{6R^2 LU\eta}{c^2}\right) \qquad \ldots\ldots\ldots \qquad (4.15)$$

Hence the expression for coefficient of friction is given as:

$$\mu = \frac{F}{W} = \frac{\left(\frac{RL\eta U}{c}\right)}{\left(\frac{6R^2 LU\eta}{c^2}\right)} \frac{F^*}{W^*} = \left(\frac{c}{6R}\right)\left(\frac{F^*}{W^*}\right) \qquad \ldots\ldots\ldots\ldots\ldots\ (4.16)$$

hence,
$$\frac{F^*}{W^*} = \left(\frac{6R}{c}\right)\mu \qquad \ldots\ldots\ldots\ldots\ldots\ (4.17)$$

Film Thickness For Piston Skirts & Its Derivatives.

Dimensionless film thickness equation is given by:

$$\bar{h}^* = E_t(t)\cos x^* + \left[E_b(t) - E_t(t)\right] y^* \cos x^* + 1 \qquad \ldots\ldots\ldots\ldots\ldots\ (4.18)$$

Where, E_t = Eccentricity ratio of skirt at the top = e_t/C; E_b = Eccentricity ratio of skirt at the bottom = e_b/C

The derivatives of 'h^*' are found by direct differentiation of equation (4.18), i.e.,

$$\frac{d\bar{h}^*}{dx^*} = -E_t(t)\sin x^* - \left[E_b(t) - E_t(t)\right] y^* \sin x^* \qquad \ldots\ldots\ldots \qquad (4.19)$$

$$\frac{d\bar{h}^*}{dy^*} = \left[E_b(t) - E_t(t)\right]^* \cos x^* \qquad \ldots\ldots\ldots\ldots \qquad (4.20)$$

$$\frac{d^2\bar{h}^*}{dx^{2*}} = -E_t(t)\cos x^* - \left[E_b(t) - E_t(t)\right] y^* \cos x^* \qquad \ldots\ldots\ldots\ldots \qquad (4.21)$$

4.4 Numerical Procedure for EHL of Piston Skirts & Inverse Solution Technique

The processes that have been used to obtain the EHD results of suggested dimensionless model are as follows:

1. Reynolds equation is integrated to give the pressure distribution.
2. The inverse solution of the Reynolds equation, which gives a specified pressure distribution.
3. The calculation of surface deformations.

The Inverse Solution Of The Reynolds Equation.

At the outer end of the pressure profile the pressure gradient is negative and there is no change in film thickness in the direction of sliding of piston. At the inlet where the film is convergent the change in film thickness is not equal to zero. At that instant the change in pressure profiles is the product of piston speed and viscosity of the lubricant divided by square of Film thickness. Thus for known speed and viscosity the film thickness at the point, where second order pressures are obtained whose difference is equal to zero, can be found for given pressure curve. We call all these points (transient case) as respective 'a' points at particular instants. Once film thickness 'h_a' is found from the above-mentioned relationship between pressure gradient and piston speed, oil viscosity & lubricant film thickness, the entire film shape corresponding to the given pressure curve can be calculated from the integrated form of the Reynolds equation. When this relationship is substituted into two-dimensional transient Reynolds equation we get the value of film thickness *'h_m'* which is 1.5 times the value of film thickness at instantaneous points 'a' respectively.

At other points *'h'* can be found by solving the cubic equation in *'h'* obtained by rearranging Reynolds equation. The resultant cubic equation is given by

$$K\overline{h}^{3} + \overline{h} - 1 = 0$$

where, $K = \frac{h_m^{\,2}}{12\eta u}\frac{dp}{dx}$ and $\overline{h} = \frac{h}{h_m}$

At any point on the instantaneous inlet pressure sweep up to the maximum pressure *'K'* is positive and above cubic equation presents one negative and two positive roots where positive roots coincide at point *'a'*. Between the maximum pressure and outlet, *'K'* is negative. In this region cubic equation has only one real root, which is positive and gives the required film thickness. The only tricky feature of this inverse solution is the location of respective instantaneous points on the transient inlet side where the condition of having second order pressure differentials equal to zero is met. Numerically this involves finding the zero of the second differences of a list of instantaneous pressures at each time step. This extensive iterative repetitions at each time step in order to arrive at desired pressure difference values. Computation work involves repeated smoothing of achieved pressure values in the last repetitive cycle and their first differences to be used for next iterative cycle until the desirable pressures and their first differences facilitate the accurate location of respective instantaneous point in each time step.

4.5 EHL Film Solution Involving Non-Newtonian Lubricant Rheology

Upper convected Maxwell model is used by incorporating constant density, viscosity and a small fluid relaxation time. The continuity, momentum and constitutive equations for the incompressible non Newtonian fluid flow are solved by using a regular perturbation method. Specifically, we assume an asymptotic solution in the form of a double perturbation expansion in powers of ε and De.

The leading term in the conventional lubrication solution is denoted by [ℓ] while the two perturbation corrections are denoted by [ε] and [De].

The leading term of Partial derivative of pressure is obtained from the simple Reynolds equation.

$$\frac{\partial}{\partial x}\left(\overline{h^3}\frac{\partial p_h}{\partial x}\right)+\frac{\partial}{\partial y}\left(\overline{h^3}\frac{\partial p_h}{\partial y}\right)=6\eta U\frac{d\bar{h}}{dy} \qquad \text{……..} \qquad (4.22)$$

The correction term of the pressure is obtained by taking double derivative of leading term of velocities [31].

$$\frac{\partial \mathrm{P}^{(\varepsilon)}}{\partial \mathrm{x}}=2\frac{\partial^2 \mathrm{U}^{(\ell)}}{\partial \mathrm{x}^2}+\frac{\partial^2 \mathrm{U}^{(\ell)}}{\partial \mathrm{y}^2} \qquad \text{……} \qquad (4.23)$$

which gives

$$\frac{\partial \mathrm{P}^{(\varepsilon)}}{\partial \mathrm{x}}=12\left(\frac{\mathrm{h}^3-\mathrm{h_m}}{\mathrm{h}^3}\right)+2\left(\frac{3\mathrm{h_m}}{\mathrm{h}^3}+\frac{2}{\mathrm{h}^2}\right)\frac{\mathrm{dh}}{\mathrm{dx}} \qquad \text{……} \qquad (4.24)$$

For the Deborah term of pressure, modified Reynolds equation is solved [1], which gives,

$$\frac{\partial \mathrm{P}^{(\mathrm{De})}}{\partial \mathrm{x}}=-18\frac{{\mathrm{h_m}}^2}{\mathrm{h}^5}\frac{\mathrm{dh}}{\mathrm{dx}}+18\frac{\mathrm{h_m}}{\mathrm{h}^4}\frac{\mathrm{dh}}{\mathrm{dx}}-\frac{4}{\mathrm{h}^3}\frac{\mathrm{dh}}{\mathrm{dx}}-12\frac{\mathrm{h_d}}{\mathrm{h}^3} \qquad \text{……} \qquad (4.25)$$

where

$$h_d=\left\{\frac{\frac{3}{8}\left(\frac{h_m{}^2}{h_1{}^4}-\frac{h_2{}^2}{h_0{}^4}\right)-\frac{1}{2}\left(\frac{\mathrm{h_m}}{\mathrm{h_1}^3}-\frac{\mathrm{h_m}}{\mathrm{h_0}^3}\right)+\frac{1}{6}\left(\frac{1}{\mathrm{h_1}^2}-\frac{1}{\mathrm{h_0}^2}\right)}{\int_0^1\frac{1}{\overline{h^3(x)}}dx}\right\} \qquad \text{……..} \qquad (4.26)$$

Now total $\frac{\mathrm{dp}}{\mathrm{dx}}$ is calculated using asymptotic solutions.

$$\frac{\mathrm{dp}}{\mathrm{dx}}=\frac{\partial \mathrm{P}^{(\ell)}}{\partial \mathrm{x}}+\frac{\partial \mathrm{P}^{(\varepsilon)}}{\partial \mathrm{x}}+\frac{\partial \mathrm{P}^{(\mathrm{De})}}{\partial \mathrm{x}} \qquad \text{……} \qquad (4.27)$$

The resulting expression will be used in the calculation of shear stress, which will further give hydrodynamic friction force.

CHAPTER 5

SIMULATION RESULTS & ANALYSIS OF NON-NEWTONIAN (VISCOELASTIC) ELASTOHYDRODYNAMIC LUBRICATION OF PISTON SKIRTS IN THE INITIAL ENGINE START UP

5.1 Results & Analysis of Viscoelastic Piston Skirts EHL Model

5.1.1 Hydrodynamic Film Thickness

Refer to Figures: 5.1, in the non-Newtonian viscoelastic isothermal regime, maximum and minimum hydrodynamic film thickness profiles as a function of 720 degree crank rotation are plotted to represent film thickness magnitudes against corresponding piston positions for the four engine strokes. Film thicknesses remain very less in the initial 90 degree of crank rotation in induction stroke. The general trend is the gradual rise, subsequent fall (in the power stroke). It implies that there is less shearing and reduced frictional losses when hydrodynamic film thickness is minimum. It is only when the film thickness starts increasing significantly that there is corresponding increase in frictional losses as more shear stresses are generated. When observing it in the context of 720 degree crank rotation then it can safely be assumed that despite minimum film thickness up to 90 degree crank rotation, there are less frictional losses and energy dissipation due to reduced shear heating and hence less viscosity drop leading to better hydrodynamic load carrying capabilities under theses specified conditions.

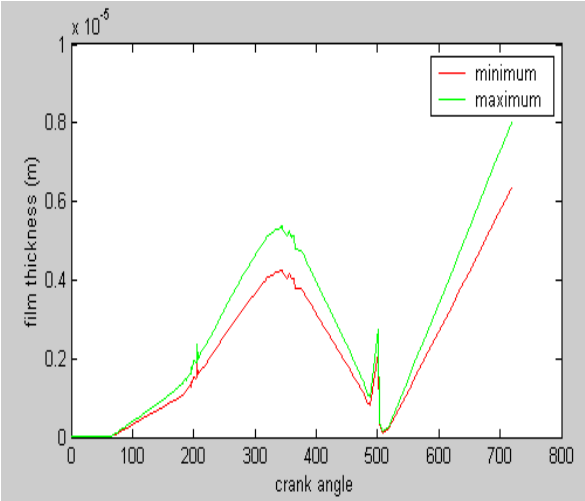

Fig.5.1: Film Thickness profiles vs crank angle

5.1.2 Hydrodynamic Pressure Fields

Refer to figures 5.2(a), 5.2(b) and 5.2(c), which show pressure fields over the skirts surface in the induction/intake piston stroke at 60, 120 and 180 degree crank rotation respectively. Positive pressures generate from mid to the skirt top surface. The slope is gentle till the mid-stroke after it starts getting steep, peak pressures shift towards right and all this happens with increasing film thickness. It implies that an increase in frictional losses and more

shear stress generation could shift hydrodynamic peak pressures along with an increase in steepness of profile slopes.

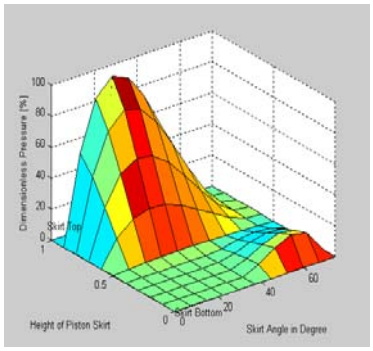

Fig 5.2(a) Pressure profiles at 60 deg

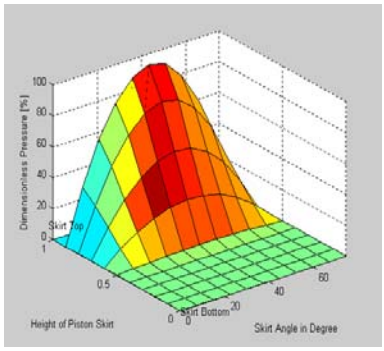

Fig 5.2(b) Pressure profiles at 120 deg

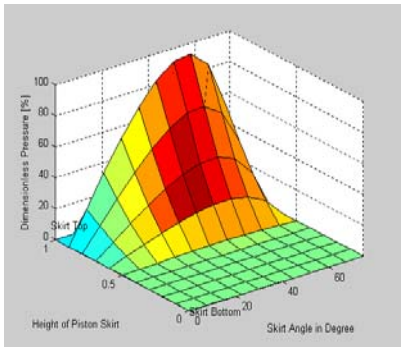

Fig 5.2(c) Pressure profiles at 180 deg

Refer to figures 5.3(a), 5.3(b) and 5.3(c), which show pressure fields over the skirts surface in the compression piston stroke at 240, 300 and 360 degree crank rotation respectively. Positive pressures generate from mid to the skirt top surface till 240 degree angle. The slope gets steeper till one-third of the compression stroke after which positive pressures start shifting towards skirts bottom and all this happens with further rise in the film thickness. It implies that increase in frictional losses and more shear stress generation shift hydrodynamic pressure fields towards skirts bottom along slight increase in steepness of profile slopes.

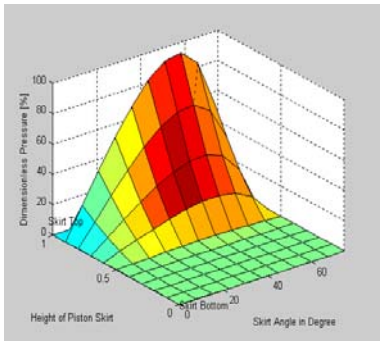

Fig 5.3(a) Pressure profiles at 240 deg

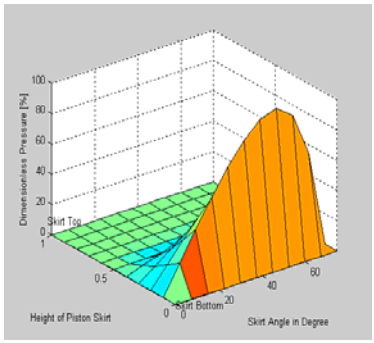

Fig 5.3(b) Pressure profiles at 300 deg

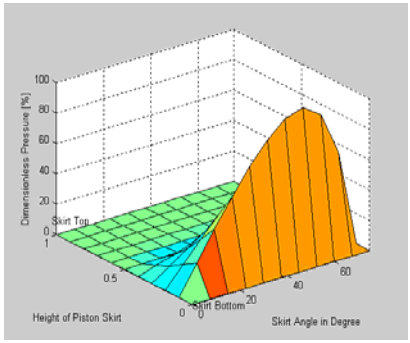

Fig 5.3(c) Pressure profiles at 360 deg

Refer to figures 5.4(a), 5.4(b) and 5.4(c), which show pressure fields over the skirts surface in the power/expansion stroke of piston at 420, 480 and 540 degree crank rotation respectively. Positive pressures generate from mid to the skirt bottom surface till 540 degree angle. The slope gets steep till one-third of the stroke after which positive pressures slightly shift in the mid values over the skirts bottom and all this happens with further rise in the film thickness, coefficient of friction and shear stress. It implies that further increase in frictional losses and more shear stress generation with instantaneous reduction and then rise in film thickness keep hydrodynamic pressure fields at the skirts bottom along slight increase in steepness of profile slopes.

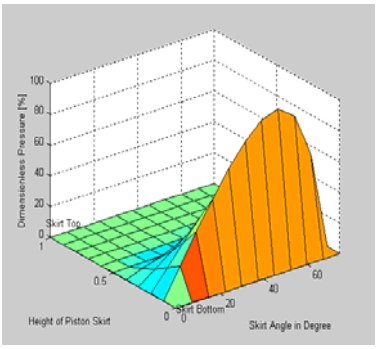

Fig 5.4(a) Pressure profiles at 420 deg

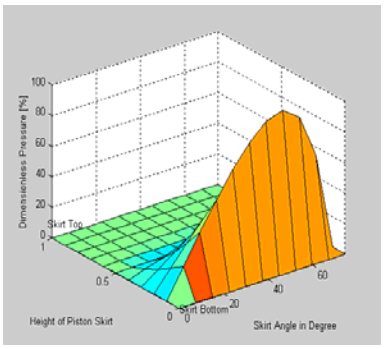

Fig 5.4(b) Pressure profiles at 480 deg

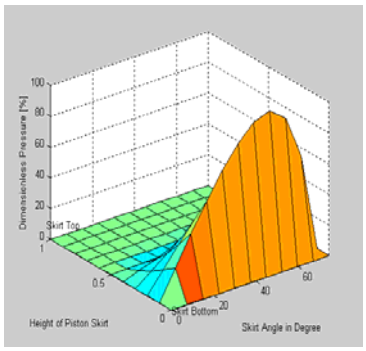

Fig 5.4(c) Pressure profiles at 540 deg

Refer to figures 5.5(a), 5.5(b) and 5.5(c), which show pressure fields over the skirts surface in the exhaust stroke of piston at 600, 660 and 720 degree crank rotation respectively. Positive pressures generate from mid to the skirt bottom surface till 540 degree angle. The slope gets further steep till mid of the stroke after which positive pressures slightly shift in the mid values over the skirts bottom and all this happens with further rise in the film thickness. It implies that a further increase in frictional losses and more shear stress generation with instantaneous reduction and then rise in film thickness keep hydrodynamic pressure fields at the skirts bottom along with slight increase in steepness of profile slopes.

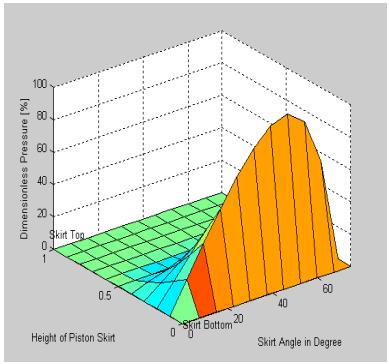

Fig 5.5(a) Pressure profiles at 600 deg

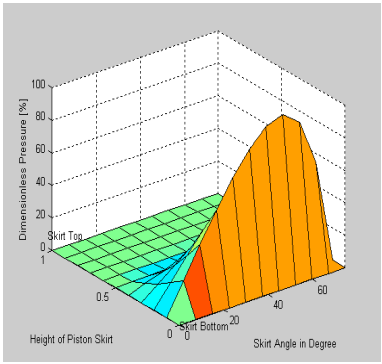

Fig 5.5(b) Pressure profiles at 660 deg

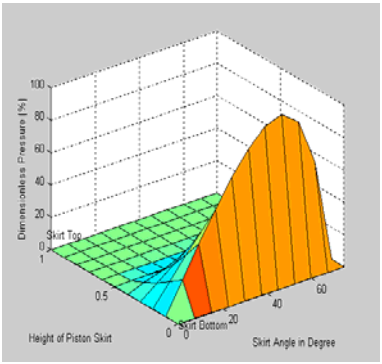

Fig 5.5(c) Pressure profiles at 720 deg

5.1.3 Piston Secondary Motion & Eccentricities

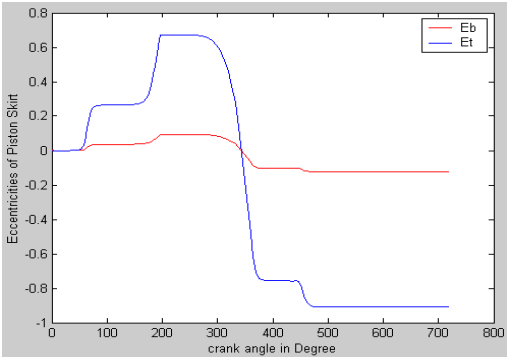

Fig 5.6 Eccentricities of Piston Vs Crank angle

Refer to Figure 5.6 'E_t' & 'E_b' are negligible from the start to the mid of intake stroke, then shifts toward minor thrust side although are safely away from the upper horizontal line. During

the piston compression stroke both piston eccentricities curves remain on the minor thrust side and move closer to the upper horizontal line. 'E_t' & 'E_b' curves shift towards the center line and cross it at the end of compression stroke.

During the expansion stroke of piston the piston 'E_t' curve goes close to the lower horizontal line during piston travel from mid point to BDC but there is no solid-to- solid contact till the end of expansion stroke. In the exhaust stroke the values of 'E_t' & 'E_b' remain the same as the previous stroke.

5.2 Comparative Analysis of Newtonian & Viscoelastic Models

Newtonian model

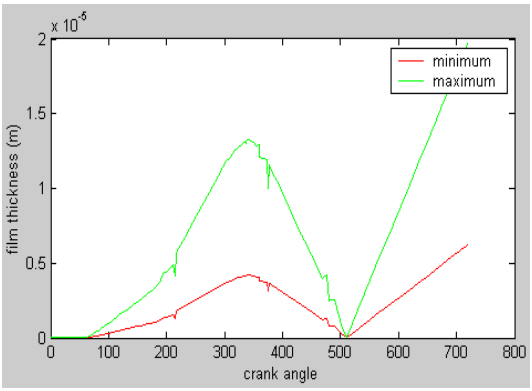

Fig 5.7(a) Hydrodynamic Film Thickness Vs Crank angle

Viscoelastic non-Newtonian model

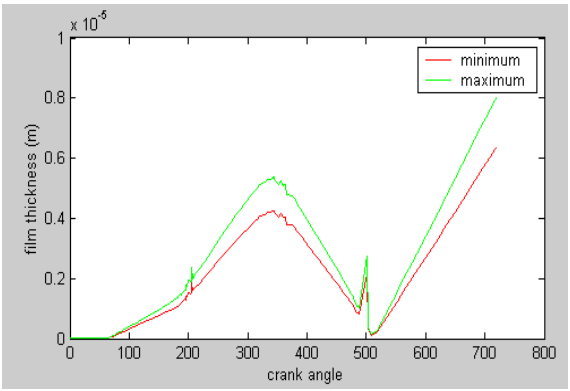

Fig 5.7(b) Hydrodynamic Film Thickness Vs Crank angle

In the Fig 5.7(a) & Fig 5.7(b) non-Newtonian viscoelastic isothermal Film Thicknesses are compared with Newtonian isothermal Film Thicknesses, maximum and minimum hydrodynamic film thickness profiles as a function of 720 degree crank rotation are plotted to represent film thickness magnitudes against corresponding piston positions for the four engine strokes. The sudden rise and fall of film thickness value indicates that at that particular point of time there is sudden corresponding drop in the EHD pressures, which is restored again after that brief interval. It is clearly seen from the plots that the maximum Film thickness in the viscoelastic model has decreased compared to that of Newtonian model, which when related to the values of Shear Stress and Coefficient of Friction shows that Shear Stress and Coefficient of Friction has also decreased. It implies that there is lesser shearing and reduced frictional losses when viscoelasticity has been incorporated and hence the maximum value of Film Thickness has reduced which shows drop in viscosity which leads to better load carrying capacity.

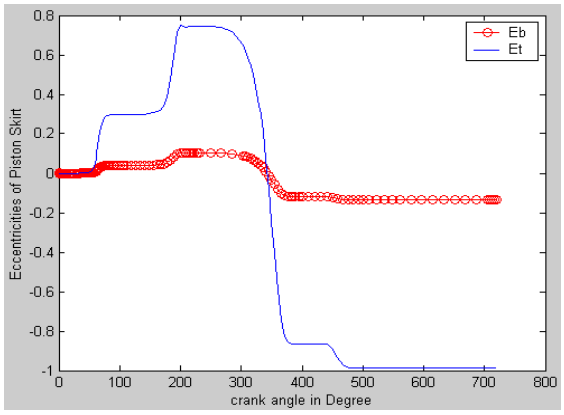

Fig 5.8(a) Eccentricities Of Piston Skirt Vs Crank angle

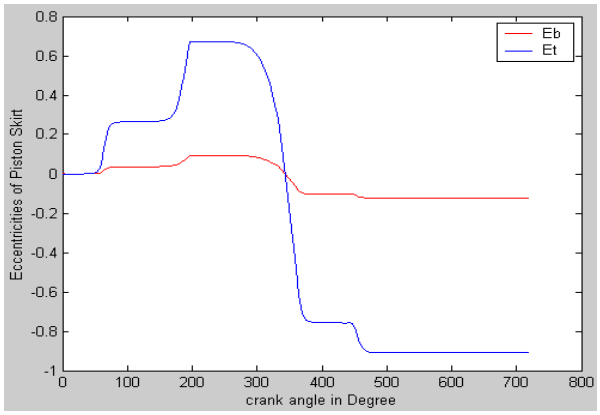

Fig 5.8(b) Eccentricities Of Piston Skirt Vs Crank angle

In Newtonian lubrication model, dimensionless piston eccentricities 'E_t' & 'E_b' are clearly shifted towards the major thrust side as well as minor thrust side in the entire cycle of piston motion. In Viscoelastic case 'E_t' & 'E_b' are negligible from the start and then shifts toward minor thrust side and finally shifts towards major thrust side and is more safely away from the upper and lower horizontal lines.

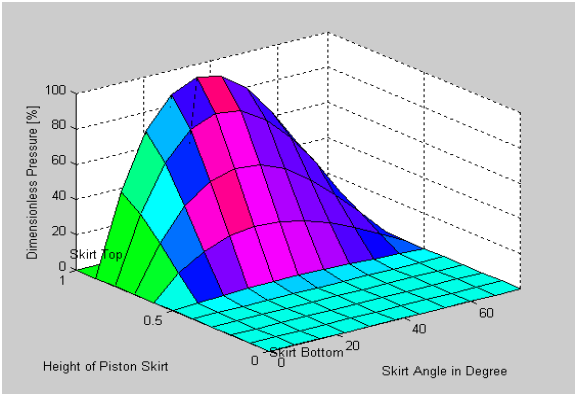

Fig 5.9(a) Pressure profiles at 120 deg crank angle

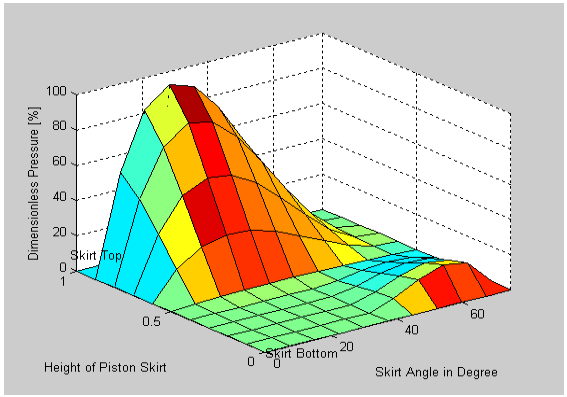

Fig 5.9(b) Pressure profiles at 120 deg crank angle

Refer to figure 5.9(a), In Newtonian model the pressure distribution is uniform through the entire crank rotation angles, which indicates perfectly aligned piston skirts model, maintaining desirable clearances throughout the entire cycle. Refer to figure 5.9(b), in viscoelastic model Positive pressures generate from mid to the skirt top surface. The slope is gentle till the mid-stroke after it starts getting steep, peak pressures shift towards right and all this is happening with increasing film thickness, coefficient of friction and shear stress. It implies that an increase in frictional losses and more shear stress generation could shift hydrodynamic peak pressures along with an increase in steepness of profile slopes.

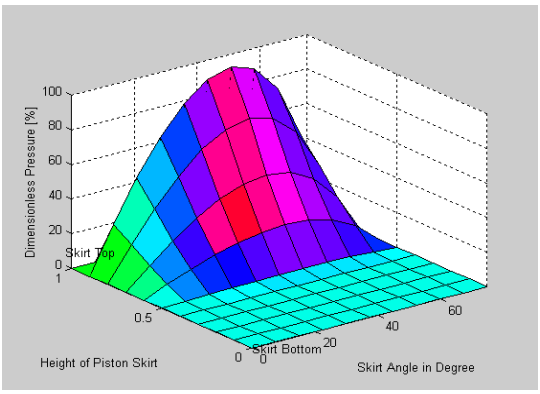

5.10(a) Pressure profiles at 240 deg crank angle

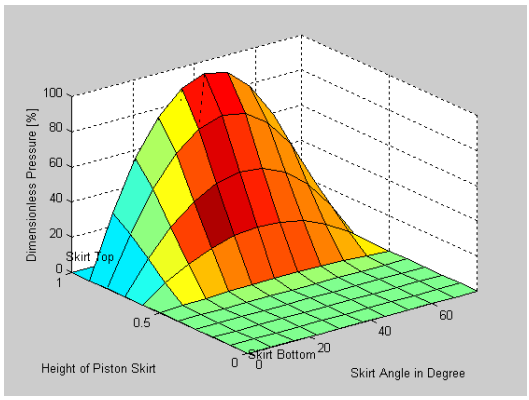

Fig 5.10(b) Pressure profiles at 240 deg crank angle

Refer to figures 5.10(a) and 5.11(a), In the Newtonian model the intake stroke peak hydrodynamic pressure values are closer to the piston skirt top surface showing gentle slope of instantaneous pressure fields. While in the compression stroke slopes of instantaneous pressure fields start getting steep with corresponding sharp rise in peak pressures but still these peak values develop closer to the skirt top surface plane. Refer to figures 5.10(b), and 5.11(b), Viscoelastic model positive pressures generate from mid to the skirt top surface till 240 degree angle. The slope gets steeper till one-third of the compression stroke after which positive pressures start shifting towards skirts bottom and all this happens with further rise in the film thickness, coefficient of friction and shear stress. It implies that increase in frictional losses and more shear stress generation shift hydrodynamic pressure fields towards skirts bottom along slight increase in steepness of profile slopes.

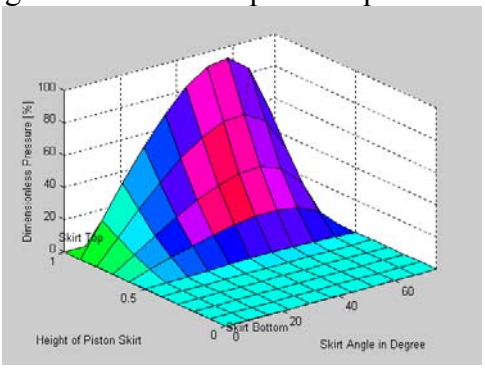

Fig 5.11(a) Pressure profiles at 360 deg Crank angle

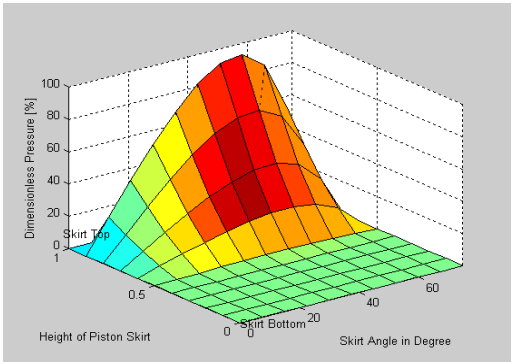

Fig 5.11(b) Pressure profiles at 360 deg Crank angle

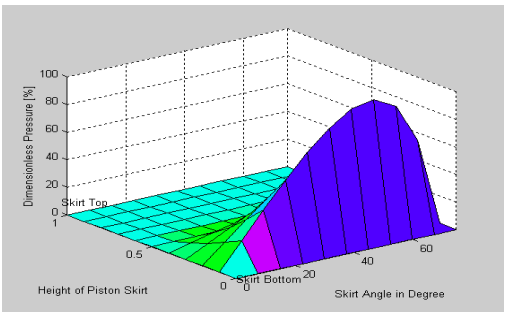

Fig 5.12(a) Pressure profiles at 480 deg crank angle

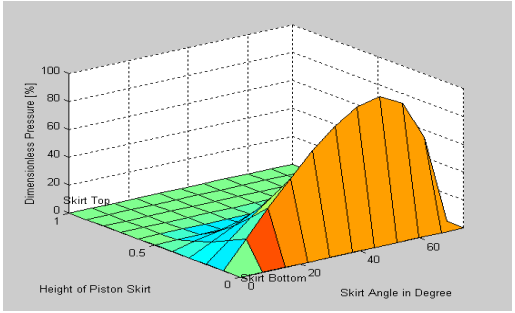

Fig 5.12(b) Pressure profiles at 480 deg crank angle

Refer to figure 5.12(a), In the Newtonian model piston expansion strike the slope of instantaneous pressure fields gets steeper and peak pressures shift towards the right side of piston skirt top surface plane till the mid of expansion stroke. From the mid-point of the expansion stroke to the end of it when piston reaches the bottom dead center (BDC), the pressure field gradients as well as peak values shift towards piston skirt bottom surface from the top edge. This is a very significant change in the entire cycle. In the exhaust stroke the pressure fields develop over the piston skirt bottom surface plane and we witness peak values of pressure to be developing at the extreme edges of skirt bottom surface .Refer to figure 5.12(b), viscoelastic model which show pressure fields over the skirts surface in the power/expansion stroke of piston at 420, 480 and 540 degree crank rotation respectively. Positive pressures generate from mid to the skirt bottom surface till 540 degree angle. The slope gets steep till one-third of the stroke after which positive pressures slightly shift in the mid values over the skirts bottom and all this happens with further rise in the film thickness, coefficient of friction and shear stress. It implies that further increase in frictional losses and more shear stress generation with instantaneous reduction and then rise in film thickness keep hydrodynamic pressure fields at the skirts bottom along slight increase in steepness of profile slopes.

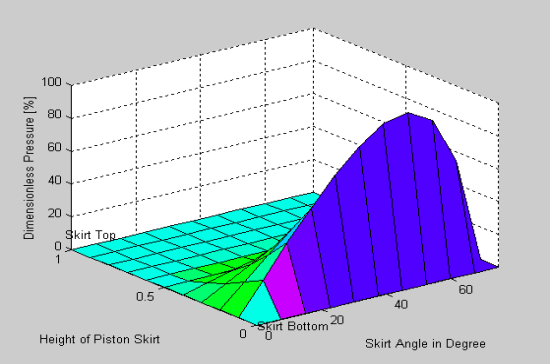

Fig 5.13(a) Pressure profiles at 600 deg crank angle

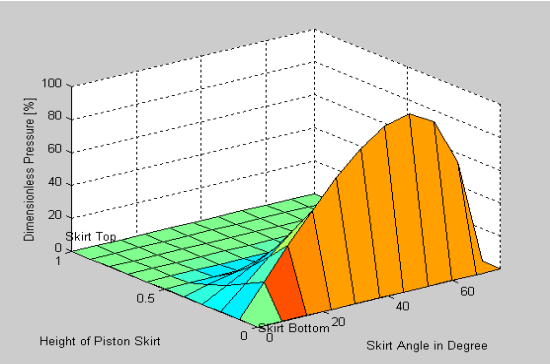

Fig 5.13(b) Pressure profiles at 600 deg crank angle

Refer to figures 5.13(a) and 5.14(a). In the exhaust stroke the pressure fields develop over the piston skirt bottom surface plane and we witness peak values of pressure to be developing at the extreme edges of skirt bottom surface. Refer to figures 5.13(b) and 5.14(b) which show pressure fields over the skirts surface in the exhaust stroke of piston at 600, 660 and 720 degree crank rotation respectively. Positive pressures generate from mid to the skirt bottom surface till 540 degree angle. The slope gets further steep till mid of the stroke after which positive pressures slightly shift in the mid values over the skirts bottom and all this happens with further rise in the film thickness, coefficient of friction and shear stress. It implies that a further increase in frictional losses and more shear stress generation with instantaneous reduction and then rise in film thickness keep hydrodynamic pressure fields at the skirts bottom along with slight increase in steepness of the profile.

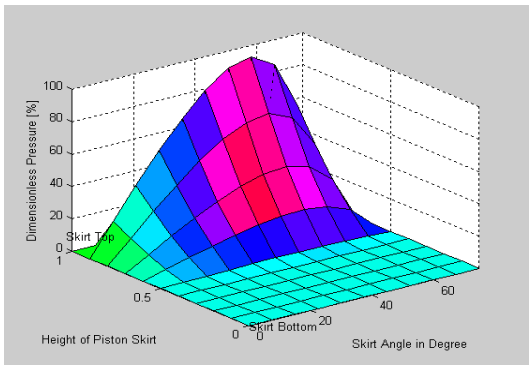

Fig 5.14(a) Pressure profiles at 720 deg crank angle

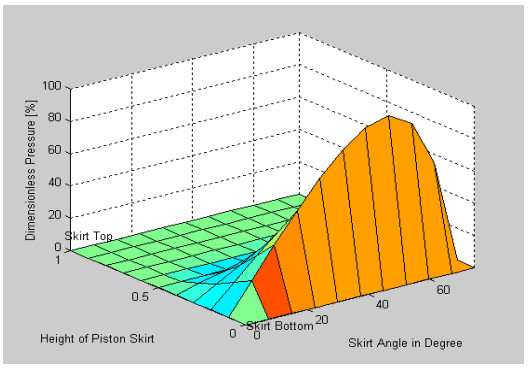

Fig 5.14(b) Pressure profiles at 720 deg crank angle

5.3 Parametric Studies & Analysis of Viscoelastic Model

Parametric Study-1

Viscosity = 0.016 Pa.s
Radial Clearence = 5 micron

Engine speed (RPM)

500 | 600 | 700 | 800 | 900 | 1000 | 1200 | 1400 | 1500 | 2000

Parametric Study-2

Viscosity = 0.016 Pa.s
Radial Clearence = 10 micron

Engine speed (RPM)

500 | 600 | 700 | 800 | 900 | 1000 | 1200 | 1400 | 1500 | 2000

Parametric Study-3

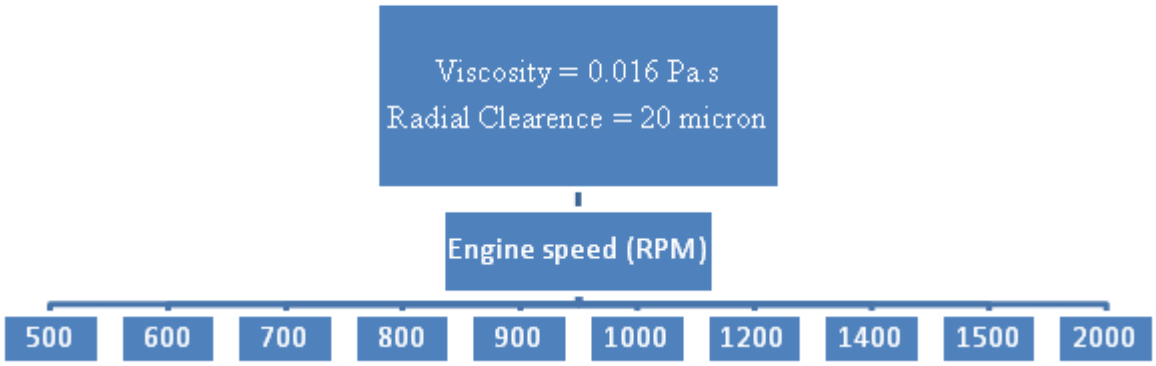

Parametric Study-4

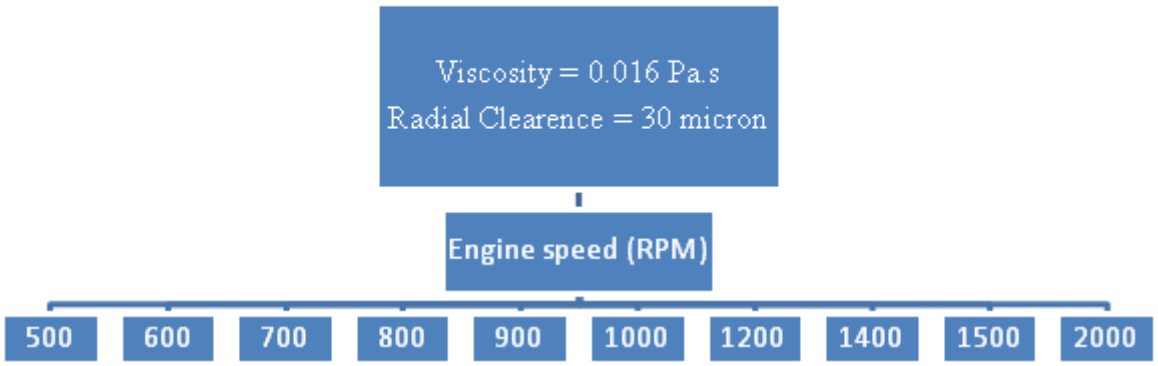

Parametirc Study-5

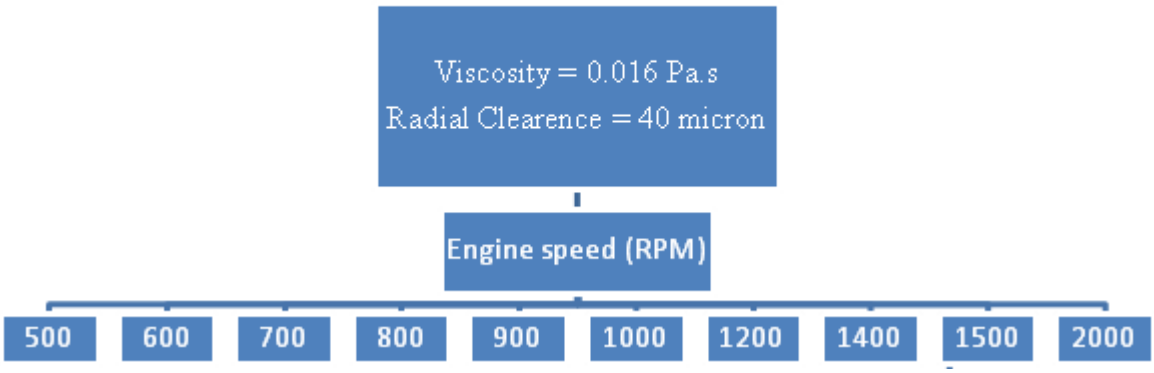

Parametric Study-6

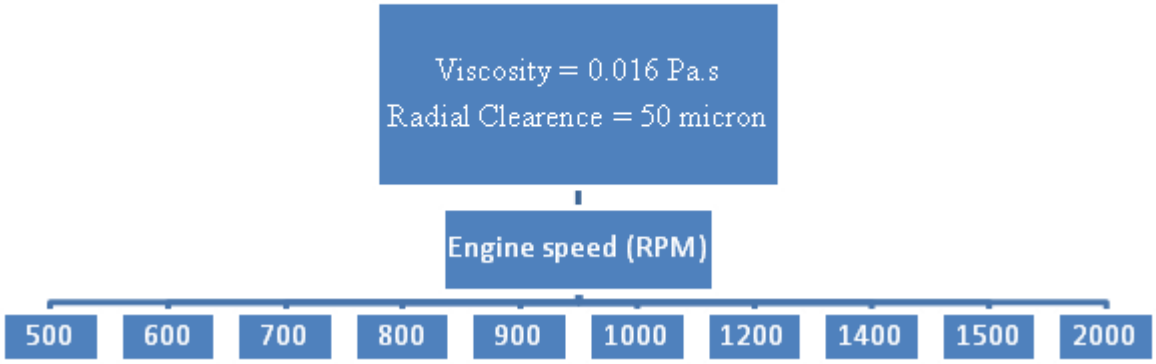

Parametric Study-7

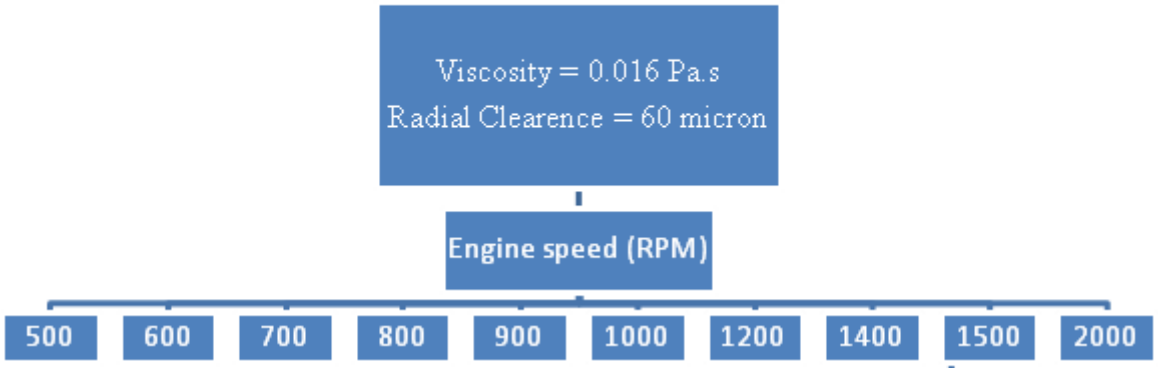

Parametric Study-8

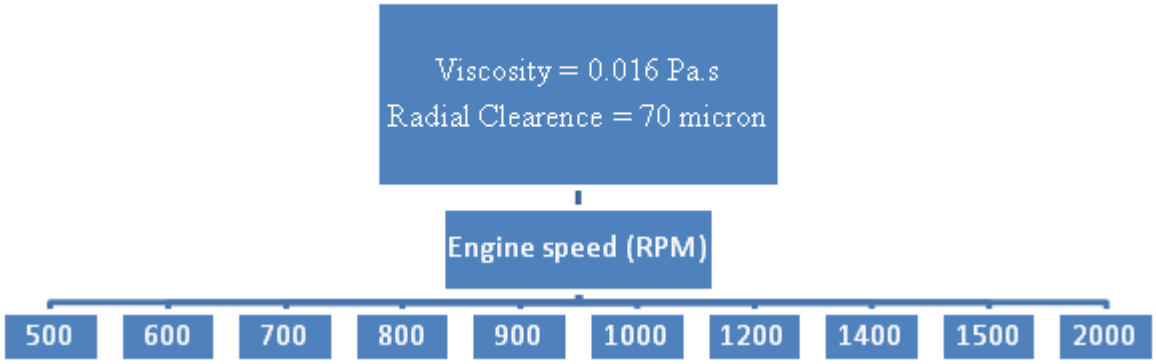

Parametric Study-9

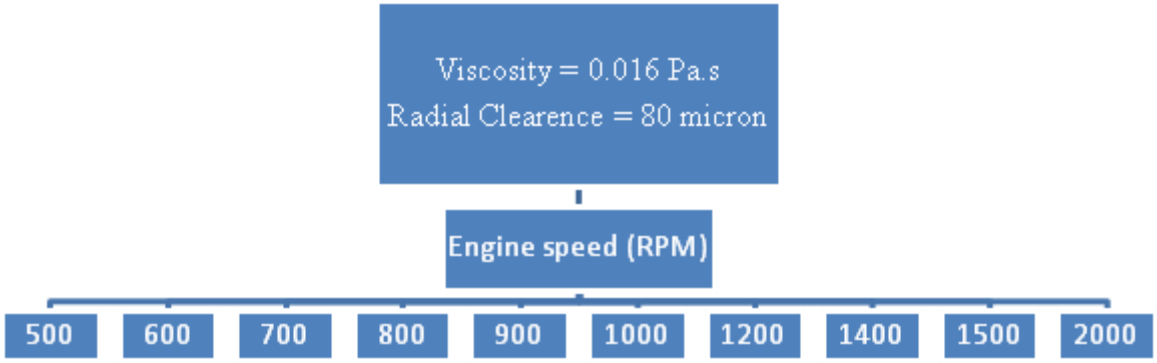

Parametric Study-10

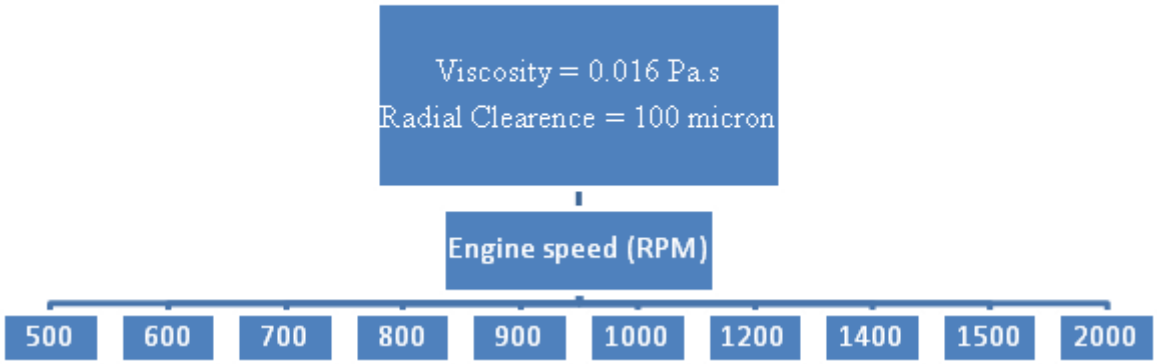

Parametric Study-11

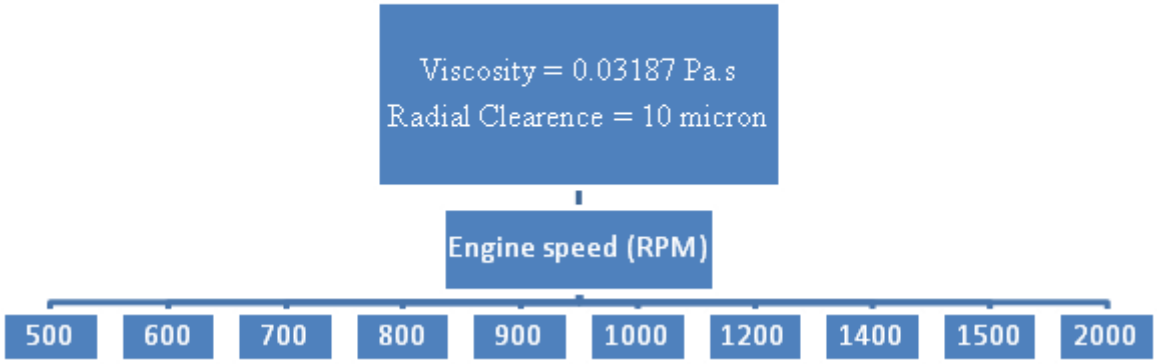

Parametric Study-12

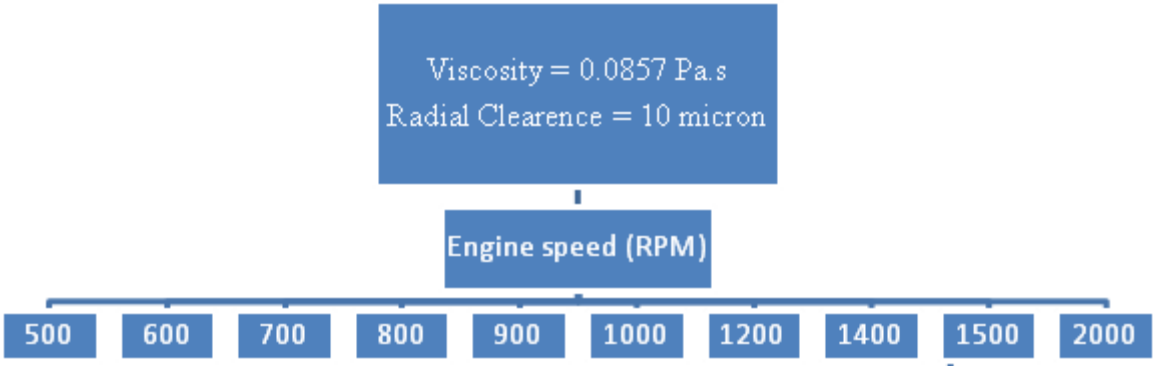

Parametric Study-13

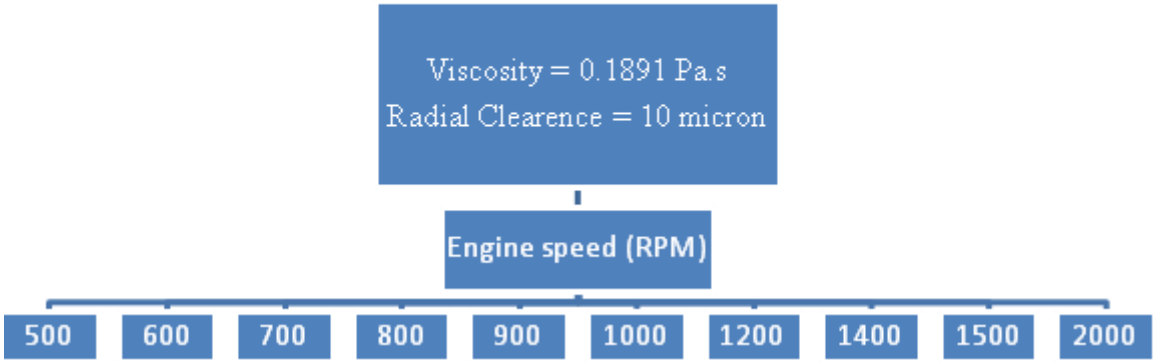

5.3.1 'SPEED' Parameter Analysis

In the speed Parameter analysis, Variations in different parameters are analyzed on the speed range between 500-2000 rpm. The brief overviews of the results that vary with speed are shown in general and then the overview of results in particular at different initial start up speed ranges are shown:

Briefly, we analyze those results one by one:

In the basic piston skirts lubrication model we have following observations on the results:

1. Oil film thickness suddenly rises just before 500 degree crank rotation and then falls.
2. Peak values of maximum & minimum film thickness slightly rise in magnitude.

3. There is little change in the oil film thickness profile between 500-550 degree crank angles.
4. Piston eccentricity at the skirt top (E_t) does not go very close to the lower line (major thrust side). There is no two-step drop in 'E_t' towards lower line as compared to the original case.

Piston Eccentricities:

Comparison of 'E_t' and 'E_b' is made from 500 to 2000 rpm and the results at 600, 1000, 1400 and 2000 rpms are shown.

600 rpm

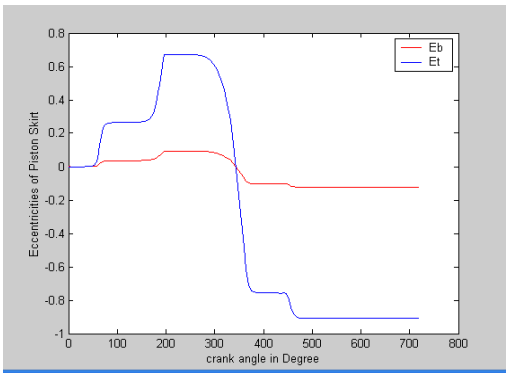

Fig 5.15(a) Piston Eccentricities at 600 rpm

1000 rpm

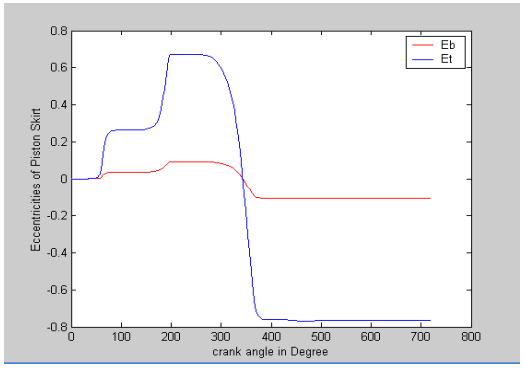

Fig 5.15(b) Piston Eccentricities at 1000 rpm

In the first few rpms ie., 500 to 1000, we can see that the eccentricities are closer to major and minor thrust sides and as the initial start up rpms are increasing the eccentricities are getting closer and closer to major thrust sides which means more chances of Solid to solid contact.

1400 rpm

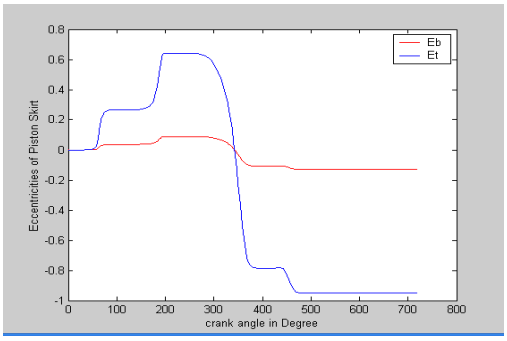

Fig 5.15(c) Piston Eccentricities at 1400 rpm

2000 rpm

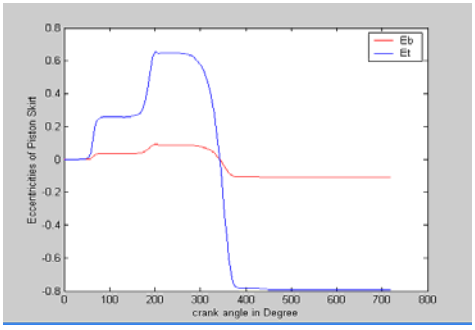

Fig 5.15(d) Piston Eccentricities at 2000 rpm

From here we can easily conclude that high initial engine start up speeds are detrimental to engine smooth operation and can cause adhesive wear and hence high initial start up speeds

(near 2000 rpm) will reduce the engine life. Therefore the engine start speed must not be higher than 1000 rpms.

EHL Film Thickness and EHL Pressure Profiles at different speeds:

Comparison of results between EHL Film Thickness profiles and pressure profiles are shown below.

Following comments are made on the results of EHD Film Thickness profiles:

1. There is a large change in film thickness profiles which takes the shape of an EHD film profile after applying the inverse solution technique.
2. The film thickness profiles obtained closely follow the bench marked EHD film thickness profile.
3. The rise in peak hydrodynamic pressures is exponentially generated than the earlier drawn pressure fields such that they enter into EHD domain.
4. The resulting pressure rise is so high that the new values are several times higher than the earlier pressure values.
5. The opposing surfaces are unable to sustain high pressures and hence they get elastically deformed to allow the EHD oil film to enter inside the contacts and establish an EHD layer of minimum thickness.

EHD Film Thickness profiles are shown at 600, 1200 and 1800 rpms.

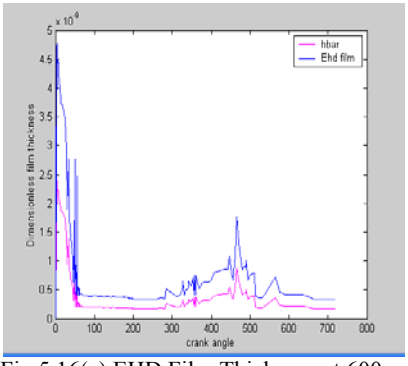

Fig 5.16(a) EHD Film Thickness at 600 rpm

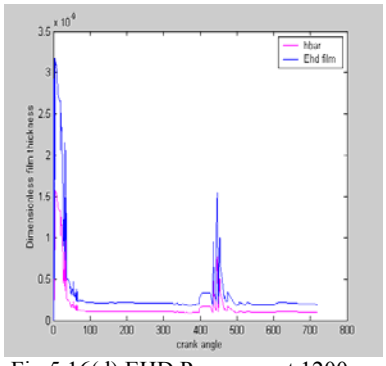

Fig 5.16(d) EHD Pressures at 1200 rpm

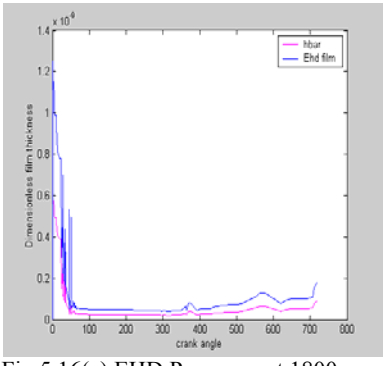

Fig 5.16(c) EHD Pressures at 1800 rpm

The generated peak EHD pressures are many times more than the generated hydrodynamic pressures; hence it is nearly impossible to draw a 3-D pressure field of both types of pressures (Hydrodynamic and EHD) in percentage terms for comparative analysis. In order to get 3-D EHD pressure profiles in percentage terms for 720 degree cycle of crank rotation we have plotted the required graph shown below giving such profiles. The peak hydrodynamic pressure

values are taken as base line of these EHD pressures. In our case the peak percentage EHD pressure values are around 50% of the maximum possible pressures compared to the base line (bottom surface) peak hydrodynamic pressures as shown on the graph in the figure below. These pressures are mostly in the medium range and in case of oil starvation these pressures would be the Hertzian pressures much higher in magnitude and hence causes plastic flow of material. If we manage oil flooding in the initial engine start up phase then there is no possibility of Hertzian pressures replacing EHD pressures and hence there is less chance of adhesive wear expected, during the initial engine start up.

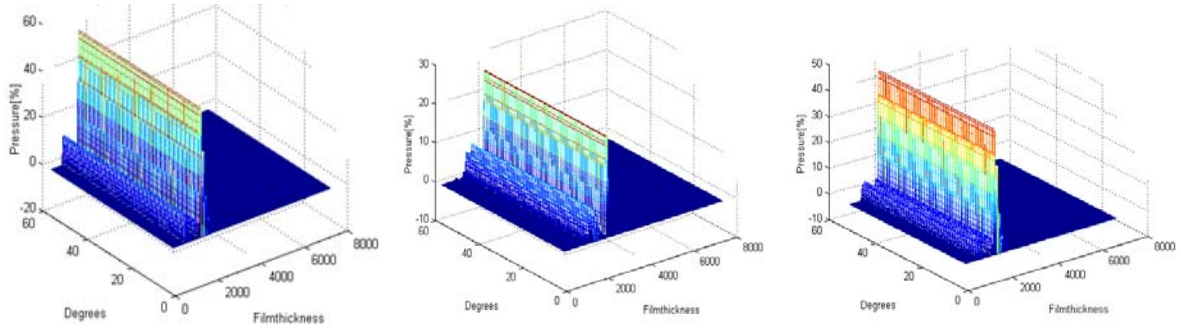

Fig 5.17(a) EHD Film Thickness at 600 rpm Fig 5.17(b) EHD Pressures at 1200 rpm Fig 5.17(c) EHD Pressures at 1800 rpm

Low Start up Speed: 500-900 rpm

In the low start up speed range, maximum variations from the original model are at 700 rpm and Hydrodynamic Pressure profiles (from 60 deg to 240 deg), Ehl film Thickness, Piston Eccentricities and Hydrodynamic Film Thickness profiles are shown at 700 rpm.

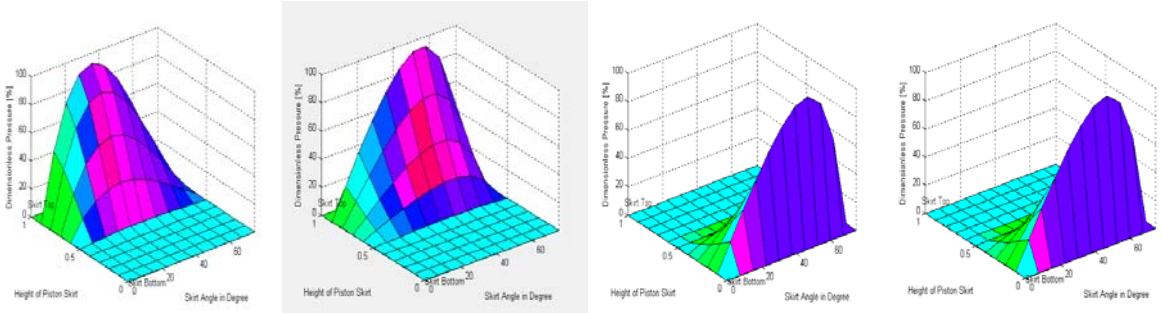

Fig 5.18(a) Pressure profile at 60 deg Fig 5.18(b) Pressure profiles at 120 deg Fig 5.18(c) Pressure profiles at 180 deg Fig 5.18(d) Pressure profiles at 240 deg

Briefly, we analyze the results one by one. In the basic piston skirts lubrication model we have following observations on the results:

1. Oil film thickness profiles have generally same trends as before except few new spikes.

2. Maximum & minimum film thickness profile curves do not show rapid rise & fall around 500 degree in sharp contrast to the case before.
3. There is one noticeable spike downward in the oil film thickness profile at 370 degree crank angle.
4. Piston eccentricity at the skirt top (E_t) drops much closer to the lower line (major thrust side) straight from upper line (minor thrust side) just after 372 degree and remains their until the end of cycle at 720 degree. It even touches the lower line before 500 degree, which means that solid-to-solid contact does get established at this speed.
5. The peak pressure profiles in the induction stroke are at skirt top surface as before but the values are closer to 100%. The slopes of pressure rise are gentle.
6. Peak pressures shift to the right side skirt top surface during the compression stroke.
7. Pressure profiles in expansion & exhaust strokes shift to the skirt bottom surface but slightly high peak pressures are obtained as compared to when the speed is 600 rpm.

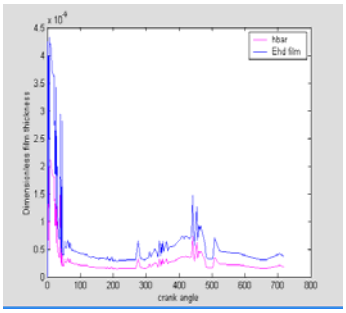

Fig 5.18(e) EHD Film Thickness

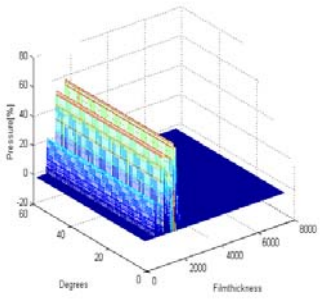

Fig 5.18(f) EHD Pressures

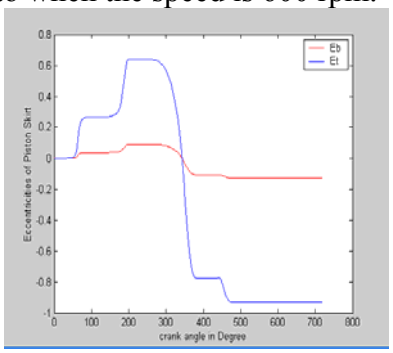

Fig 5.18(g) Piston Eccentricities

Medium Start up speed: 1000-1400 rpm

In the medium start up speed range, maximum variations from the original model are at 1200 rpm and Hydrodynamic Pressure profiles, Ehl film Thickness, Piston Eccentricities, Hydrodynamic Film Thicknesses, Shear Stress and Coefficient of Friction are shown at 1200 rpm. Also hydrodynamic Friction forces and Hydrodynamic Friction moments are shown at 1200 rpm.

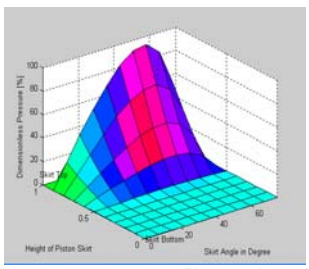
Fig 5.19(a) Pressure profile at 60 deg

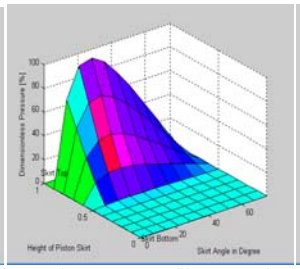
Fig 5.19(b) Pressure profiles at 120 deg

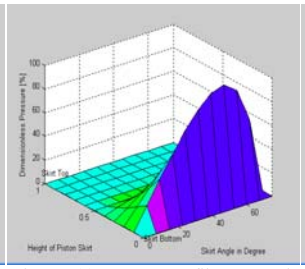
Fig 5.19(c) Pressure profiles at 180 deg

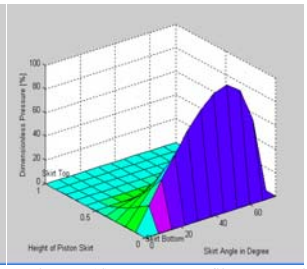
Fig 5.19(d) Pressure profiles at 240 deg

We have following comments on the EHL model simulation results in medium speed range:

1. Piston eccentricity at the top i.e. 'E_t' goes very close to the lower line and touches it.
2. There are some notable instantaneous spikes seen in the maximum & minimum film thickness profiles.

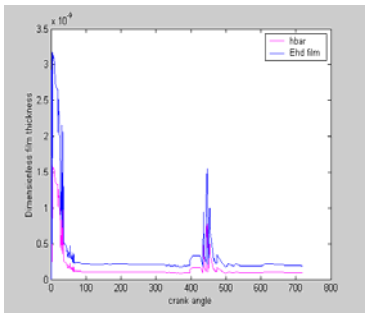

Fig 5.19(e) EHD Film Thickness

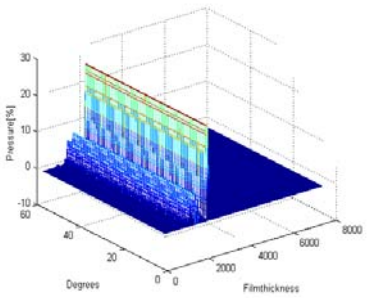

Fig 5.19(f) EHD Pressures

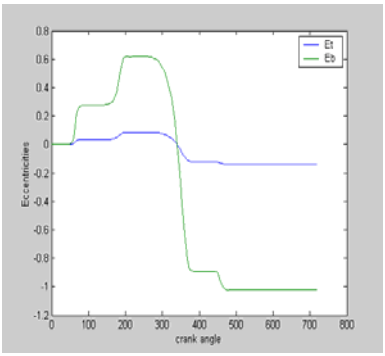

Fig 5.19(g) Piston Eccentricities

3. EHD film thickness profile curve generally follows same trend in the beginning as before. The values remain negligibly small during the induction & compression strokes.
4. EHD film thickness remains at minimum values till 476 degree angle when there is exponential rise to a significantly high value & then a rapid drop to minimum value which remains till 720 degree.
5. Peak values of EHD pressures rise from originally around 55% to exceed 130%. This indicates extreme EHD pressures developing with the start up speed of 1500 rpm.
6. With the increase in speed from 600rpm to 1500 rpm in the initial engine start up EHD film thickness values reduce considerably, which is very important to consider. This is due to the corresponding build up of extremely high EHD pressures. Hence, our initial deduction stands validated that we must be very careful to select initial engine start up speed as an increase in speed means increased EHD pressures build up, which may be very damaging to the piston and rings during the initial engine start up especially when (in reality) it is oil starvation between the opposing surfaces

High Start up Speed: 1500-2000 rpm

In the medium start up speed range, maximum variations from the original model are at 1500 rpm and Hydrodynamic Pressure profiles, EHL film Thickness, Piston Eccentricities, Hydrodynamic Film Thicknesses, Shear Stress and Coefficient of Friction are shown at 1500 rpm. Also hydrodynamic Friction forces and Hydrodynamic Friction moments are shown at 1500 rpm.

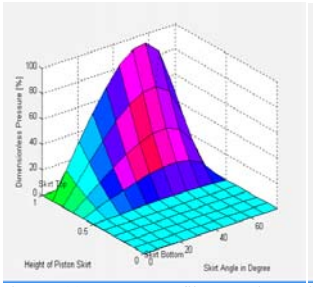
Fig 5.20(a) Pressure profile at 60 deg

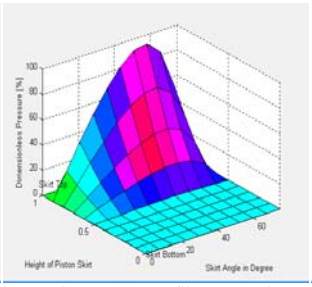
Fig 5.20(b) Pressure profiles at 120 deg

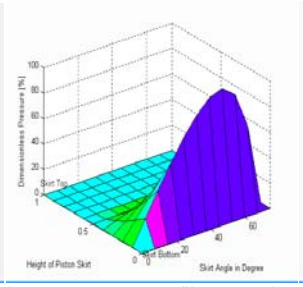
Fig 5.20(c) Pressure profiles at 180 deg

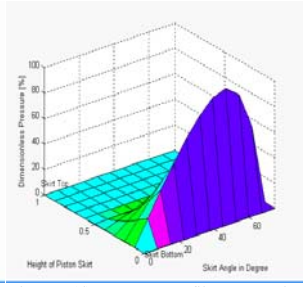
Fig 5.20(d) Pressure profiles at 240 deg

We have following comments on the EHL model simulation results in high speed range:

1. Piston eccentricity at the top i.e. 'E_t' goes very close to the lower line and touches it.
2. There are spikes seen in the maximum & minimum film thickness profiles.
3. The values of minimum and maximum EHD Film thickness profiles remain negligibly small during the induction & compression strokes.

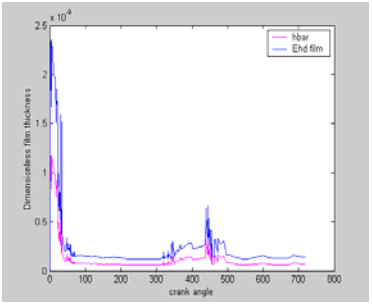

Fig 5.20(e) EHD Film Thickness

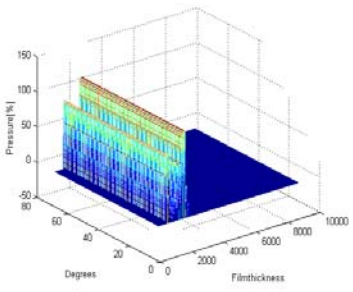

Fig 5.20(f) EHD Pressures

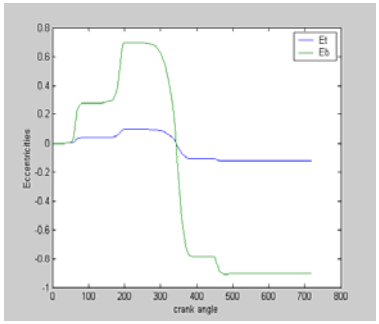

Fig 5.20(g) Piston Eccentricities

4. EHD film thickness remains at minimum values till 473 degree angle when there is exponential rise to a significantly high value & then a rapid drop to minimum value which remains till 720 degree.
5. Peak values of EHD pressures rise from originally around 57% to exceed 121%. This indicates extreme EHD pressures developing with the start up speed of 2000 rpm.

5.3.2 'VISCOSITY' Parameter Analysis

In the viscosity Parameter analysis, we have considered four different viscosities, 0.016 is the benchmarked viscosity form the benchmarked research paper, while 0.03187,0.05187 and 0.189 are viscosities of three SAE standard oils, which are SAE 10, SAE 30 and SAE 50. The behavior of different parameters is analyzed on these different viscosities.

0.016 Pa.s

Comparison is given at 0.016 Pa.s respectively and Hydrodynamic Pressure profiles, Ehl film Thickness, EHL Pressure profiles, Hydrodynamic Film Thicknesses are shown at 0.016 Pa.s.

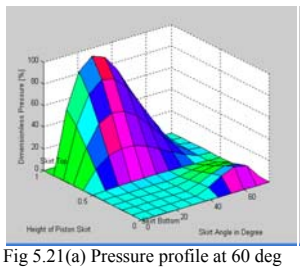

Fig 5.21(a) Pressure profile at 60 deg

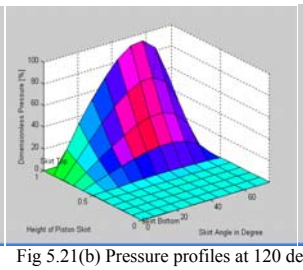

Fig 5.21(b) Pressure profiles at 120 deg

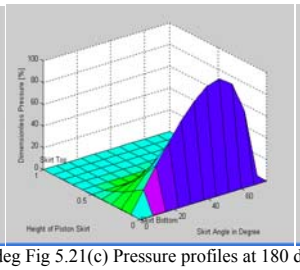

Fig 5.21(c) Pressure profiles at 180 deg

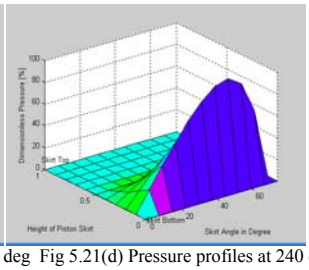

Fig 5.21(d) Pressure profiles at 240 deg

1. There are two very prominent and high surges noticed in the overall EHD film thickness curves. More significant among these is a very sharp and high peak value obtained at 236 degree, which drops down to minimum value again at around 280 degree.
2. EHD film thickness curves have minimum values till 465 degree crank rotation. Then there is a notable surge with peak values (less than before) obtained at 478 degree angle. This peak values drop down to minimum magnitudes at 490 degree. The minimum values of profile curves are maintained till 720 degree when the rotation cycle completes.

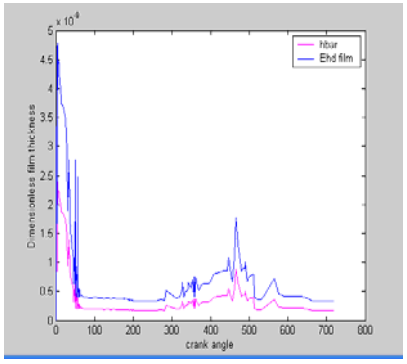

Fig 5.21(e) EHD Film Thickness

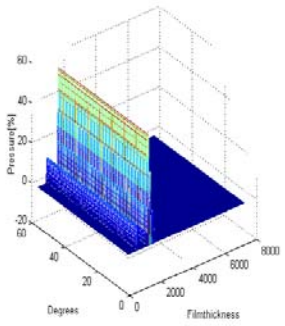

Fig 5.21(f) EHD Pressures

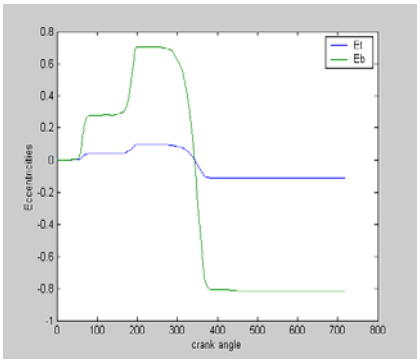

Fig 5.21(g) Piston Eccentricities

3. The overall pressure fields have mostly similar slopes as in the original case. Peak pressure values are at the skirt top surface during the induction stroke.
4. In the compression stroke the pressure fields indicate steep slopes instead of gentle ones. Peak pressure values rise to above 90% towards the skirt top surface.
5. At the end of compression stroke and in the initial half of expansion stroke the slopes of pressure fields become steeper and peak pressures acting on the skirt top surface have values as high as above 95%. This is a notable change witnessed in this case.

SAE-10 :

Comparison is given for SAE -10 respectively and Hydrodynamic Pressure profiles, Ehl film Thickness, Piston velocities, Hydrodynamic Film Thicknesses, are shown at 0.03187 Pa.s.

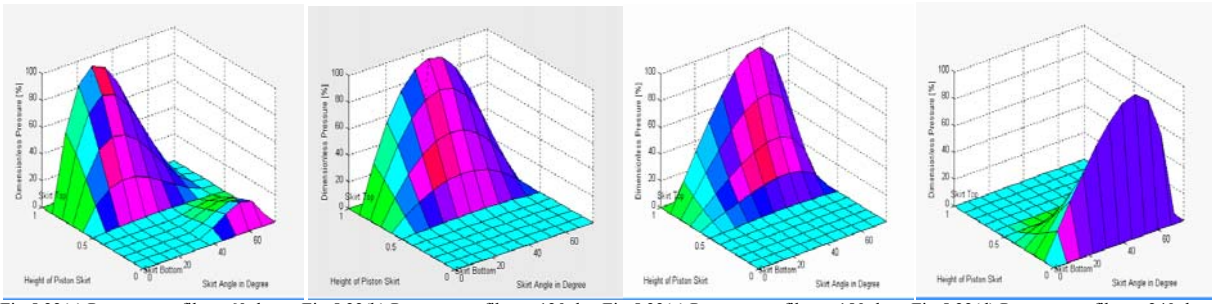

Fig 5.22(a) Pressure profile at 60 deg Fig 5.22(b) Pressure profiles at 120 deg Fig 5.22(c) Pressure profiles at 180 deg Fig 5.22(d) Pressure profiles at 240 deg

Briefly, we analyze these results one by one. In the basic piston skirts lubrication model we have following observations on the results:

1. Maximum and minimum film thickness profile curves have some instantaneous changes between the peak values & values at 400 degree. The general trend after that point is mostly the same.

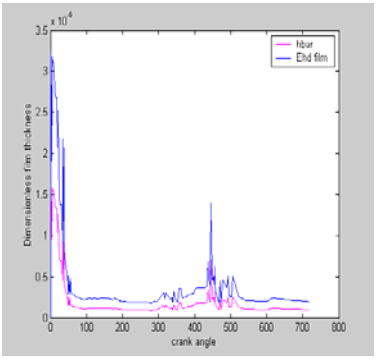

Fig 5.22(e) EHD Film Thickness

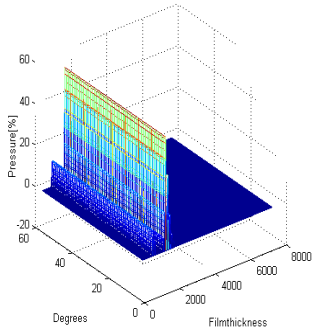

Fig 5.22(f) EHD Pressures

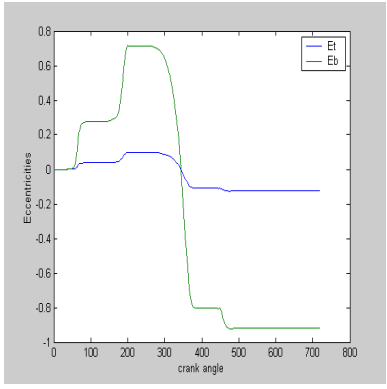

Fig 5.22(g) Piston Eccentricities

2. The curves representing piston eccentricities at the skirt top (E_t) and at the bottom (E_b) are generally the same. 'E_t' curve shows improvement when shifted to the major thrust side (lower line) after 372 degree. Instead of getting closer to the lower line it shifts up to a safe distance from it. This means that there are lesser chances for possible solid-to-solid contact between piston and cylinder liner surfaces than before.
3. The overall pressure fields have mostly similar slopes as in the original case. Peak pressure values are at the skirt top surface during the induction stroke.
4. In the compression stroke the pressure fields indicate steep slopes instead of gentle ones. Peak pressure values rise to above 90% towards the skirt top surface.
5. At the end of compression stroke and in the initial half of expansion stroke the slopes of pressure fields become steeper and peak pressures acting on the skirt top surface have values as high as above 95%. This is a notable change witnessed in this case.
6. Pressure fields shift towards the bottom of skirt surface nearing the end of expansion stroke. Peak pressures act on skirt bottom surface. There is a notable shift in peak pressures towards the right.

SAE-30 :

Comparison is given for SAE-30 respectively, and Hydrodynamic Pressure profiles, Ehl film Thickness, Piston velocities, Hydrodynamic Film Thicknesses, are shown at 0.0857 Pa.s.

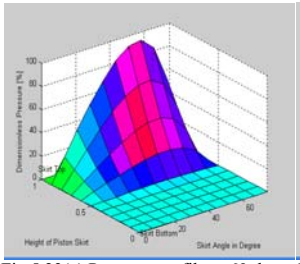

Fig 5.23(a) Pressure profile at 60 deg

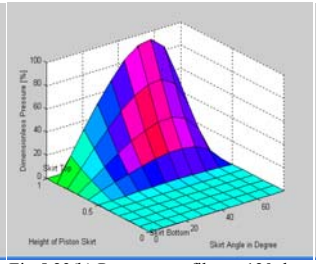

Fig 5.23(b) Pressure profiles at 120 deg

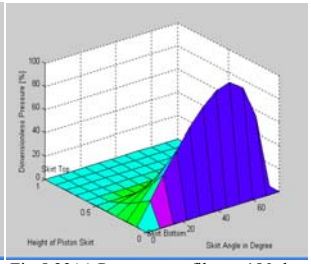

Fig 5.23(c) Pressure profiles at 180 deg

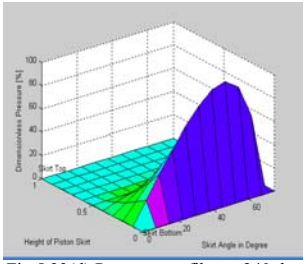

Fig 5.23(d) Pressure profiles at 240 deg

We have following comments on the EHL model simulation results:

1. There are two very prominent and high surges noticed in the overall EHD film thickness curves. More significant among these is a very sharp and high peak value obtained at 236 degree, which drops down to minimum value again at around 280 degree.
2. EHD film thickness curves have minimum values till 465 degree crank rotation. Then there is a notable surge with peak values (less than before) obtained at 478 degree angle.

This peak values drop down to minimum magnitudes at 490 degree. The minimum values of profile curves are maintained till 720 degree when the rotation cycle completes.

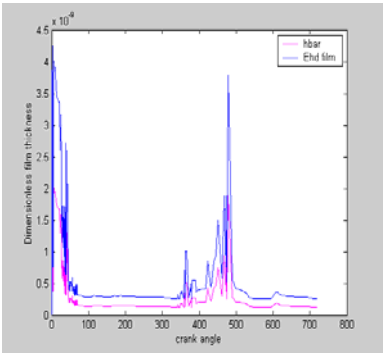

Fig 5.23(e) EHD Film Thickness

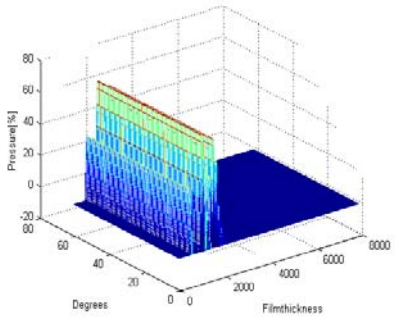

Fig 5.23(f) EHD Pressures

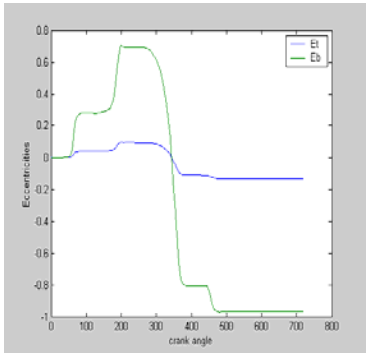

Fig 5.23(g) Piston Eccentricities

3. There are three small surges in the maximum and minimum film thickness profiles, which occur between 350 degree and 400 degree of crank rotation.
4. Peak values of EHD pressures rise from originally around 55% to 95%. This increase in EHD pressures is quite significant as elastic deformations increase due to shift in EHD pressures from medium to high ranges. Hence we must be very careful to decide the viscosity of lubricant in the initial engine start up as any reduction in oil viscosity means increased EHD pressures generation and build up.

SAE 50 :

Comparison is given at SAE-50 respectively, and Hydrodynamic Pressure profiles, Ehl film Thickness, Hydrodynamic Film Thicknesses profiles are shown at 0.1891 Pa.s. Also hydrodynamic Friction forces and Hydrodynamic Friction moments are shown at 0.1891 Pa.s.

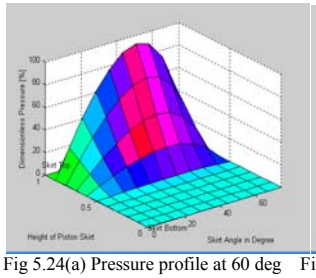
Fig 5.24(a) Pressure profile at 60 deg

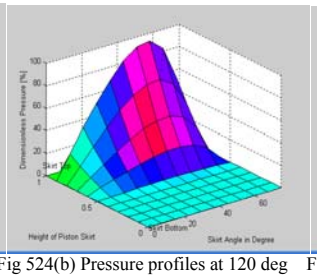
Fig 524(b) Pressure profiles at 120 deg

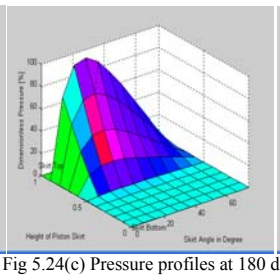
Fig 5.24(c) Pressure profiles at 180 deg

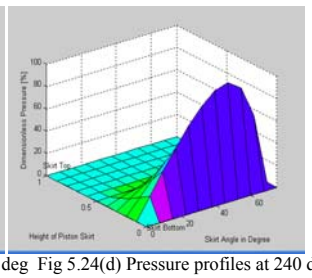
Fig 5.24(d) Pressure profiles at 240 deg

In the basic piston skirts lubrication model we have following observations on the results:

1. There a change in the general oil film thickness profiles. Maximum and minimum film thickness profile curves have some instantaneous changes between the peak values & values at 360 degree.
2. The curves representing piston eccentricities at the skirt top (E_t) and at the bottom (E_b) are generally the same. 'E_t' curve shows improvement when shifted to the major thrust side (lower line) after 372 degree. Instead of getting closer to the lower line it shifts up to a safe distance from it. This means that there are lesser chances for possible solid-to-solid contact between piston and cylinder liner surfaces than before.
3. The overall pressure fields have mostly similar slopes as in the original case. Peak pressure values are at the skirt top surface during the induction stroke.
4. In the compression stroke the pressure fields indicate steep slopes instead of gentle ones. Peak pressure values rise to above 90% towards the skirt top surface.

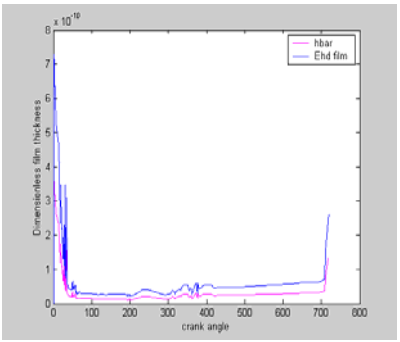

Fig 5.24(e) EHD Film Thickness

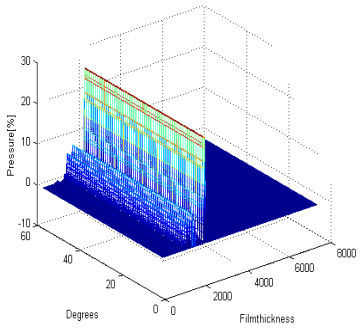

Fig 5.24(f) EHD Pressures

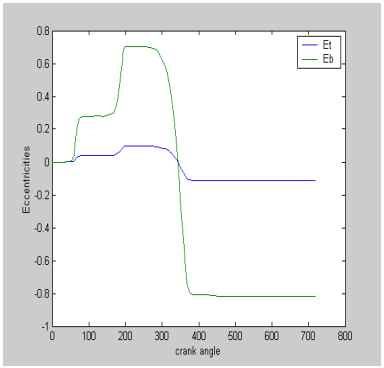

Fig 5.24(g) Piston Eccentricities

5. At the end of compression stroke and in the initial half of expansion stroke the slopes of pressure fields become steeper and peak pressures acting on the skirt top surface have values as high as above 95%. This is a notable change witnessed in this case.
6. Pressure fields shift towards the bottom of skirt surface nearing the end of expansion stroke. Peak pressures act on skirt bottom surface. There is a notable shift in peak pressures towards the right.

5.3.3 'RADIAL CLEARANCE' Parameter Analysis

We changed the radial clearance between piston and cylinder bore from 5 micron (original model) to 100 micron. It was with the knowledge that existing engine designs normally have relatively bigger values of such clearances when an engine is assembled. Hence, such relatively

large radial clearances are actually there when an engine is started. It is after few minutes of engine running when engine acquires its optimum operating conditions and relatively large clearances are reduced to smaller values (e.g. 5 micron or a value similar to it). In this study we did not change the value of any other parameter. We achieved results, which varied, from our original results. The results are shown below.

10 micron

Comparison is given at 10 micron radial clearance respectively

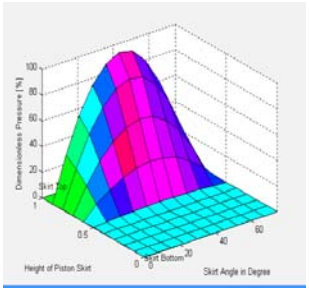

Fig 5.25(a) Pressure profile at 60 deg

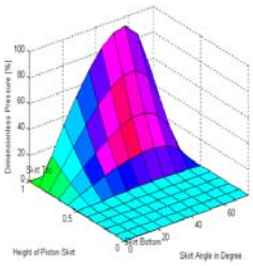

Fig 5.25(b) Pressure profiles at 120 deg

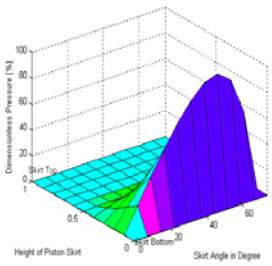

Fig 5.25(c) Pressure profiles at 180 deg

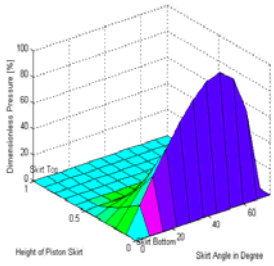

Fig 5.25(d) Pressure profiles at 240 deg

Briefly, we analyze those results one by one. In the basic piston skirts lubrication model we have following observations on the results:

1. There is little change in the general oil film thickness profile. Maximum and minimum film thickness values have minor instantaneous changes in their values but those are insignificant. The general trend is mostly the same.
2. The curve for piston eccentricity at the skirt top (E_t) shows improvement when shifted to the major thrust side (lower line) after 372 degree. Instead of getting closer to the lower line it shifts little up towards the center line representing piston concentricity. This means that there are reduced chances of possible solid-to-solid contact between piston and cylinder liner surfaces.

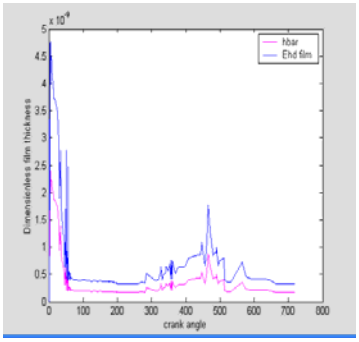

Fig 5.25(e) EHD Film Thickness

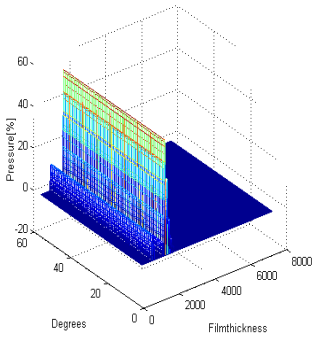

Fig 5.25(f) EHD Pressures

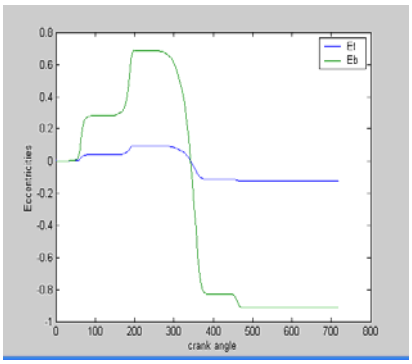

Fig 5.25(g) Piston Eccentricities

3. The overall pressure fields do not change their profiles significantly except that the peak pressures slightly shift to the right and insignificant rise in their magnitudes.

50 micron

Comparison is given at 20 micron radial clearance respectively

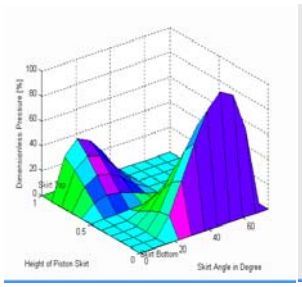

Fig 5.26(a) Pressure profile at 60 deg

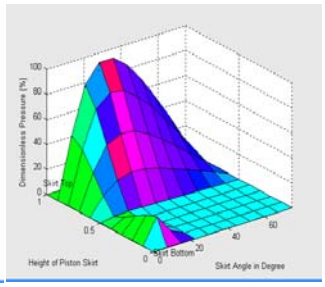

Fig 5.26(b) Pressure profiles at 120 deg

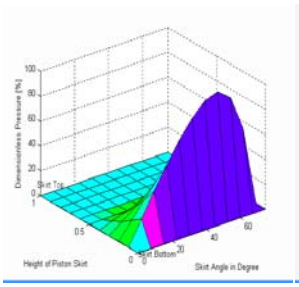

Fig 5.26(c) Pressure profiles at 180 deg

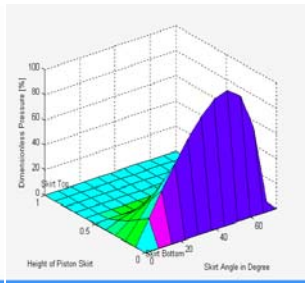

Fig 5.26(d) Pressure profiles at 240 deg

We have following comments on the EHL model simulation results:

1. EHD film thickness profile curves change visibly. The EHD film curves rise higher than peak maximum film thickness between 200-300 degree rotations.
2. The film curves rise sharply to very high value & then drops between 430-500 degrees.
3. EHD film thickness profile follows the same trend as that of film thickness profile determined using inverse solution. The magnitudes of both EHD films vary further.

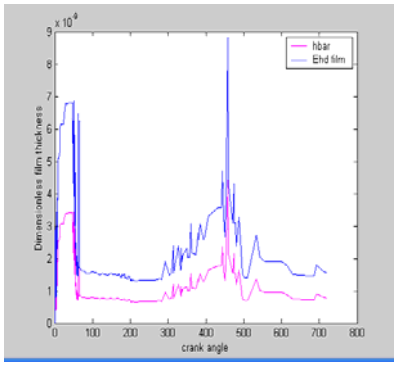

Fig 5.26(e) EHD Film Thickness

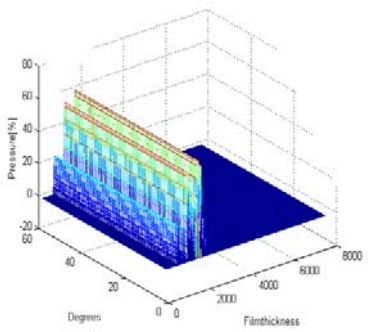

Fig 5.26(f) EHD Pressures

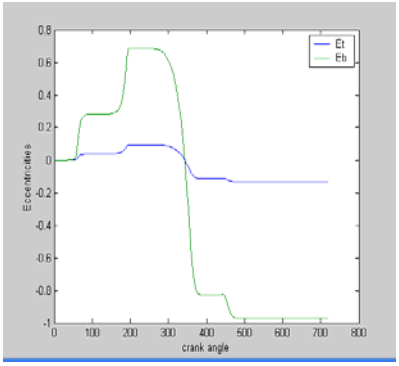

Fig 5.26(g) Piston Eccentricities

4. Peak values of EHD pressures rise from originally around 55% to 78%. This increase is quite significant as elastic deformations increase due to intense pressures.
5. With this increase in radial clearance from initial value of 10 microns to 50 microns in the initial engine start up EHD film thickness values change further, which is very

important to consider. This is because corresponding EHD pressures raise is quite significant.

100 micron

Comparison is given at 100 micron radial clearance respectively

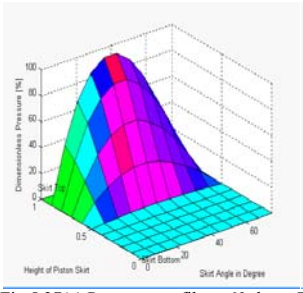

Fig 5.27(a) Pressure profile at 60 deg

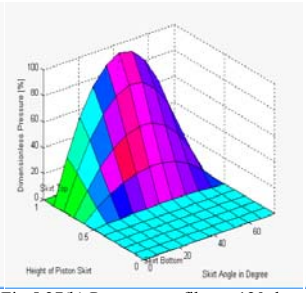

Fig 5.27(b) Pressure profiles at 120 deg

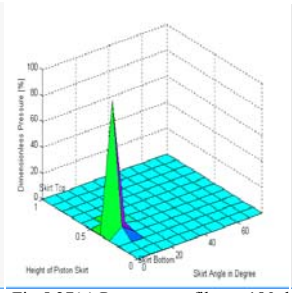

Fig 5.27(c) Pressure profiles at 180 deg

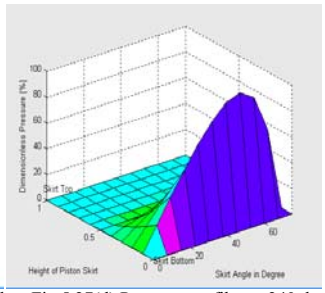

Fig 5.27(d) Pressure profiles at 240 deg

Briefly, we analyze those results one by one. In the basic piston skirts lubrication model we have following observations on the results:

1. There are some significant changes in the maximum & minimum oil film thickness profiles curves. There are no sudden spikes in the profile curves from 350 to 500 degree of crank rotation.
2. The film thickness profile curves do not have any sudden sharp rise and fall after 500 degree in contrast to the original case.
3. The curve for piston eccentricity at the skirt top (E_t) when shifted to the major thrust side (lower line) touches the lower line at 474 degree angle. Hence solid-to-solid contact is established between piston skirt top and cylinder liner surfaces, which remain till the end of cycle at 720 degree. Hence, there is real damage to piston skirts surface during this period.
4. In the expansion and exhaust strokes the pressure fields deteriorate such that very sharp and very concentrated pressures at particular points of piston skirt surface are witnessed. These pressures are no more hydrodynamic pressures but are generated due to solid-to-solid contacts. Such pressures could cause significant damage to the skirts surface.

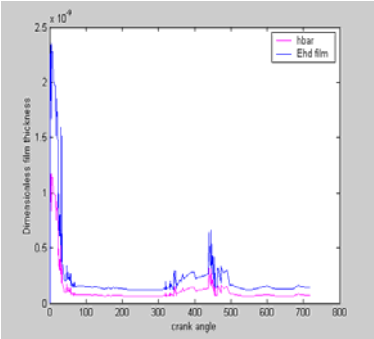

Fig 5.28(e) EHD Film Thickness

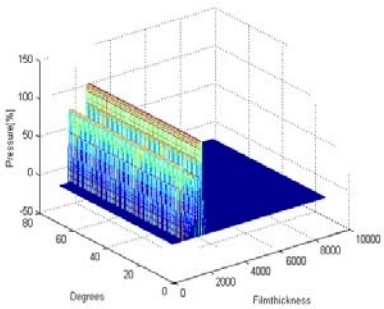

Fig 5.28(f) EHD Pressures

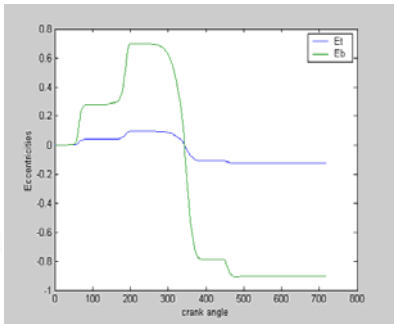

Fig 5.28(g) Piston Eccentricities

5. Steeper and concentrated pressure fields in the initial crank rotation angles indicate misalignment of piston skirts with the cylinder walls especially during the intake and compression strokes.
6. This misalignment affects the actual clearances between skirts and bore resulting in difficulty in maintaining actual operating clearances during normal engine operation.

CHAPTER-6

SIMULATION RESULTS & ANALYSES OF NON-NEWTONIAN RHEOLOGY BASED EHL OF PISTON SKIRTS IN THE INITIAL ENGINE START UP

6.1 Comparative Analysis of Viscoelastic & Rheological Models

Viscoelastic model

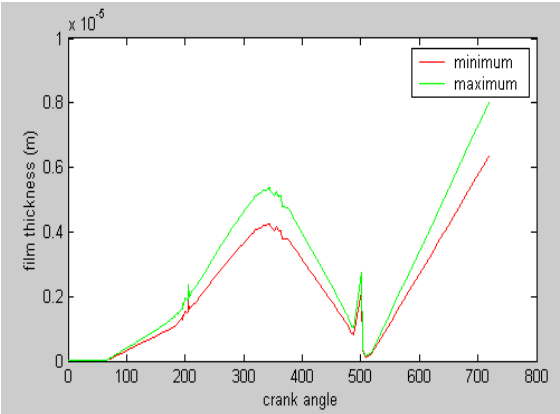

Fig 6.1(a) Film Thickness profiles of viscoelastic model

Rheological model

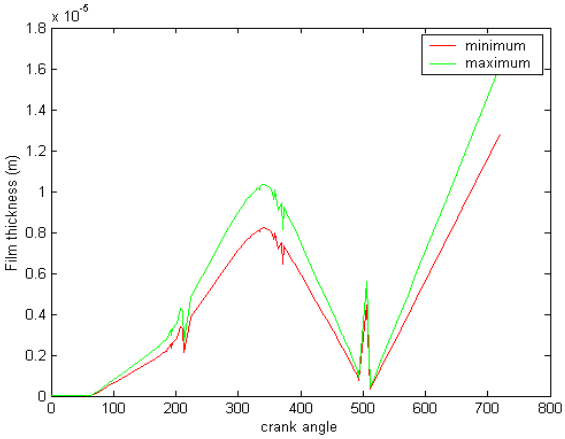

Fig 6.1(b) Film thickness profiles of Rheological model

In the Fig 6.1(a) & Fig 6.1(b) non-Newtonian viscoelastic isothermal Film Thicknesses are compared with Viscoelastic Adiabatic Film Thicknesses, maximum and minimum hydrodynamic film thickness profiles as a function of 720 degree crank rotation are plotted to represent film thickness magnitudes against corresponding piston positions for the four engine strokes. The sudden rise and fall of film thickness value indicates that at that particular point of time the there is sudden corresponding drop in the EHD pressures, which is restored again after that brief interval. It is clearly seen from the plots that the maximum Film thickness in the viscoelastic model has increased compared to that of Newtonian isothermal model, which when related to the values of Shear Stress and Coefficient of Friction shows that Shear Stress and Coefficient of Friction has also decreased. It implies that there are lesser shearing and reduced frictional losses when adiabatic phenomenon has been incorporated and hence the maximum value of Film Thickness has reduced which shows drop in viscosity which leads to better load carrying capacity.

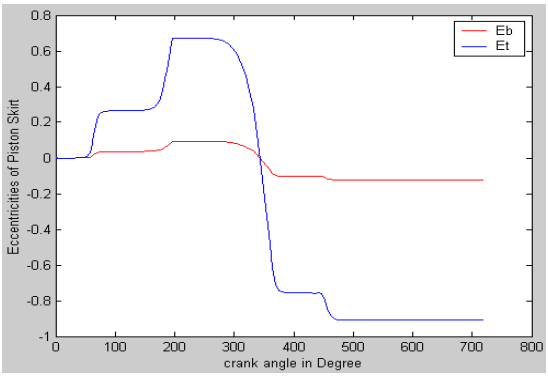

Fig 6.2(a) Piston Eccentricities vs Crank angle

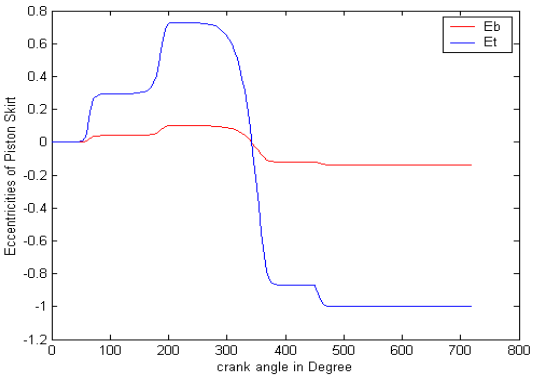

Fig 6.2(b) Piston Eccentricities vs Crank angle

In isothermal viscoelastic lubrication model, dimensionless piston eccentricities 'E_t' & 'E_b' are clearly shifted towards the major thrust side as well as minor thrust side in the entire cycle of piston motion. In adiabatic viscoelastic case 'E_t' & 'E_b' are negligible from the start and then shifts toward minor thrust side and finally shifts towards major thrust side and is more safely away from lower horizontal line.

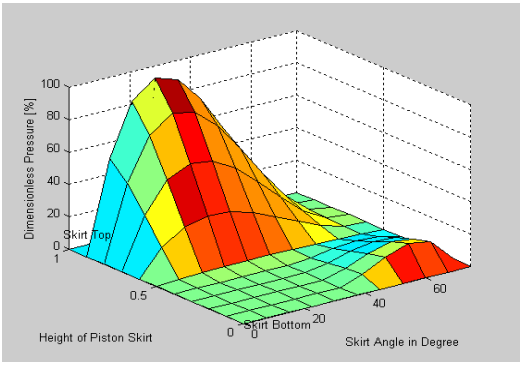

Fig 6.3(a) Hydrodynamic pressures at 120 deg

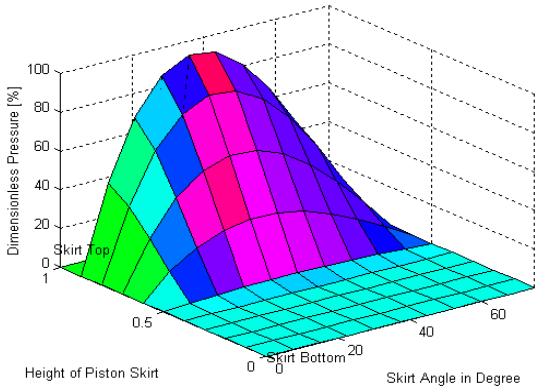

Fig 6.3(b) Hydrodynamic Pressures at 120 deg

Refer to figure 6.3(a), in viscoelastic isothermal model Positive pressures generate from mid to the skirt top surface. Refer to figures 6.3(b), In adiabatic viscoelastic model the pressure distribution is uniform through the entire crank rotation angles, which indicates perfectly aligned piston skirts model, maintaining desirable clearances throughout the entire cycle when shear thermal effects are incorporated. The slope is gentle till the mid-stroke after it starts getting steep, peak pressures shift towards right and all this happening with increasing film thickness, coefficient of friction and shear stress. It implies that an increase in frictional losses and more shear stress generation could shift hydrodynamic peak pressures along with an increase in steepness of profile slopes.

Fig 6.4(a) Hydrodynamic pressures at 240 deg

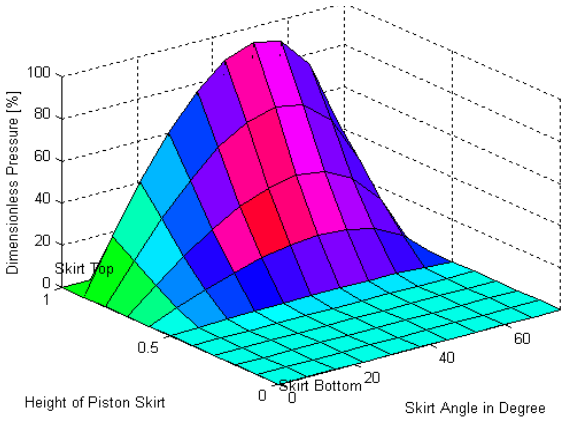

Fig 6.4(b) Hydrodynamic Pressures at 240 deg

Refer to figure 6.4(a), Viscoelastic isothermal model positive pressures generate from mid to the skirt top surface till 240 degree angle. Refer to figure 6.4(b), in the adiabatic viscoelastic model the intake stroke peak hydrodynamic pressure values are closer to the piston skirt top surface showing gentle slope of instantaneous pressure fields. While in the compression stroke slopes of instantaneous pressure fields start getting steep with corresponding sharp rise in peak pressures but still these peak values develop closer to the skirt top surface plane. The slope gets steeper till one-third of the compression stroke after which positive pressures start shifting towards skirts bottom and all this happens with further rise in the film thickness, coefficient of friction and shear stress. It implies that increase in frictional losses and more shear stress generation shift hydrodynamic pressure fields towards skirts bottom along slight increase in steepness of profile slopes.

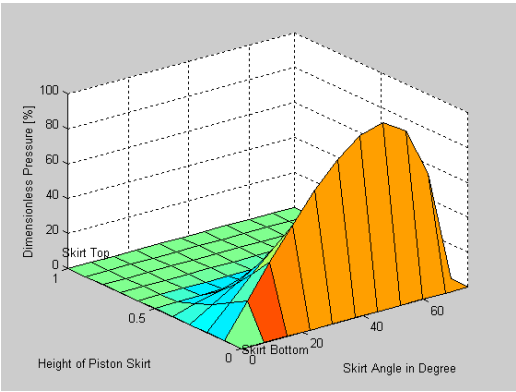

Fig 6.5(a) Hydrodynamic pressures at 360 deg

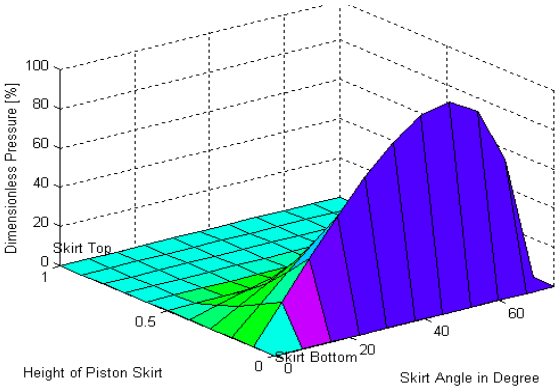

Fig 6.5(b) Hydrodynamic Pressures at 360 deg

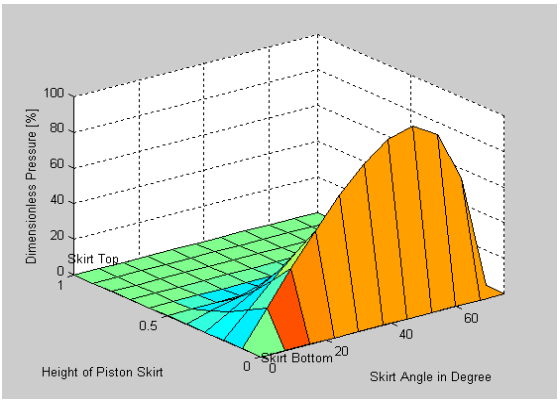

Fig 6.6(a) Hydrodynamic pressures at 480 deg

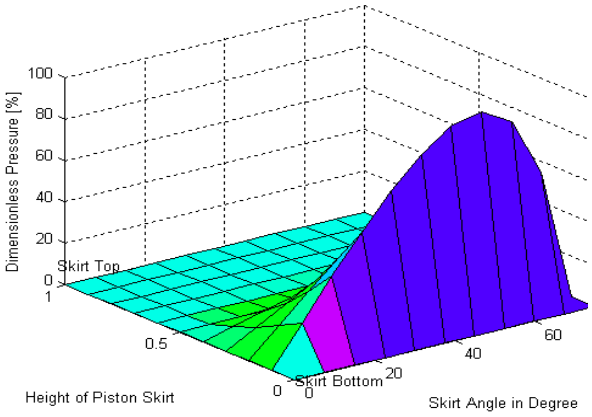

Fig 6.6(b) Hydrodynamic Pressures at 480 deg

Refer to figures 6.5(a) and 6.6(a) In the Newtonian model piston expansion strike the slope of instantaneous pressure fields gets steeper and peak pressures shift towards the right side of piston skirt top surface plane till the mid of expansion stroke. From the mid-point of the expansion stroke to the end of it when piston reaches the bottom dead center (BDC), the pressure field gradients as well as peak values shift towards piston skirt bottom surface from the top edge. This is a very significant change in the entire cycle. In the exhaust stroke the pressure fields develop over the piston skirt bottom surface plane and we witness peak values of pressure to be developing at the extreme edges of skirt bottom surface .Refer to figures 6.5(b) and 6.6(b), In viscoelastic model which show pressure fields over the skirts surface in the power/expansion stroke of piston at 480 and 540 degree crank rotation respectively. Positive pressures generate from mid to the skirt bottom surface till 540 degree angle. The slope gets steep till one-third of the stroke after which positive pressures slightly shift in the mid values over the skirts bottom and all this happens with further rise in the film thickness, coefficient of friction and shear stress. It implies that further increase in frictional losses and more shear stress generation with instantaneous reduction and then rise in film thickness keep hydrodynamic pressure fields at the skirts bottom along slight increase in steepness of profile slopes.

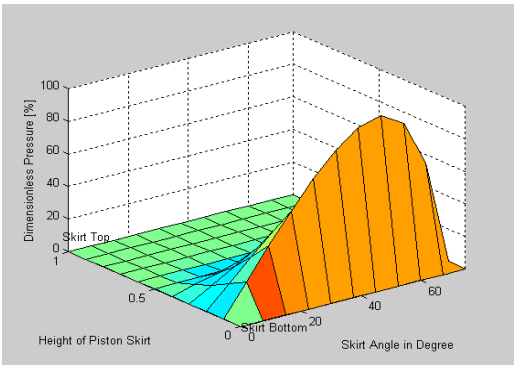

Fig 6.7(a) Hydrodynamic pressures at 600 deg

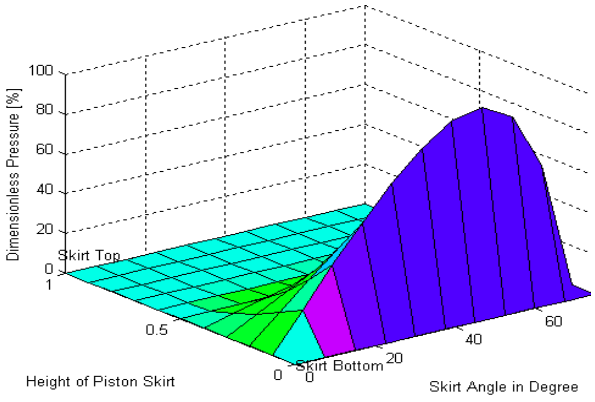

Fig 6.7(b) Hydrodynamic Pressures at 600 deg

Refer to figures 6.7(a) and 6.8(a), In the exhaust stroke the pressure fields develop over the piston skirt bottom surface plane and we witness peak values of pressure to be developing at the extreme edges of skirt bottom surface. Refer to figures 6.7(b) and 6.8(b), which show pressure fields over the skirts surface in the exhaust stroke of piston at 600 and 720 degree crank rotation respectively. Positive pressures generate from mid to the skirt bottom surface till 540 degree

angle. The slope gets further steep till mid of the stroke after which positive pressures slightly shift in the mid values over the skirts bottom and all this happens with further rise in the film thickness, coefficient of friction and shear stress. It implies that a further increase in frictional losses and more shear stress generation with instantaneous reduction and then rise in film thickness keep hydrodynamic pressure fields at the skirts bottom along with slight increase in steepness of the profile.

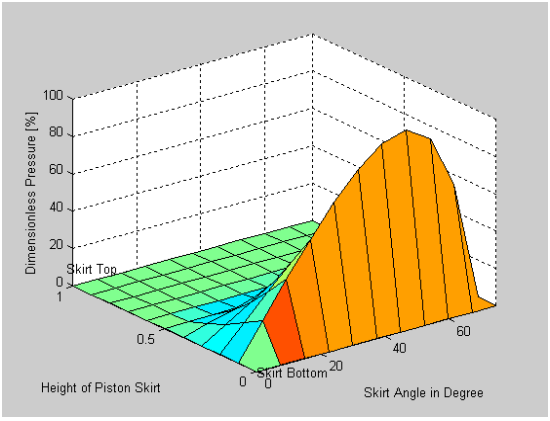

Fig 6.8(a) Hydrodynamic pressures at 720 deg

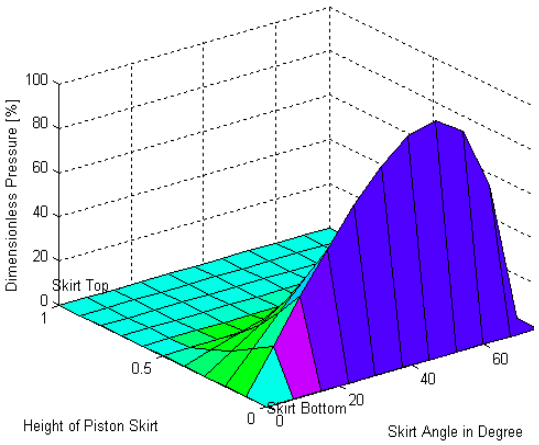

Fig 6.8(b) Hydrodynamic Pressures at 720 deg

6.2 Parametric Studies & Analysis of Rheological EHL Model

Parametric study-1

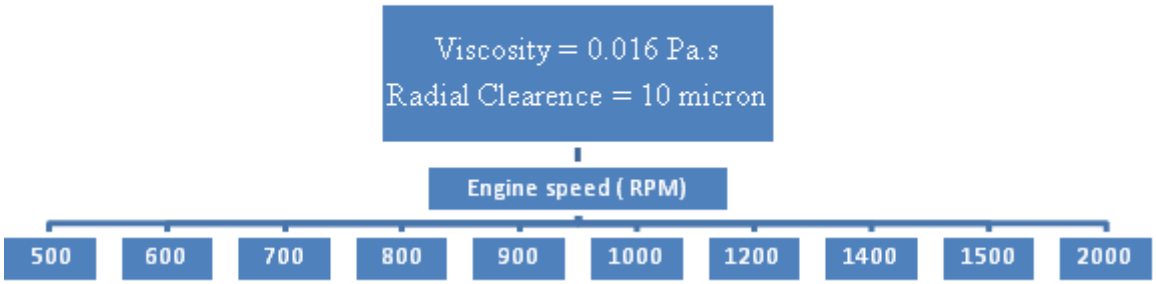

Parametric study-2

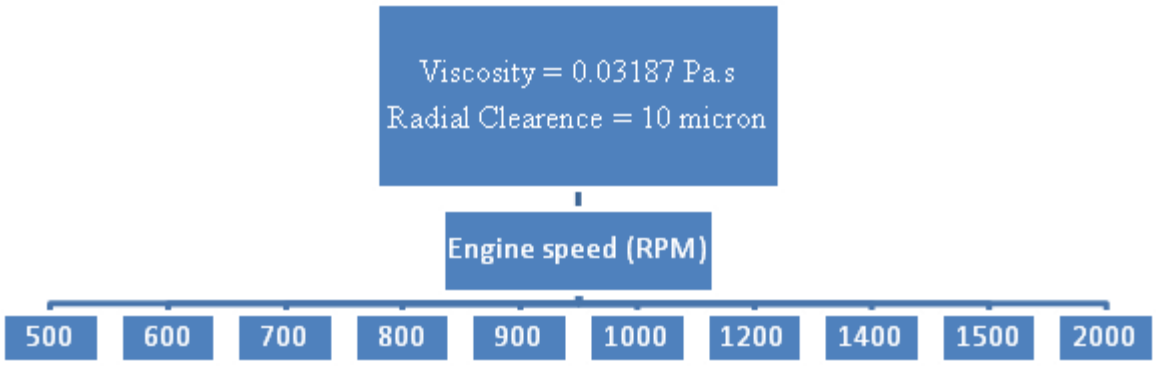

Parametric study-3

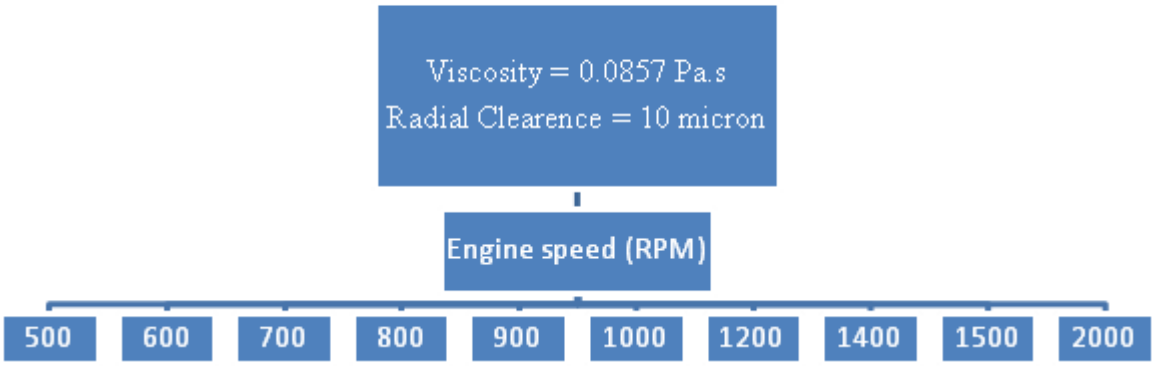

Parametric study-4

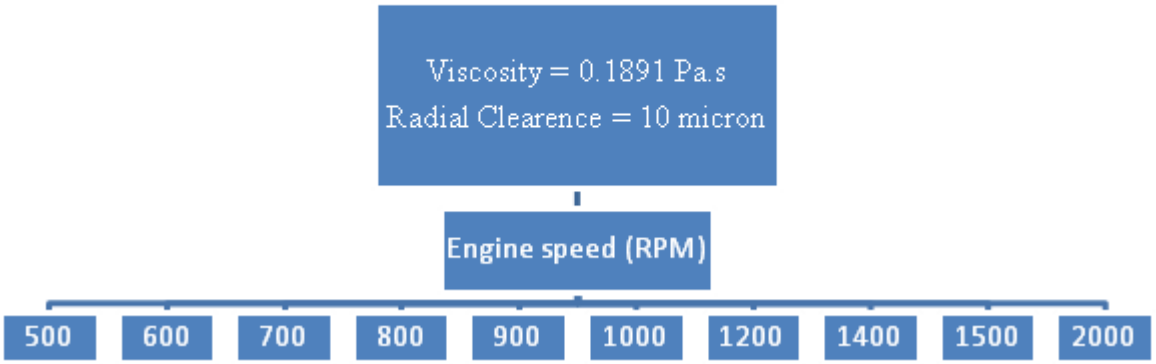

6.2.1 'SPEED' Parameter Analysis

In the speed Parameter analysis, Effects of rheology on different parameters are analyzed in the speed range between 500-2000 rpm. The brief overview of the results that vary with speed are shown in general and then the overview of results in particular at different initial start up speed ranges are shown, The initial start up speed ranges are defined as low start up speed range, medium start up speed range and high start up speed range and are discussed in detail in the coming section.

600 rpm

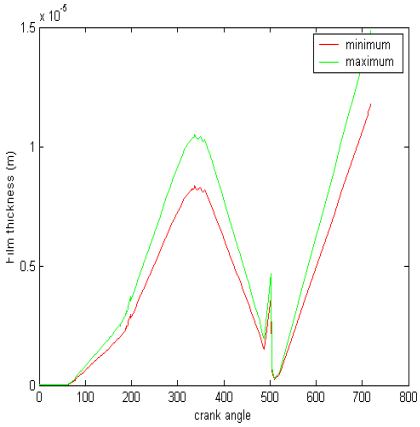

Fig 6.9(a) Film Thickness profiles

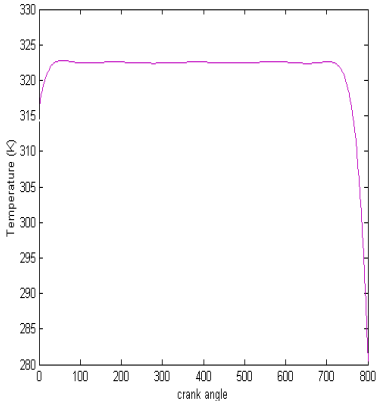

Fig 6.9(b) Temperature Profile

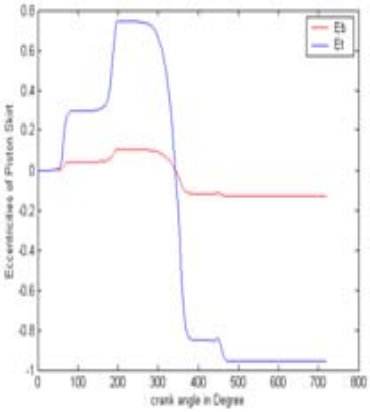

Fig 6.9(c) Piston Eccentricities

We have following comments on the EHL model simulation results:

1. In the piezoviscous regime EHD film thickness profiles are not reduced as drastically as when clearance is 10 micron.
2. EHD film thickness is very small up to 42 degree rotation then rises, attains a reduced peak value at 230 degree and then drops down to a small value.
3. EHD film thickness curve rises to peak value at 478.5-degree crank rotation. It drops down to minimum value at 550-degree crank angle and maintains same magnitude till the end of crank rotation cycle.
4. Since EHD film thickness values do not drop much, these are in comparable proportion to the hydrodynamic film thickness values. This was not the case when radial clearance was taken as 10 micron. This means that here, film thickness is still in the rigid & mixed hydrodynamic range. Once this is so, then no EHD pressure profiles could be generated.
5. At piston-to-bore radial clearance of 100 micron, solid-to-solid contact gets established due to which rigid hydrodynamic pressure fields change into extremely high Hertzian pressures (due to solid-to-solid contacts) & hence EHD pressure field cannot be generated.

1000 rpm

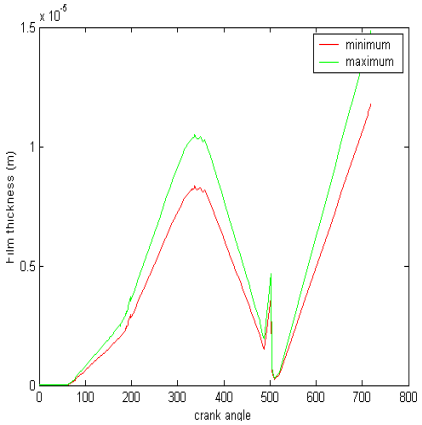

Fig 6.10(a) Film Thickness profiles

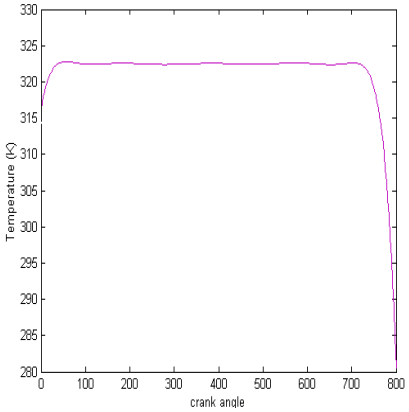

Fig 6.10(b) Temperature profiles

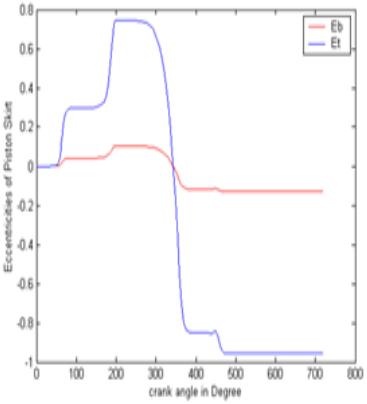

Fig 6.10(c) Piston Eccentricities

We have following comments on the EHL model simulation results:

1. There are two very prominent and high surges noticed in the overall EHD film thickness curves. More significant among these is a very sharp and high peak value obtained at 236 degree, which drops down to minimum value again at around 280 degree.
2. EHD film thickness curves have minimum values till 465 degree crank rotation. Then there is a notable surge with peak values (less than before) obtained at 478 degree angle. This peak values drop down to minimum magnitudes at 490 degree. The minimum values of profile curves are maintained till 720 degree when the rotation cycle completes.
3. There are three small surges in the maximum and minimum film thickness profiles, which occur between 350 degree and 400 degree of crank rotation.
4. Peak values of EHD pressures rise from originally around 55% to 95%. This increase in EHD pressures is quite significant as elastic deformations increase due to shift in EHD pressures from medium to high ranges. Hence we must be very careful to decide the viscosity of lubricant in the initial engine start up as any reduction in oil viscosity means increased EHD pressures generation and build up.

2000 rpm

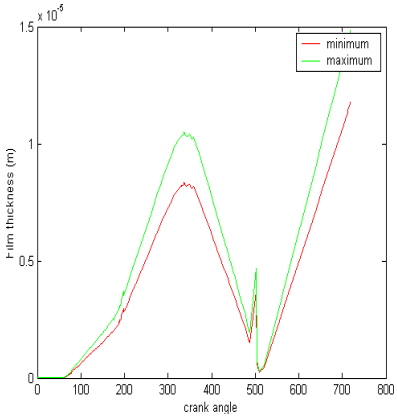

Fig 6.11(a) Film Thickness profiles

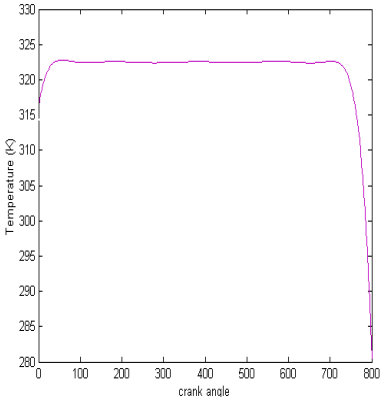

Fig 6.11(b) Temperature profiles

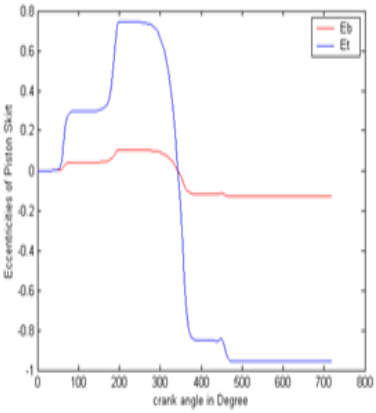

Fig 6.11(c) Piston Eccentricities

6.2.2 'VISCOSITY' Parameter Analysis

In the viscosity Parameter analysis, to see the effects of Shear heating in initial engine start up we have considered three different viscosity oils, SAE-10, SAE-30 and SAE-50. The behavior of Film Thickness profiles and temperature profiles are analyzed on these different viscosities and the general trend is the same.

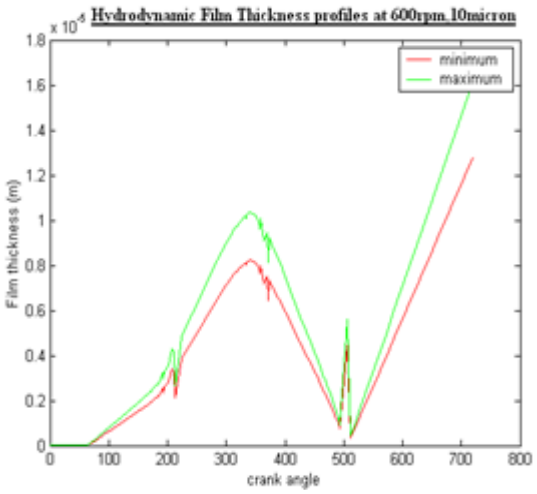

Fig 6.12(a) Hydrodynamic Film Thickness Profiles

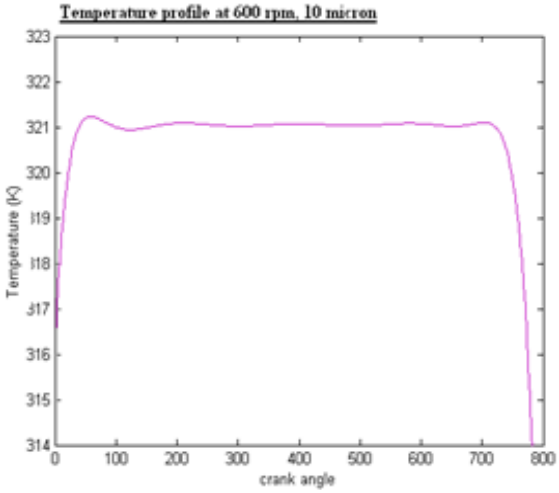

Fig 6.12(b) Temperature vs Crank angle

CHAPTER 7

COCLUSIONS & RECOMMENDATIONS

Conclusions:

According to our EHD model analysis of piston skirt and liner surface, it can safely be inferred that in order to avoid adhesive wear of piston skirts during initial engine start up, an extensive research effort at PhD level must be done, using modern modeling and simulation techniques along with the experimental work, fundamental engine design parameters must be incorporated and analyzed. And hence a very comprehensive and more realistic model can be developed, which will make future researchers understand the engine start up wear phenomenon in more detail. For that matter our model could serve as a foundation stone on which a more realistic research based structure could be built in future.

Based on the findings of our existing EHL model of piston in the initial engine start up we draw following useful conclusions:

1. It is possible to establish EHD lubricating film at initial engine start up which is shown in our parametric studies.
2. Engine start up speed of 500 rpm is more appropriate than that of higher engine start up values i.e., 2000 rpm. At 2000 rpm instantaneous EHD film thickness values rise in significant proportion to the maximum & minimum film thickness values. Percentage peak EHD pressures at 2000 rpm also rise to around 79% from around 43% at 500 rpm.
3. At 2000 rpm there is clear indication of solid-to-solid contact between piston skirt top and major thrust side of cylinder liner surfaces despite having fully flooded regime. Moreover, instantaneous EHD film thickness values raise further to still more significant proportions to the maximum & minimum film thickness values. Percentage peak EHD pressures at 2000 rpm also rise to more than 130% from around 55% at 500 rpm.
4. An increase in engine start up speed from 500 rpm to 2000 rpm and beyond means generating very high EHD pressures as compared to medium range of EHD pressures at 500 rpm. Transforming EHD pressures from medium to high ranges in the initial engine

start up could lead to significant damage under adverse engine operating conditions. So, we must try to keep EHD pressures within medium ranges.

5. In case of radial clearance between piston and cylinder liner walls, we conclude that 5 micron clearance is most appropriate as compared to 50 micron or 100 micron.
6. At 50 micron radial clearance instantaneous EHD film thickness values raise significantly on at least two occasions as compared to the maximum & minimum film thickness values. Percentage peak EHD pressures at 50 micron rise to around 78% at 50 micron clearance from around 55% at 10 micron clearance.
7. At 100 micron radial clearance it is not possible to avoid solid-to-solid contact between piston skirt top and major thrust side of cylinder liner surfaces despite having oil flooded regime. At such clearance the hydrodynamic pressure fields break down to intense pressures due to solid-to-solid contacts. The damage will be more severe in such a case.
8. Lubricant viscosity value of 0.03187 Pa.S seems more appropriate than other oils as percentage peak EHD pressures at other oils rise to around 85% from around 50% at 0.03187 Pa.S.

RECOMMENDATIONS:

In our research work we have developed a simplified EHL model of piston skirt and cylinder liner surfaces in the initial engine start up by exploring key fundamental aspects of transient EHD phenomenon. This model was simplified by considering number of logical assumptions to avoid certain non-linear and highly complex aspects of actual piston lubrication phenomenon. All these assumptions make our existing model as more close to ideal situations than applicable to actual ground realities. Now there is a need to explore all such complex non-linearities to reach to some final definite conclusions. By considering this model as the starting point for future researchers some of the more complex aspects are indicated below for further research and exploration of EHL phenomenon in the initial engine start up:

1. Thermoelastohydrodynamic (TEHD) lubrication phenomenon of piston in the initial engine start up.

2. Incorporation of ‘Squeeze Film Effect’ phenomenon in the calculation of hydrodynamic pressures.
3. Incorporation of (actual) rough piston skirt & cylinder liner surface profiles & textures with associated surface roughness & waviness factors & their effects on EHD film generation.
4. Exploration of all other forms of elastic deformations of piston and liner surfaces as applicable to the initial engine start up conditions and their incorporation into existing model of EHL phenomenon
5. Incorporation of thermally induced deformation of piston.
6. Incorporation of Different material properties of Piston and Liner.

‘MATLAB’ PROGRAM CODE FOR INTERFACE-SIMULATION OF EHL OF PISTON SKIRTS

```
function triboloy(action)
munlock; global  tbs tbgp tbp tbt tbge tbgr tbr;
if  nargin < 1, action = 'initialize'; end;
action = 'initialize'
if  strcmp (action,'initialize')
  oldFigNumber = watchon;
figNumber = figure('Name','EHD Lubricaton of Piston And Rings','NumberTitle','off','Visible','off','Color',[0.85
0.6 0],'ColorMap',[0 0 1])
figDefaultAxesPos = [0.10 0.10 0.63 0.80]; set(figNumber,'DefaultAxesPosition',figDefaultAxesPos);
  axes('Units','normalized','Position',figDefaultAxesPos);
  top = 0.35; left = 0.05; right = 0.75; bottom = 0.05; labelHt = 0.05; spacing = 0.005;
  %=============================================
      labelColor = [0.2 0.2 0.2]; top = 0.95; left = 0.78; btnWid = 0.18; btnHt = 0.06; spacing = 0.03;
  %=============================================
  % The CONSOLE frame
      frmBorder = 0.02; yPos = 0.05 - frmBorder; frmPos = [left - frmBorder yPos btnWid + 2 * frmBorder 0.9
+ 2 * frmBorder];
      uicontrol('Style','frame','Units','normalized','Position',frmPos,'BackgroundColor', [0 0.5 1]);
  %=============================================
      % The piston button
      btnNumber = 1; yPos = top - (btnNumber - 1) * (btnHt + spacing); labelStr = 'Piston Basic Model';
callbackStr = 'tribology("tribobutton")';
      btnPos = [left yPos - btnHt btnWid btnHt];    tbs = uicontrol('Style','radiobutton', ...'Units','normalized', ...
  'Position', btnPos, ...'BackgroundColor',[0.9 0.5 0], ...'ForegroundColor',[1 1 1], ...'FontWeight','bold', ... 'String',
labelStr,....
        'Callback',str2mat('partial'));
  %=============================================
  btnNumber = 2; yPos = top - (btnNumber - 1) * (btnHt + spacing); labelStr = 'Graphs-Piston Model';
callbackStr = 'tribology("tribobutton")';        btnPos = [left yPos - btnHt btnWid btnHt];    tbgp =
uicontrol('Style','radiobutton', ...Units','normalized', ...
      'Position', btnPos, ...'BackgroundColor',[0.9 0.5 0], ... 'ForegroundColor',[1 1 1], ...'FontWeight','bold', ...
'String', labelStr,....
        'Callback',str2mat('graphpis'));
  %=============================================
```

```
% The PARTIAL button
    btnNumber = 3; yPos = top - (btnNumber - 1) * (btnHt + spacing); labelStr = 'EHD Model'; callbackStr =
'tribology("tribobutton")';  btnPos = [left yPos - btnHt btnWid btnHt];   tbp = uicontrol('Style','radiobutton', ...
    'Units','normalized', ...      'Position',btnPos, ...'BackgroundColor',[0.9 0.5 0], ...  'ForegroundColor',[1 1
1], ...
      'FontWeight','bold', ...  'String',labelStr, ... 'Callback',str2mat('partailehd'));
%==============================================
% The DEFLECTION button
    btnNumber = 4; yPos = top - (btnNumber - 1) * (btnHt + spacing); labelStr = 'Graphs- EHD '; callbackStr
= 'tribology("tribobutton")';          btnPos = [left yPos - btnHt btnWid btnHt];   tbge =
uicontrol('Style','radiobutton', ...'Units','normalized', ...
    'Position',btnPos, ...BackgroundColor',[0.9 0.5 0], ...'ForegroundColor',[1 1 1], ...'FontWeight','bold',
...'String',labelStr, ...
    'Callback', str2mat('graphehd'));
%==============================================
watchoff(oldFigNumber); figure(figNumber);
 elseif  strcmp(action,'tribobutton'),   cmdStr = get(gco,'UserData'); mcwHndl = findobj(gcf,'Tag','mcw');
set(mcwHndl,'String',cmdStr); evalmcw(mcwHndl);   pause 'tributton' elseif  strcmp(action,'eval'),
mcwHndl = findobj(gcf,'Tag','mcw'); cmdStr = get(mcwHandl,'String'); evalmcw(mcwHndl); pause 'eval' elseif
strcmp(action,'info'),
strhlp = {'Tribology' help('introduction');          'Viscosity'          help('viscosity'); 'Simple'   help('simple');
'Partial'   help('partial');
    'Thermal'   help('thermal');   'Deflection' help('deflection');    'Groove'    help('groove');  'Stability'
help('stability');};
    helpwin(strhlp,'Tribology','Engineering Triboloyy - Info');   pause 'info' end;
```

GOVERNING 'MATLAB' CODE FOR ODE SOLUTION-BASIC CODE FOR PISTON SKIRTS MODEL

```
function [de]=dedtp(t,y)
global h22 h33 h44 ;global stno; global residp;global reslim1;global alpha;global inode;global jnode;global
N;global C;global nlim1; global factor1;global I;global wFh;global M;global t1;global ffh1;global h;global
h0;global beta;global reslim2;global residb; global nlim2;global factor2;global Pressure;global indx;global
p44;global visc;global P;global cou;global P1;global dpdx;global d2pdx2;
global deltax;global flag1;global RP;global RC;global hh244;global H1;global H2;global indx1;global
nTORR;global Torr;global myu;
global hhbar;global visc;global hhbar1;global mfh1;
```

```
e2b=y(1);2t=y(2);eb=y(3);et=y(4);indx=indx+1;hbar=[];
%*****************************************************
de = zeros(4,1);    % a column vector
%*****************************************************
CP=.001;r=0.0418;l=0.15;visc=0.0016;u=0.1;V=2*pi*N*r/60;w=V/r;w=w/57.29578;Et=et/C;Eb=eb/C;
A1=[0 90 180 270 310 360 372 378  450 540 630  720  810  900  990  1080 1120  1170  1182 1188  1260  1350
1440 1530 1620 ...        1710        1800        1840        1890        1902        1908
  1980 2070 2160        2250        2340        2430        2520        2610 ...
 2650  2700 2712        2718        2790        2880        2970        3060]';
A2=[0.1 0.1 0.1  500 1020 11500 20500 19000 2200 0.1 0.1 0.1 0.1  500 1020 11500 20500 19000 2200 0.1 0.1
0.1 0.1  500 1020 11500 20500 19000 2200 0.1 0.1  0.1 0.1  500 1020 11500 20500 19000 2200 0.1 0.1 ]';
FG=interp1(A1,A2,t*3600, 'cubic');tdispm=4*.0836;    A=CP+r*sin((I)/57.29578);    Y=((l+r)^2-CP^2)^.50-
(l^2-A^2)^0.50-r*cos(I/57.29578);    U=r*w*sin(I/57.29578)+r*w*A*cos(I/57.29578)*((l^2-A^2)^-0.5);
    aY=r*w^2*cos((I)/57.29578)+(r*w*A*cos((I)/57.29578))^2*(l^2-A^2)^-1.5+((r*w*cos((I)/57.29578))^2-
r*w^2*A*sin((I)*57.29578))*(l^2-A^2)^-0.5;    phi=atan(A*(l^2-A^2)^-0.5);
    FIC=-MPIS*aY;    FIP=-MPIN*aY;    FS=(tan(phi))*(FG+FIP+FIC);    MS=FG*CP-FIC*CG;
L=.0338; B=(2*pi*.0836)/2;  slender = B/L; deltax = alpha/(inode-1); deltay = 1/(jnode-1);
M = zeros(inode, jnode); P = zeros(inode, jnode);EA=200*(10^9); EBB=200*(10^9);  density=.7;
 n2 = 0; betas = 0; residb = reslim2 + 10;
while (residb > reslim2) & (n2 < nlim2),
  n2 = n2 + 1;
 for i = 1: inode,
   xaux = (i-1)*deltax + pi - 0.5 * alpha;     x1=xaux*C;
   for j = 1: jnode,
      y = (j-1) * deltay - 0.5;  y1=y*C;   yaux=y1;        h0=Et*cos(xaux)-(Et-Eb)*y*cos(xaux)+1;
h0=abs(h0);
       dhdx0  = -Et*sin(xaux)+(Et-Eb)*y*sin(xaux); d2hdx20 = -Et*cos(xaux)+(Et-Eb)*y*cos(xaux);  dhdy0  =
-(Et-Eb)*cos(xaux);
         dhdy0  =  -(et-eb)*cos(xaux/r); d2hdy20 = 0; ho=Et-(Et-Eb)*y+1; h1=Et*cos(1/C)-(Et-
Eb)*y*cos(1/C)+1;        H(i,j) =h0;
       G(i,j) = dhdx0/h0^1.5;        F(i,j) = 0.75*(dhdx0^2 + (slender*dhdy0)^2)/h0^2 + 1.5*(d2hdx20 +
d2hdy20*slender^2)/h0;
hm = mean(H(i,j));
hd(i,j) =((3/8*((hm^2/h1^4)-(hm^2/ho^4)))-(-1/2*(hm/h1^3)-(hm/ho^3))+((1/6)*((1/h1^2)-
(1/ho^2))))/(2*(1/ho^2-1/h1^2));
 dpdxe(i,j)=(12*((H(i,j)^3-hm)/H(i,j)^3))+ (2*(3*(hm/H(i,j)^3)+(2/H(i,j)^2)*dhdx0));
 dpdxd(i,j)=(-18*(hm^2/h0^5)*(dhdx0))+(18*(hm/h0^4)*dhdx0)-(4*(1/h0^3)*(dhdx0))-(12*(hd(i,j)/h0^3));
 if i>1 dpdxl(i,j) = ((P(i,j)-P(i-1,j)))/deltax; end;
```

```
      if i == 1, dpdxl(i,j) = P(2,j)/deltax; end;
      dpdx(i,j)=dpdxl(i,j)+(0.9*dpdxe(i,j))+(0.9*dpdxd(i,j));      dpdx(i,j)=dpdx(i,j)+(dpdx(i,j)==0)*eps;
  end;  end;
   coeff1 = 1/deltax^2;  coeff2 = (slender/deltay)^2;
   %================================
   %SUBROUTINE TO SOLVE THE VOGELPOHL EQUATION
   sum2 = 0; n1 = 0; residp = reslim1 + 10;
   while (residp > reslim1) & (n1 < nlim1),
     n1 = n1 + 1; sum = 0;
     for i = 2: inode-1,
       for j = 2: jnode-1,
         store = ((M(i+1,j) + M(i-1,j))*coeff1 + (M(i,j+1) + M(i,j-1))*coeff2-G(i,j))/(2*coeff1 + 2*coeff2 + F(i,j));
         M(i,j) = M(i,j) + factor1*(store-M(i,j));
         if  M(i,j) < 0, M(i,j) = 0; end;
         sum = sum + M(i,j);
       end;   end;
    if(sum==0)
       sum=0.0001;
    end
    residp = abs((sum - sum2)/sum); sum2 = sum;
  end;
 % ========================
   % FIND PRESSURE FIELD FROM VOGELPOHL PARAMETER
   for i = 2: inode-1,
     for j = 2: jnode-1,
       P(i,j) = M(i,j)/H(i,j)^1.5;
     end;  end;
   % CALCULATE TRANSVERSE AND AXIAL LOADS
    % ====================================
  for i = 1: inode,
      SUMY(i) = 0;
      for j = 2: jnode, SUMY(i) = SUMY(i) + P(i,j) +P(i,j-1); end;
      SUMY(i) = SUMY(i)*0.5*deltay;
   end;
     axialw =0; transw = 0;
   for i= 2: inode,
      x = (i-1)*deltax + pi-0.5*alpha; x2 = (i-2)*deltax + pi - 0.5*alpha;
```

```
      axialw = axialw - cos(x)*SUMY(i)-cos(x2)*SUMY(i-1);     transw = transw + sin(x)*SUMY(i) +
sin(x2)*SUMY(i-1);
    end;
      axialw = axialw*deltax*0.5;      transw = transw*deltax*0.5;
    %================================
    loadw = sqrt(axialw^2 + transw^2);
    if  (axialw == 0)      axialw=0.0001;  end
     attang = atan(transw/axialw);   if  (axialw > 0)        attang1 = attang;    end;
     if  (axialw < 0)       attang1 = -attang;    end;
       beta = beta + factor2*attang1;   residb = abs((beta-betas)/beta);    betas = beta; end;
  % ==========================
  % SUBROUTINE TO CALCULATE PETROFF MULTIPLIER
  for j = 1: jnode, ICAV(j) = 1000; end;
  for j = 2: jnode-1,   for i = 2: inode,
      if  (M(i,j) == 0) & (ICAV(j) == 1000), ICAV(j) = i; end;
    end;end;
  % EXTRAPOLATED VALUES OF ICAV(J) AT EDGES OF BEARING
  ICAV(1) = 2*ICAV(2)-ICAV(3);if ICAV(1) < 1, ICAV(1) = 1; end;if ICAV(1) > inode, ICAV(1) = inode;
    ICAV(jnode) = 2*ICAV(jnode-1)-ICAV(jnode-2);end;if ICAV(jnode) < 1, ICAV(jnode) = 1; end;
  if ICAV(jnode) > i, ICAV(jnode) =0; end;
  % FIND VALUES OF DIMENSIONLESS SHEAR STRESS
  for i = 1: inode,
    for j = 1: jnode,
   if i == ICAV(jnode),  TORR(i,j) = 1*1/H(i,j) + 3*(dpdx(i,j)*H(i,j));
          TORR(i,j)=TORR(i,j)*(U*visc/C);
       end;
        if i > ICAV(jnode), TORR(i,j) = 1/H(i,j);  TORR(i,j)=TORR(i,j)*(U*visc/C);   end;     i10 = ICAV(j);
      if i < ICAV(jnode),  TORR(i,j) = 1*H(i10,j)/H(i,j)^2;      TORR(i,j)=TORR(i,j)*(U*visc/C);end;
  nTORR=nTORR+1;    end;  end; Torr=(mean(TORR));[ka,ia]=max(M);[la,ja]=max(ka);
kkk=max(H(ia(ja),ja));pmax = 0;
  for i = 2: inode-1,   for j = 2: jnode-1,
      if P(i,j) > pmax, pmax = P(i,j); end;
    end;end;
  if(mod(cou,2)==0)    h22=[h22 min(max(H))];    h33=[h33 min(min(H))];  h44=[h44 kkk(1,1)];
pp44=1/max(max(H));p44=[p44 pp44]; t1=[t1 t];hh244=hhbar*2;end; Ecy=200e+09; Ep=200e+09;%Pa
  %*************** Double Integration of Pressure*************************
  for i=1:inode
     SumY(i)=0;
```

```
      for j=2:jnode
         SumY(i)=SumY(i)+P(i,j)+P(i, j-1);        SumY(i)=SumY(i)*0.5*deltay;
      end;end;
   Prees=0;
   for i=2:inode
      Prees=Prees+SumY(i)+SumY(i-1);
   end
   DUBP=Prees*5*deltax;
   sigma1=0.5;sigma2=0.5;cfg1=(1-(sigma1)^2)/Ep;cfg2=(1-
(sigma2)^2)/Ecy;cfg=cfg1+cfg2;Ebar=2/cfg;dismue=(2/(pi*Ebar))*DUBP;
   for ind=1:inode
      for j=1:jnode
   hehd(ind, j)=kkk(1,1)+((ind^2)/2*RC)+dismue;end;end;
   %************************************************************************
   % INTEGRATE FOR TORR(i,j) OVER  X AND Y
   for i = 1: inode,
     % LINE INTEGRAL IN Y-SENSE for FFh
     SUMY(i) = 0;
     for j = 2: jnode,
        SUMY(i) = SUMY(i) + TORR(i,j) +TORR(i,j-1); end;
     SUMY(i) = SUMY(i)*0.5*deltay;
   end;
   friction = 0;
   for i = 2: inode,
      friction = friction + SUMY(i) + SUMY(i-1); end;friction = friction*0.5*deltax;  myu =
friction/loadw;Ffh=friction; ffh1=[ffh1 Ffh];
   %***********************Mfh**********************************
   %Mfh Moment about Pin due to Hydrodynamic friction
   mfh = 0;
   for i = 2: inode,
      x1 = (i-1)*deltax + pi - 0.5 * alpha;   x2=(i-2)*deltax + pi - 0.5 * alpha;    x1=x1*C;     x2=x2*C;
      mfh = mfh - cos(x1)*SUMY(i) -cos(x2)*SUMY(i-1); end;mfh = mfh*0.5*deltax; Mfh=(mfh)-CP*Ffh;
mfh1=[mfh1 Mfh];
   %================================
   %CALCULATE DIMENSIONLESS FRICTION COEFFICIENT
   if(flag1==1) hmax = 0;
   for i = 2: inode-1,
     for j = 2: jnode-1,
```

```
      P(i,j)=P(i,j)*(6*U*visc*B)/C^2; end;  end;end; pmax = 0;
  for i = 2: inode-1,
    for j = 2: jnode-1,
      if P(i,j) > pmax, pmax = P(i,j); end;
   end; end;
  % EXPRESS ALL PRESSURES AS PERCENTAGE OF MAXIMUM PRESSURE
  if(pmax==0)
     pmax=0.0001;
  end
  pmax=abs(pmax);
  for i = 1: inode,
    for j = 1: jnode,
       P(i,j) = abs(P(i,j))*100/pmax;
    end;end;
  P1(:,:,indx1)=P;H2(:,:,indx1)=H;indx1=indx1+1;cou=cou+1;IPIS=.5*MPIS*(Radius)^2;
  %**************************Fh
force************************************************************
  for i = 1: inode,
     for j = 1: jnode,
       FFH(i,j) = ((M(i,j)/H(i,j)^1.5))*(6*U*visc*B)/C^2;
     end;  end;
  for i = 1: inode,
   fhSUMY(i) = 0;  for j = 2: jnode, fhSUMY(i) = fhSUMY(i) + FFH(i,j) +FFH(i,j-1); end; fhSUMY(i) =
fhSUMY(i)*0.5*deltay;
    end; fh = 0;
  for i = 2: inode,
     x1 = (i-1)*deltax + pi - 0.5 * alpha;     x2=(i-2)*deltax + pi - 0.5 * alpha; x1=x1*C;     x2=x2*C;
     fh = fh - cos(x1)*fhSUMY(i) - cos(x2)*fhSUMY(i-1); end;fh = fh*0.5*deltax; Fh=fh;
  %*************************************************************************************
*****
  for i = 1: inode,
     for j = 1: jnode,
       FFH(i,j) = ((M(i,j)/H(i,j)^1.5));
     end;  end;
  for i = 1: inode,
      fhSUMY(i) = 0;
      for j = 2: jnode, fhSUMY(i) = fhSUMY(i) + FFH(i,j) +FFH(i,j-1); end; fhSUMY(i) = fhSUMY(i)*0.5*deltay;
end;  fh = 0;
```

```
   for i = 2: inode,
      x1 = (i-1)*deltax + pi - 0.5 * alpha;x2=(i-2)*deltax + pi - 0.5 * alpha; fh = fh - cos(x1)*fhSUMY(i) -
cos(x2)*fhSUMY(i-1); end;
   fh = fh*0.5*deltax;  wFh=fh;
   %**********************Mh**************************************************************************
****
    for i = 1: inode,
            xaux = (i-1)*deltax + pi - 0.5 * alpha;
      for j = 1: jnode,
        MH(i,j) = (M(i,j)/H(i,j)^1.5)*(6*U*visc*B)/C^2;   end;  end;
     for i = 1: inode,
          for j = 2: jnode,
         mfhSUMY(i) = mfhSUMY(i) + (a-j)*MH(i,j) +(a-j-1)*MH(i,j-1); end; mfhSUMY(i) =
mfhSUMY(i)*0.5*deltay;  end;
     for i = 2: inode,
      x1 = (i-1)*deltax + pi - 0.5 * alpha;x2=(i-2)*deltax + pi - 0.5 * alpha;  x1=x1*C;    x2=x2*C;
      mfh = mfh -cos(x1)*mfhSUMY(i) -cos(x2)*mfhSUMY(i-1); end;mfh = mfh*0.5*deltax;
   %**********************************************************************************************
*****
   A=[MPIN*(1-a/L)+MPIS*(1-b/L) MPIN*a/L+MPIS*b/L;MPIS*IPIS/L+MPIS*(a-b)*(1-b/L) MPIS*(a-b)*b/L-
MPIS*IPIS/L];
   BT=[Fh+FS+Ffh*tan(phi);MH+MS+Mfh];
   X=lsqr(A, BT);indx=indx+1;det=X(1);deb=X(2);de(1)=deb;de(2)=det;de(3)=e2b;de(4)=e2t;
```

‘MATLAB’ CODE FOR 2-D & 3-D GRAPHS OF PISTON SKIRTS BASIC MODEL SIMULATION

```
   clear all;clear global;
   global tbv tbs tbp tbt tbd tbg tbge tbgr tbgp tbr tba;global h22 h33 h44;global epsilon;global I;global
residp;global reslim1;global alpha;global inode;global jnode;global N;global C;global nlim1; global factor1;global
stno;global wFh;global M;global t1;global ffh1;global h;global h0;global beta;global reslim2;global residb;global
nlim2;global factor2;global indx;global Pressure;global p44;global visc;global P;global cou;global P1;global
dpdx;global d2pdx2;global hh244;global flag1;global RP;global RC;global H1;global H2;global indx1;global
hhbar;global TORR;global visc0;global hhbar1;global y; global T;global nTORR,global myu;global tbinfo;global
visc1;global fh;global Mfh;global mfh1;global Torr;
   indx=1;indx1=1; ffh1=[]; t1=[]; ia=[]; h44=[]; hh244=[]; h22=[]; h33=[]; p44=[]; PQ=[]; flag1=0; hhbar=[];
hhbar1=[];
   set([tbv tbs tbt tbd tbg tbgr tbge tbr ],'Enable','off');
```

```
indx=0;cou=1;
%BEGIN OF INPUT DATA
prompt = {'Speed(RPM)','Radial Clearance (m)','L/D ratio:','Piston skirt angle [o]:', 'Misalignment parameter
from interval [0,0.5]:', 'Viscosity [Pa.s]','Radius of Piston [m]'};
title = 'INPUT DATA (PISTON-Basic Model)'; lineno = 1; ep=num2str(epsilon);def = {'600','.00001','.5','75','0',
'0.01600', '0.0415'}; answer = inputdlg(prompt,title,lineno,def, 'off');
if  size(answer) == 0, %PROGRAM IS TERMINATED
   set(tbs,'Value',get(tbs,'Min')); set([tbv tbp tbt tbd tbg tba tbinfo tbclose],'Enable','on'); break; end;
[N,C,loverd, alpha, t, visc, RP] = deal(answer{:});  loverd = str2num(loverd);C = str2num(C);N =
str2num(N);RP = str2num(RP);
alpha = str2num(alpha); t = str2num(t); slender = 0.5/loverd; alpha = alpha*pi/180;visc=str2num(visc);
if t < 0, t = 0; end; if t > 0.5, t = 0.5; end;
% SET MESH CONSTANTS
prompt ={'Number of nodes in the i or x direction:','Number of nodes in the j or y direction:',
      'Terminating value of residual for iter. to solve Vogelpohl equation:','Terminating value of residual for iter.
to find attitude angle:',
      'Relaxation factor of iter. to solve Vogelpohl equation:','Relaxation factor of iter. to find attitude angle:',
      'Max number of cycles during iter. to solve Vogelpohl equation:', 'Max number of cycles during iter. to find
attitude angle:'};
title = 'INPUT DATA (PISTON-Basic Model)'; lineno = 1; def = {'11','11','0.000001','0.0001','1.2','1','100','30'};
answer = inputdlg(prompt, title, lineno, def);if  size(answer) == 0,
  set(tbp, 'Value', get(tbp, 'Min')); set([tbv tbs tbt tbd tbg tba tbinfo tbclose],'Enable','on'); break; end;
[inode, jnode, reslim1, reslim2, factor1, factor2, nlim1, nlim2] = deal(answer{:});
inode = str2num(inode); jnode = str2num(jnode); reslim1 = str2num(reslim1); reslim2 = str2num(reslim2);
factor1 = str2num(factor1); factor2 = str2num(factor2); nlim1 = str2num(nlim1); nlim2 = str2num(nlim2);
r=(.08360)/2; wFh=.000001; N=2*pi*r*N/60;N=N;y0(1)=0;y0(2)=0;y0(3)=0;y0(4)=0;tot=N/60;tot=(1/(tot))*2;
stno=tot/(4*pi/N); stno=4320/stno; h22=[]; tot=1.2; RCY=RP+C; RC=(RP+RCY)/(RP*RCY); RC=1/RC;
visc0=visc [T,y]=ode45(@dedtp, [0 tot], y0);fprintf(' \n'); fprintf(' PROGRAM  HAS BEEN COMPLETED\N');
set(tbp, 'Value',get(tbp, 'Min')); set([tbv tbs tbt tbd tbg tbgr tbge tbr ],'Enable','on');
figure(1) h44=h44*C^2; h33=h33*C^2; h22=h22*C^2; hh244=hh244*C^2;  hhbar=hhbar*C^2; [ta,ia]=sort(t1);
 plot(ta*3600/6,real((h33(ia)/200)),'g');hold on; plot(ta*3600/6,real((h22(ia)/200)),'r');hold off; ylabel('film
thickness (m)')
xlabel('crank angle'); legend('minimum','maximum'); figure(2); [ta,ia]=sort(ia);
```

‘MATLAB’ FUNCTION CODE TO COMPUTE AN EHD FILM PROFILE IN EHL MODEL SIMULATION

```
function [de]=dedt(t,y)
global h22 h33 h44 ;global stno; global residp;global reslim1;global alpha;global inode;global jnode;global N;global C;global nlim1; global factor1;global I;global wFh;global M;global t1;global ffh1;global h;global h0;global beta;global reslim2;global residb; global nlim2;global factor2;global Torr;global myu;global Pressure;global indx;global p44;global visc;global P;global cou;global P1;global dpdx;global d2pdx2;
global deltax;global flag1;global RP;global RC;global hh244;global H1;global H2;global indx1;global hhbar;global visc0;global hhbar1;global ia;global ta;global p44;
e2b=y(1);e2t=y(2);eb=y(3);et=y(4);indx=indx+1;hbar=[];
%*****************************************************
de = zeros(4,1);    % a column vector
%*****************************************************
CP=.001;r=0.0418;l=0.15;V=2*pi*N*r/60;w=V/r;w=w/57.29578;Et=et/C;Eb=eb/C;MPIS=0.295;MPIN=.09;CG=.005;a=.0125;b=.0015;I=(t*stno);
A1=[0 90 180 270 310 360 372 378  450 540 630  720  810  900  990  1080 1120  1170  1182 1188  1260  1350  1440 1530 1620 ...        1710        1800        1840        1890        1902        1908
  1980 2070 2160        2250        2340        2430        2520        2610 ...
 2650  2700 2712        2718        2790        2880        2970        3060]';
A2=[0.1 0.1 0.1  500 1020 11500 20500 19000 2200 0.1 0.1 0.1 0.1  500 1020 11500 20500 19000 2200 0.1 0.1 0.1 0.1  500 1020 11500 20500 19000 2200 0.1 0.1  0.1 0.1  500 1020 11500 20500 19000 2200 0.1 0.1 ]';
FG=interp1(A1,A2,t*3600, 'cubic');tdispm=4*.0836;    A=CP+r*sin((I)/57.29578);Y=((l+r)^2-CP^2)^.50-(l^2-A^2)^0.50-r*cos(I/57.29578);
    U=r*w*sin(I/57.29578)+r*w*A*cos(I/57.29578)*((l^2-A^2)^-0.5);
 aY=r*w^2*cos((I)/57.29578)+(r*w*A*cos((I)/57.29578))^2*(l^2-A^2)^-1.5+((r*w*cos((I)/57.29578))^2-r*w^2*A*sin((I)*57.29578))*(l^2-A^2)^-0.5;
    phi=atan(A*(l^2-A^2)^-0.5);    FIC=-MPIS*aY;    FIP=-MPIN*aY;    FS=(tan(phi))*(FG+FIP+FIC);    MS=FG*CP-FIC*CG;
%=================
L=.0338;B=(2*pi*.0836)/2;slender = B/L; deltax = alpha/(inode-1); deltay = 1/(jnode-1);
% INITIALIZE VALUES OF M(I,J), SWITCH(I,J) AND P(I,J)
M = zeros(inode, jnode); P = zeros(inode, jnode);
% ENTER Et and Eb ITERATION CYCLE, CALCULATE H, F AND G VALUES (Vogelpohl Parameters)
EA=200*(10^9);EBB=200*(10^9);density=.7;  n2 = 0; betas = 0; residb = reslim2 + 10;
 while (residb > reslim2) & (n2 < nlim2),
   n2 = n2 + 1;
  for i = 1: inode,
    xaux = (i-1)*deltax + pi - 0.5 * alpha;      x1=xaux*C;
   for j = 1: jnode,
       y = (j-1) * deltay - 0.5; y1=y*C; yaux=y1;  h=C+et*cos(x1)-(et-eb)*y1*cos(x1) ;  h0=Et*cos(xaux)-(Et-Eb)*y*cos(xaux)+1;    h0=abs(h0);  dhdx0  = -Et*sin(xaux)+(Et-Eb)*y*sin(xaux); d2hdx20 = -Et*cos(xaux)+(Et-
```

```
Eb)*y*cos(xaux); dhdy0  =  -(Et-Eb)*cos(xaux); d2hdy20 = 0;H(i,j) =h0;    G(i,j) = dhdx0/h0^1.5;  F(i,j) = 0.75*(dhdx0^2 +
(slender*dhdy0)^2)/h0^2 + 1.5*(d2hdx20 + d2hdy20*slender^2)/h0;  ho=Et-(Et-Eb)*y+1;              h1=Et*cos(1/C)-(Et-
Eb)*y*cos(1/C);  hmm = mean(H(i,j));l=0.15; u=0.1;d2pdx2(i,j)=(((12*visc*u*l)/h0^3)*((-0.3+(1.5*(hmm*ho)/h0)-
(1.5*(hmm^2*ho^2)/h0^2)*(d2hdx20))+((visc*u*l*ho*hmm)/h0^5)*((-1.5+(3*hmm*ho)/h0)*(dhdx0)^2)));d(i,j)
=((3/8*((hmm^2/h1^4)-(hmm^2/ho^4)))-(-1/2*(hmm/h1^3)-(hmm/ho^3))+((1/6)*((1/h1^2)-(1/ho^2))))/(2*(1/ho^2-1/h1^2));
dpdxe(i,j)=(12*((H(i,j)^3-hmm)/H(i,j)^3))+ (2*(3*(hmm/H(i,j)^3)+(2/H(i,j)^2)*dhdx0)); dpdxd(i,j)=(-
18*(hmm^2/h0^5)*(dhdx0))+(18*(hmm/h0^4)*dhdx0)-(4*(1/h0^3)*(dhdx0))-(12*(hd(i,j)/h0^3));
    if i>1 dpdxl(i,j) = ((P(i,j)-P(i-1,j)))/deltax; end; if i == 1, dpdxl(i,j) = P(2,j)/deltax; end;
        dpdx(i,j)=dpdxl(i,j)+dpdxe(i,j)+dpdxd(i,j);      dpdx(i,j)=dpdx(i,j)+(dpdx(i,j)==0)*eps; end;    end;
     coeff1 = 1/deltax^2;  coeff2 = (slender/deltay)^2;
     %================================
     %SUBROUTINE TO SOLVE THE VOGELPOHL EQUATION
     sum2 = 0; n1 = 0; residp = reslim1 + 10;
     while (residp > reslim1) & (n1 < nlim1),
       n1 = n1 + 1; sum = 0;
       for i = 2: inode-1, for j = 2: jnode-1,
         store = ((M(i+1,j) + M(i-1,j))*coeff1 + (M(i,j+1) + M(i,j-1))*coeff2-G(i,j))/(2*coeff1 + 2*coeff2 + F(i,j));M(i,j) = M(i,j)
+ factor1*(store-M(i,j));
            if  M(i,j) < 0, M(i,j) = 0; end; sum = sum + M(i,j);end; end; if(sum==0) sum=0.0001; end; residp = abs((sum -
sum2)/sum); sum2 = sum; end;
      % ========================
    % FIND PRESSURE FIELD FROM VOGELPOHL PARAMETER
    for i = 2: inode-1,    for j = 2: jnode-1,
        P(i,j) = M(i,j)/H(i,j)^1.5;
      end;  end;
     % CALCULATE TRANSVERSE AND AXIAL LOADS
     % ====================================
     % SUBROUTINE TO INTEGRATE FOR FORCES
     for i = 1: inode,
       SUMY(i) = 0;     for j = 2: jnode, SUMY(i) = SUMY(i) + P(i,j) +P(i,j-1); end;    SUMY(i) = SUMY(i)*0.5*deltay;  end;
axialw =0; transw = 0;
     for i= 2: inode,
       x = (i-1)*deltax + pi-0.5*alpha; x2 = (i-2)*deltax + pi - 0.5*alpha;  axialw = axialw - cos(x)*SUMY(i)-cos(x2)*SUMY(i-
1);     transw = transw + sin(x)*SUMY(i) + sin(x2)*SUMY(i-1);  end;  axialw = axialw*deltax*0.5; transw =
transw*deltax*0.5;
     %================================
     loadw = sqrt(axialw^2 + transw^2);   if  (axialw == 0)  axialw=0.0001;  end;   attang = atan(transw/axialw);   if  (axialw > 0)
attang1 = attang; end;
      if  (axialw < 0)  attang1 = -attang;   end;   beta = beta + factor2*attang1;    residb = abs((beta-betas)/beta);   betas =
beta;end;
   % ========================
   % SUBROUTINE TO CALCULATE PETROFF MULTIPLIER
```

```
for j = 1: jnode, ICAV(i) = 1000; end;
for j = 2: jnode-1,   for i = 2: inode,
    if  (M(i,j) == 0) & (ICAV(i) == 1000), ICAV(j) = i; end;   end;end;Radius=RP;
% EXTRAPOLATED VALUES OF ICAV(J) AT EDGES OF BEARING
ICAV(1) = 2*ICAV(2)-ICAV(3); if ICAV(1) < 1, ICAV(1) = 1; end;if ICAV(1) > inode, ICAV(1) = inode;
 ICAV(jnode) = 2*ICAV(jnode-1)-ICAV(jnode-2);end;if ICAV(jnode) < 1, ICAV(jnode) = 1; end; if ICAV(jnode) > 1,
ICAV(jnode) = 0; end;
for i = 1: inode,   for j = 1: jnode
 if i>1 dpdx(i,j) = ((P(i,j)-P(i-1,j)))/deltax; end;  if i == 1, dpdx(i,j) = P(2,j)/deltax; end;    if i == ICAV(jnode),TORR(i,j) =
1*1/H(i,j) + 3*(dpdx(i,j)*H(i,j)); TORR(i,j)=TORR(i,j)*(U*visc/C);  end; if i > ICAV(jnode), TORR(i,j) =
1/H(i,j);TORR(i,j)=TORR(i,j)*(U*visc/C);end;
            i10 = ICAV(j); if i < ICAV(jnode), TORR(i,j) = 1*H(i10,j)/H(i,j)^2;   TORR(i,j)=TORR(i,j)*(U*visc/C);end; end;
end;
  Torr=(mean(TORR)); [ka,ia]=max(M);[la,ja]=max(ka); kkk=max(H(ia(ja),ja));pmax = 0;
for i = 2: inode-1,   for j = 2: jnode-1,
    if P(i,j) > pmax, pmax = P(i,j); end;  end;end;
if(mod(cou,2)==0)    h22=[h22 min(max(H))];    h33=[h33 min(min(H))];  h44=[h44 kkk(1,1)]; pp44=1/max(max(H));
p44=[p44 pp44]; t1=[t1 t];hh244=hhbar*2;end;
%**********************EHD Effects**************************
for i=1:inode    for j=1:jnode
      dpdx(i,j)=dpdx(i,j)+dpdx(i,j)*eps;    if (d2pdx2(i,j)==0 & abs(dpdx(i,j))>0)       dpdX=dpdx(i,j);
       flag=1;         dpdX=dpdX+dpdX*eps;       ha=sqrt(4*visc0*abs(U)/dpdX);       hm=(ha)^(2/3);
K=(hm^2/12*visc0*abs(U))*dpdX;
      if(P(i,j)==pmax)
         flag1=1;       end;       if(flag1==0)          K=K;       else          K=-1*K;       end;       cubeq=[K 0 1 -1];
      [hbar]=roots(cubeq);       rl=[real(hbar(1)) real(hbar(2)) real(hbar(3))]';       alfa=29;     visc1=visc0*exp(alfa*pmax);
end; end;end;
if(flag==0)    hbar=[0.1 0.1 0.1];end; Ecy=200e+09;Ep=200e+09;%Pa
%*************** Double Integration of Pressure**************************
for i=1:inode    SumY(i)=0;
   for j=2:jnode
      SumY(i)=SumY(i)+P(i,j)+P(i, j-1); SumY(i)=SumY(i)*0.5*deltay;end;end;Prees=0;
for i=2:inode
   Prees=Prees+SumY(i)+SumY(i-1);end;DUBP=Prees*5*deltax;sigma1=0.3;sigma2=0.3;cfg1=(1-(sigma1)^2)/Ep;cfg2=(1-
(sigma2)^2)/Ecy;
cfg=cfg1+cfg2;Ebar=2/cfg;dismue=(2/(pi*Ebar))*DUBP;
for ind=1:inode    for j=1:jnode
hehd(ind, j)=kkk(1,1)+((ind^2)/2*RC)+dismue;h44=[hehd(ind,j) kkk(1,1)];end;end;
%*************************************************************************
% INTEGRATE FOR TORR(i,j) OVER  X AND Y
for i = 1: inode,
  % LINE INTEGRAL IN Y-SENSE for FFh
```

```
    SUMY(i) = 0;
    for j = 2: jnode, SUMY(i) = SUMY(i) + TORR(i,j) +TORR(i,j-1); end;   SUMY(i) = SUMY(i)*0.5*deltay; end;friction =
0;for i = 2: inode,
   friction = friction + SUMY(i) + SUMY(i-1);end;friction = friction*0.5*deltax; myu = friction/loadw;Ffh=friction;ffh1=[ffh1
Ffh];
  %**********************Mfh**********************************
  mfh = 0;
  for i = 2: inode,
     x1 = (i-1)*deltax + pi - 0.5 * alpha;x2=(i-2)*deltax + pi - 0.5 * alpha; x1=x1*C;x2=x2*C;  mfh = mfh - cos(x1)*SUMY(i)
-cos(x2)*SUMY(i-1);
  end; mfh = mfh*0.5*deltax;Mfh=(mfh)-CP*Ffh;
  %================================
  %CALCULATE DIMENSIONLESS FRICTION COEFFICIENT
  % SEARCH FOR MAXIMUM PRESSURE
  if(flag1==1) hmax = 0;
  for i = 2: inode-1,   for j = 2: jnode-1,
      P(i,j)=P(i,j)*(6*U*visc*B)/C^2; end;   end;end; pmax = 0;
  for i = 2: inode-1,   for j = 2: jnode-1,
      if P(i,j) > pmax, pmax = P(i,j); end;   end;end;
  % EXPRESS ALL PRESSURES AS PERCENTAGE OF MAXIMUM PRESSURE
  if(pmax==0)   pmax=0.0001;end
  for i = 1: inode,   for j = 1: jnode,
      P(i,j) = P(i,j);   end;end; if(mod(cou,6)==0)
  P1(:,:,indx1)=P;P44(:,:,indx1)=p44;H1(:,:,indx1)=hehd;H2(:,:,indx1)=H;maxhbar1=max(hbar);hhbar1=[hhbar1 maxhbar1];
  indx1=indx1+1;end; if(mod(cou,2)==0)
[maxhehda]=max(hehd);maxhehd=max(maxhehda);maxhbar=max(hbar);hh244=[hh244 maxhehd]; hhbar=[hhbar
maxhbar];end;cou=cou+1;IPIS=.5*MPIS*(Radius)^2;
  %************************Fh force*************************************************************
  for i = 1: inode,    for j = 1: jnode,
       FFH(i,j) = ((M(i,j)/H(i,j)^1.5))*(6*U*visc0*B)/C^2;end;end;
  for i = 1: inode,
      fhSUMY(i) = 0; for j = 2: jnode, fhSUMY(i) = fhSUMY(i) + FFH(i,j) +FFH(i,j-1); end;fhSUMY(i) =
fhSUMY(i)*0.5*deltay;  end;  fh = 0;
  for i = 2: inode,
     x1 = (i-1)*deltax + pi - 0.5 * alpha;x2=(i-2)*deltax + pi - 0.5 * alpha;  x1=x1*C;x2=x2*C;
   fh = fh - cos(x1)*fhSUMY(i) - cos(x2)*fhSUMY(i-1); end;fh = fh*0.5*deltax; Fh=fh;
  %*************************************************************************************************
  for i = 1: inode,     for j = 1: jnode,
       FFH(i,j) = ((M(i,j)/H(i,j)^1.5));  end;  end;
  for i = 1: inode,
      fhSUMY(i) = 0;  for j = 2: jnode, fhSUMY(i) = fhSUMY(i) + FFH(i,j) +FFH(i,j-1); end;fhSUMY(i) =
fhSUMY(i)*0.5*deltay;  end;  fh = 0;
```

```
   for i = 2: inode,
      x1 = (i-1)*deltax + pi - 0.5 * alpha;    x2=(i-2)*deltax + pi - 0.5 * alpha;
    fh = fh - cos(x1)*fhSUMY(i) - cos(x2)*fhSUMY(i-1); end; fh = fh*0.5*deltax;wFh=fh;
   %**********************Mh*********************************************************************
    for i = 1: inode,
            xaux = (i-1)*deltax + pi - 0.5 * alpha;
      for j = 1: jnode,
        MH(i,j) = (M(i,j)/H(i,j)^1.5)*(6*U*visc0*B)/C^2; end;  end;
     for i = 1: inode,
       mfhSUMY(i) = 0;
       for j = 2: jnode,
          mfhSUMY(i) = mfhSUMY(i) + (a-j)*MH(i,j) +(a-j-1)*MH(i,j-1); end;     mfhSUMY(i) = mfhSUMY(i)*0.5*deltay;
end;  mfh = 0;
   for i = 2: inode,
      x1 = (i-1)*deltax + pi - 0.5 * alpha;    x2=(i-2)*deltax + pi - 0.5 * alpha;  x1=x1*C;x2=x2*C;
      mfh = mfh -cos(x1)*mfhSUMY(i) -cos(x2)*mfhSUMY(i-1);end;mfh = mfh*0.5*deltax;MH=mfh;FS=FS;MS=MS;
   %*********************************************************************************************
   A=[MPIN*(1-a/L)+MPIS*(1-b/L) MPIN*a/L+MPIS*b/L;MPIS*IPIS/L+MPIS*(a-b)*(1-b/L) MPIS*(a-b)*b/L-
MPIS*IPIS/L];
   BT=[Fh+FS+Ffh*tan(phi);MH+MS+Mfh];
   X=lsqr(A, BT);
   indx=indx+1;
   det=X(1);deb=X(2);de(1)=deb;de(2)=det;de(3)=e2b;de(4)=e2t;
```

REFERENCES

1. D.Rh. Gwynllyw and T.N. Phillips. The effects of viscoelasticity on the performance of Journal bearings. IUTAM symposium on elastohydrodynamic and micro elastohydrodynamics, 175-186.

2. Rong Zhang and Xin kai li. Non Newtonian effects on lubricant thin film flows [J]. Journal of Engineering Mathematics (2005) 51: 1-13.

3. Waseem Akhtar , Corina Fetecau , Victor Tigoiu and Constantin Fetecau. Flow of Maxwell fluid between two side walls induced by a constantly accelerating plate. Z.angew.Math.Phys. 60 (2009) 498-510.

4. Corina Fetecau , D.Vieru , A. Mahmood , C. Fetecau. On the energetic balance for the flow of a Maxwell fluid due to a constantly accelerating plate. Acta Mech 203, 89-96 (2009).

5. A.Berker, M.G.Bouldin, S.J.Kleis, W.E.Vanarsdale. Effect of polymer on flow in journal bearing . Journal of non-Newtonian fluid mechanics, 0377-0257/95.

6. Non-Newtonian flow in the process industries. Fundamentals and Engineering applications. R.P.Chabra, J.F.Richardson.

7. Sara J .Hupp. defining the role of elastic lubricants and micro textured surfaces in lubricated, sliding friction. PhD thesis , Massachusetts institute of technology, Feb 2008.

8. I.Kudish, Rubber G.Airapetyan and Michael J.Covitch. Modeling of lubricant degradation and elastohydrodynamic lubrication, IUTAM symposium on elastohydrodynamics and micro elastohydrodynamics, 149-174. 2006. Springer

9. Punit Kumar, S.C.Jain, S.Ray. Influence of polymeric fluid additives in EHL sliding line contacts. Tribology International 41(2008) 482-492.

10. Ming-Tang Ma. An expedient approach to the non-newtonian thermal EHL in heavily loaded point contacts wear 206 (1997) 100-112.

11. Hong yiping , Chen Darong, Kong Xianmei, Wang Jiadao. Model of fluid structure interaction and its application to elastohydrodynamic lubrication. Methods Appl.Mech.Engrg. 191.(2002). 4231-4240.

12. J.Seabra, A.Sottomayor , A.Compos. Non-newtonian EHL model for traction evaluation in a roller-inner ring contact in a roller bearing. Wear 195 (1996) 53-65.

13. Hsiao-Ming Chu, Wang-Long Li, Yuh-Ping Chang. Thin film elastohydrodynamic lubrication-A power law fluid model. Tribology international 39 (2006) 1474-1481.

14. P.C.Sui, F.Sadeghi. Non Newtonian thermal elastohydrodynamic lubrication. Transactions of the ASME 390, vol.113 , April 1991.

15. Peiran yang, Shizhu wen. The behavior of non Newtonian thermal EHL film in line contacts at dynamic loads. Journal of tribology . January 1992, Vol 114/81.

16. Punit Kumar, M.M.khonsari, Scott Bair. Full EHL simulation using the actuall Ree-Eyring model for shear thinning lubricants. Journal of Tribology, January 2009, vol. 131/011802-1

17. J.P.Charmleffel, G.Dalmaz, P.Vergne. Experimental results and analytical film thickness predictions in EHD rolling point contacts. Tribology International. 40 (2007) 1543-1552.

18. J.G.Wang and J.J.Ma. on the shear stress of elastohydrodynamic lubrication in elliptical contacts. Tribology International. Vol 29. 0301-679x (96) 0005-9.

19. R.C.Bhattacharjee and N.C.Das. Power law fluid model incorporated in to ealstohydrodynamic lubrication theory of line contact. Tribology International. Vol 29, 0301-679x(95) 00096-8.

20. Dong.Zhu, Herbert S.Cheng , Takayuki Arai, Kgugo.Hamai. A numerical analysis for piston skirts in mixed lubrication. ASME. 91-Trib-66.

21. J-R Lin, M-Y.Teng and M-H.Ho. Effects of non Newtonian rheology on the film height history between non parallel sliding-sequeezing surfaces. Journal of Engineering Tribology, vol 221. DOI: 10.1243/13506501 JET 158.

22. Gwidon W. Stachowiak and Andrew W.Batchelor. Engineering Tribology, ISBN-10:0-7506-7836-4.

23. M Afzaal Malik, Syed adnan Qasim, Badar Rashid, Shahab Khushnood, Proceedings of 2004 ASME/STLE International joint tribology conference. TRIB2004-64101

24. Hoult David P., Lux Jeffrey P., Wong Victor, " Calibration of Laser fluorescence measurements of lubricant film thickness in engines", SAE Paper No. 881587.

25. Napel W.E. Ten, Bosma R., "The Influence of surface roughness on the capacitive measurement of thickness in EHD contacts", Proc. Inst. Mech Engrs, Vol. 18537/71, pp 635-639.

26. Richardson Dana E., Borman Gary L., "Theoretical & experimental investigations of oil films for application to piston ring lubrication", SAE Paper No. 922341.

27. Knopf M., Eiglmeier C., Merker G.P., “Calculation of unsteady hydrodynamic lubrication & surface contact at piston-ring/cylinder-liner interface”, SAE Paper No. 981402.
28. Hitosugi Hideshi, Nagoshi Katsuyuki, Komada Masahara, Furuhama Shoichi, “Study of mechanism of lubricating oil consumption caused by cylinder bore deformation”, SAE Paper No. 960305.
29. Shlijper A.G., Scales L.E., Rycroft J.E., “Current tools and techniques for EHL modeling”, Tribology International Vol. 29, No. 8, pp 669-673, 1996.
30. Coy R.C., “Practical Applications of lubrication models in engines”, Tribology International, Vol. 10, pp 563-571, 1998.
31. Qingwen Qu, Mei Weng, Shan Chai, Fusheng Yao, “Velocity Analysis for layered viscosity model under thin film lubrication”, Tribology International, Vol. 34, 2001, pp 517-521.
32. Taylor, C..M., “Automobile engine Tribology-design considerations for efficiency and durability”, Wear, 221 (1998), pp 1-8.
33. Pawan K. Goenka, Rohit S. Paranjpe, Yeau-Ren Jeng, “FLARE: An Integrated Software Package for Friction & Lubrication Analysis of automotive engines-Part I: Overview and Applications”, SAE Paper # 920487.
34. Rohit S. Paranjpe, Annette Cusenza, “FLARE: An Integrated Software Package for friction and lubrication analysis of automotive engines-Part II: Experimental Validation”, SAE Paper # 920488.
35. Dong Zhu, Yuan-Zhong Hu, “Effects of Rough Surface topography and orientation on the characteristics of EHD and Mixed lubrication in both circular and elliptical contacts”, Tribology transactions Vol. 44(2001), 3, pp 391-398.
36. Dong Zhu, Yuan-Zhong Hu, “A full numerical solution to the mixed lubrication in point contacts”, ASME Journal of Tribology, Jan. 2000, Vol. 122, pp 1-9.
37. Dong Zhu, “A design tool for selection and optimization of surface finish in mixed lubrication”, Tribology Transactions.
38. Dong Zhu, “Elastohydrodynamic lubrication in extended parameter ranges-Part I: Speed Effect”, Tribology Transactions, Vol. 45(2002), 4, pp 540-548.
39. Dong Zhu, “Elastohydrodynamic lubrication in extended parameter ranges-Part II: Load Effect”, Tribology Transactions, Vol. 45(2002), 4, pp 549-555.

40. Dong Zhu, Yuan-Zhong Hu, “A computer program package for the prediction of EHL and Mixed lubrication characteristics, friction, subsurface stresses and flash temperatures based on measured 3-D surface roughness”, Tribology Transactions, Vol. 44(2001), 3, pp 383-390.
41. “Saving of lubricant oil consumption by using 3Flex oil control ring”, Report prepared by Technical Department, Teikoku piston ring Co. Ltd., Japan, Number KB01-2721, pp 1-7.
42. Robert Munro, “Blow-by in relation to piston and ring features”, SAE Paper # 810932.
43. Eric W. Schneider, Daniel H. Blossfeld, Donald C. Lechman, Robert F. Hill, Richard F. Reising, “Effect of cylinder bore out-of-roundness on piston ring rotation and engine oil consumption”, SAE Paper # 930796.
44. Tasbaz O..D., Wood R.J.K., Browne M., Powrie H.E.G., Denuault G., “Electrostatic monitoring of oil lubricated sliding point contacts for early detection of scuffing”, Wear 230 (1999), pp 86-97.
45. Jaw-Ren Lin, “Squeeze film characteristics between a sphere and a flat plate: couple stress fluid model”, Elsevier Science Ltd., Computers and Structures 75 (2002) pp 73-80.
46. Mitsuhiro Soejima, Yoshito Ejima, Kenji Uemori, Masataka Kawasaki, “Studies on friction and wear characteristics of cam and follower: influences of soot contamination in engine oil”, JSAE Review 23 (2002) pp 113-119.
47. Gerges S.N.Y., “The influence of cylinder lubrication on piston slap”, Journal of Sound and Vibration (2002) 257(3), pp 527-557.
48. Manabu Wakuda, Yukihiko Yamauchi, Shuzo Kanzaki, Yoshiteru Yasuda, “Effect of surface texturing on friction reduction between ceramic and steel materials under lubricated sliding contact”, Wear 9432 (2003) pp 1-8.
49. Hao Xu, Graham J. Jones, “A study for wear and fatigue on engine bearings by using EHL analysis”, JSAE Review 21 (2002) pp 189-196.
50. Guo F., yang P., Wong P.L., “On the thermal elastohydrodynamic lubrication in opposite sliding circular contacts”, Tribology International 34 (2001), pp 443-452.
51. Daniel Nelias, “Experimental and theoretical investigation on temperature and micro-scuffing in EHL contacts”, Elsevier, Paris, Rev Gen Therm (1997) 36, pp 26-39.

52. Cris Cusano, Wang S., Conry T.F., “A Reynolds–Eyring equation for elastohydrodynamic lubrication in line contacts”, Transactions of the ASME, Tribology Division, Conference Paper No. 86-Trib-53.
53. Todor Sheiretov, Hyung Yoon, Cris Cusano, “Scuffing under dry sliding conditions-Part I: Experimental Studies”, STLE preprint No. 98-AM-1I-2.
54. Todor Sheiretov, Hyung Yoon, Cris Cusano, “Scuffing under dry sliding conditions-Part II: Theoretical Studies”, STLE preprint No. 98-AM-1I-3.
55. Cusano C., Wedeven L.D., “Elastohydrodynamic film thickness measurements of artificially-produced non-smooth surfaces”, STLE preprint No. 79-LC-IA-3.
56. Cris Cusano, Chang L., Conry T.F., “An efficient, robust, multi-level computational algorithm for elastohydrodynamic lubrication”, Transactions of the ASME, Tribology Division, Conference Paper No. 88-Trib-2.
57. Cris Cusano, Wang S., Conry T.F., “Thermal analysis of elastohydrodynamic lubrication of line contacts using the Ree-Eyring fluid model”, Transactions of the ASME, Tribology Division, Conference Paper No. 90-Trib-27.
58. Cris Cusano, Goglia P.R., Conry T.F., “The effects of surface irregularities on the elastohydrodynamic lubrication of sliding line contacts: Part I-Single Irregularities”, Transactions of the ASME, Tribology Division, Conference Paper No. 83-Lub-20.
59. Cris Cusano, Goglia P.R., Conry T.F., “The effects of surface irregularities on the elastohydrodynamic lubrication of sliding line contacts: Part II-Wavy Surfaces”, Transactions of the ASME, Tribology Division, Conference Paper No. 83-Lub-20.
60. Cusano C., Wedeven L.D., “Elastohydrodynamic film thickness measurements of artificially-produced surface dents and grooves”, ASLE Transactions, Vol. 22 (1978), 4, pp 369-381.
61. Hamilton G. M., Moore S.L., “Ring pack film thickness during running-in”, Paper VII (ii), Proc. I. Mech. E., pp 153-161.
62. Hamilton G. M., Moore S.L., “The starved lubrication of piston rings in a diesel engine”, J. Mech. Eng. Sci., 1978. Vol. 20, no. 6, pp. 345-352.
63. Hamilton G. M., Moore S.L., “The piston ring at top dead centre”, Proc. I. Mech. E., 1980, Vol. 194, pp. 373-381.

64. Taylor R.I., Brown M.A., Thompson D.M., “Validation of a piston ring-pack lubrication model that includes realistic lubricant rheology”, Lubricants and Lubrication (1995), Elsevier Science B.V., pp. 345-354.
65. Nadir Patir, Cheng H.S., “Application of average flow model to lubrication between rough sliding surfaces”, Transactions of the ASME, Lubrication Division (1978), Conference Paper no. 78-Lub-17.
66. Houpert L.G., Hamrock B.J., “Fast approach for calculating film thicknesses and pressures in elastohydrodynamically lubricated contacts at high loads”, Transactions of the ASME, Tribology Division (1985), Conference Paper no. 85-Trib-42.
67. Arthur Caines, Roger Haycock, “Automotive Lubricants Reference Book”, 1996, Published by: SAE Inc.,
68. Gwidon W. Stachowiak, Andrew W. Batchelor, Book titled “Engineering Tribology, Second Edition”, (2001) U.S.A.
69. Michael M. Khonsari, E. Richard Booser, Book titled “Applied Tribology- Bearing Design and Lubrication”, printed in 2000.
70. Stolarski T.A., Book titled “Tribology in Machine Design”, published in 1999.
71. “The Tribology of Internal Combustion Engines” Book Published in 1996, by Mech. Eng. Publications Ltd., U.K.
72. Dowson D., Higginson G.R., Book titled “Elasto-hydrodynamic Lubrication: The Fundamentals of Gear and Roller Lubrication”, printed in 1966.